

BULLETIN OF RUSSIAN STATE MEDICAL UNIVERSITY

BIOMEDICAL JOURNAL OF PIROGOV RUSSIAN NATIONAL
RESEARCH MEDICAL UNIVERSITY

EDITOR-IN-CHIEF Denis Rebrikov, DSc, professor

DEPUTY EDITOR-IN-CHIEF Alexander Oettinger, DSc, professor

EDITORS Valentina Geidebrekht, Nadezda Tikhomirova

TECHNICAL EDITOR Evgeny Lukyanov

TRANSLATORS Ekaterina Tretiyakova, Vyacheslav Vityuk

DESIGN AND LAYOUT Marina Doronina

EDITORIAL BOARD

Averin VI, DSc, professor (Minsk, Belarus)
Alipov NN, DSc, professor (Moscow, Russia)
Belousov VV, DSc, professor (Moscow, Russia)
Bogomilskiy MR, corr. member of RAS, DSc, professor (Moscow, Russia)
Bozhenko VK, DSc, CSc, professor (Moscow, Russia)
Bylova NA, CSc, docent (Moscow, Russia)
Gainetdinov RR, CSc (Saint-Petersburg, Russia)
Gendlin GYe, DSc, professor (Moscow, Russia)
Ginter EK, member of RAS, DSc (Moscow, Russia)
Gorbacheva LR, DSc, professor (Moscow, Russia)
Gordeev IG, DSc, professor (Moscow, Russia)
Gudkov AV, PhD, DSc (Buffalo, USA)
Gulyaeva NV, DSc, professor (Moscow, Russia)
Gusev EI, member of RAS, DSc, professor (Moscow, Russia)
Danilenko VN, DSc, professor (Moscow, Russia)
Zarubina TV, DSc, professor (Moscow, Russia)
Zatevakhin II, member of RAS, DSc, professor (Moscow, Russia)
Kagan VE, professor (Pittsburgh, USA)
Kzyzhkowska YuG, DSc, professor (Heidelberg, Germany)
Kobriniskii BA, DSc, professor (Moscow, Russia)
Kozlov AV, MD PhD (Vienna, Austria)
Kotelevtsev YuV, CSc (Moscow, Russia)
Lebedev MA, PhD (Darem, USA)
Manturova NE, DSc (Moscow, Russia)
Milushkina OYu, DSc, professor (Moscow, Russia)
Mitupov ZB, DSc, professor (Moscow, Russia)
Moshkovskii SA, DSc, professor (Moscow, Russia)
Munblit DB, MSc, PhD (London, Great Britain)

Negrebetsky VV, DSc, professor (Moscow, Russia)
Novikov AA, DSc (Moscow, Russia)
Pivovarov YuP, member of RAS, DSc, professor (Moscow, Russia)
Platonova AG, DSc (Kiev, Ukraine)
Polunina NV, corr. member of RAS, DSc, professor (Moscow, Russia)
Poryadin GV, corr. member of RAS, DSc, professor (Moscow, Russia)
Razumovskii AYU, corr. member of RAS, DSc, professor (Moscow, Russia)
Rebrova OYu, DSc (Moscow, Russia)
Rudoy AS, DSc, professor (Minsk, Belarus)
Rylova AK, DSc, professor (Moscow, Russia)
Savelieva GM, member of RAS, DSc, professor (Moscow, Russia)
Semiglazov VF, corr. member of RAS, DSc, professor (Saint-Petersburg, Russia)
Skoblina NA, DSc, professor (Moscow, Russia)
Slavyanskaya TA, DSc, professor (Moscow, Russia)
Smirnov VM, DSc, professor (Moscow, Russia)
Spallone A, DSc, professor (Rome, Italy)
Starodubov VI, member of RAS, DSc, professor (Moscow, Russia)
Stepanov VA, corr. member of RAS, DSc, professor (Tomsk, Russia)
Suchkov SV, DSc, professor (Moscow, Russia)
Takhchidi KhP, member of RAS, DSc, professor (Moscow, Russia)
Trufanov GE, DSc, professor (Saint-Petersburg, Russia)
Favorova OO, DSc, professor (Moscow, Russia)
Filipenko ML, CSc, leading researcher (Novosibirsk, Russia)
Khazipov RN, DSc (Marsel, France)
Chundukova MA, DSc, professor (Moscow, Russia)
Shimanovskii NL, corr. member of RAS, DSc, professor (Moscow, Russia)
Shishkina LN, DSc, senior researcher (Novosibirsk, Russia)
Yakovovskaya RI, DSc, professor (Moscow, Russia)

SUBMISSION <http://vestnikrgmu.ru/login?lang=en>

CORRESPONDENCE editor@vestnikrgmu.ru

COLLABORATION manager@vestnikrgmu.ru

ADDRESS ul. Ostrovityanova, d. 1, Moscow, Russia, 117997

Indexed in Scopus. CiteScore 2021: 0.5

Scopus[®]

SCImago Journal & Country Rank 2020: 0.14

SJR

Scimago Journal & Country Rank

Indexed in WoS. JCR 2021: 0.5

WEB OF SCIENCE[™]

Listed in HAC 31.01.2020 (№ 507)



ВЫСШАЯ
АТТЕСТАЦИОННАЯ
КОМИССИЯ (ВАК)

Five-year h-index is 8

Google
scholar

Open access to archive

CYBERLENINKA

Issue DOI: 10.24075/brsmu.2022-01

The mass media registration certificate № 012769 issued on July 29, 1994

Founder and publisher is Pirogov Russian National Research Medical University (Moscow, Russia)

The journal is distributed under the terms of Creative Commons Attribution 4.0 International License www.creativecommons.org



Approved for print 28.02.2022
Circulation: 100 copies. Printed by Print.Formula
www.print-formula.ru

ВЕСТНИК РОССИЙСКОГО ГОСУДАРСТВЕННОГО МЕДИЦИНСКОГО УНИВЕРСИТЕТА

НАУЧНЫЙ МЕДИЦИНСКИЙ ЖУРНАЛ РНИМУ ИМ. Н. И. ПИРОГОВА

ГЛАВНЫЙ РЕДАКТОР Денис Ребриков, д. б. н., профессор

ЗАМЕСТИТЕЛЬ ГЛАВНОГО РЕДАКТОРА Александр Эттингер, д. м. н., профессор

РЕДАКТОРЫ Валентина Гейдебрехт, Надежда Тихомирова

ТЕХНИЧЕСКИЙ РЕДАКТОР Евгений Лукьянов

ПЕРЕВОДЧИКИ Екатерина Третьякова, Вячеслав Виток

ДИЗАЙН И ВЕРСТКА Марины Дорониной

РЕДАКЦИОННАЯ КОЛЛЕГИЯ

В. И. Аверин, д. м. н., профессор (Минск, Белоруссия)
Н. Н. Алипов, д. м. н., профессор (Москва, Россия)
В. В. Белоусов, д. б. н., профессор (Москва, Россия)
М. Р. Богомилский, член-корр. РАН, д. м. н., профессор (Москва, Россия)
В. К. Боженко, д. м. н., к. б. н., профессор (Москва, Россия)
Н. А. Былова, к. м. н., доцент (Москва, Россия)
Р. Р. Гайнетдинов, к. м. н. (Санкт-Петербург, Россия)
Г. Е. Гендлин, д. м. н., профессор (Москва, Россия)
Е. К. Гинтер, академик РАН, д. б. н. (Москва, Россия)
Л. Р. Горбачева, д. б. н., профессор (Москва, Россия)
И. Г. Гордеев, д. м. н., профессор (Москва, Россия)
А. В. Гудков, PhD, DSc (Буффало, США)
Н. В. Гуляева, д. б. н., профессор (Москва, Россия)
Е. И. Гусев, академик РАН, д. м. н., профессор (Москва, Россия)
В. Н. Даниленко, д. б. н., профессор (Москва, Россия)
Т. В. Зарубина, д. м. н., профессор (Москва, Россия)
И. И. Затевахин, академик РАН, д. м. н., профессор (Москва, Россия)
В. Е. Каган, профессор (Питтсбург, США)
Ю. Г. Кжышковска, д. б. н., профессор (Гейдельберг, Германия)
Б. А. Кобринский, д. м. н., профессор (Москва, Россия)
А. В. Козлов, MD PhD (Вена, Австрия)
Ю. В. Котелевцев, к. х. н. (Москва, Россия)
М. А. Лебедев, PhD (Дарем, США)
Н. Е. Мантурова, д. м. н. (Москва, Россия)
О. Ю. Милушкина, д. м. н., доцент (Москва, Россия)
З. Б. Митупов, д. м. н., профессор (Москва, Россия)
С. А. Мошковский, д. б. н., профессор (Москва, Россия)
Д. Б. Мунблит, MSc, PhD (Лондон, Великобритания)

В. В. Негребский, д. х. н., профессор (Москва, Россия)
А. А. Новиков, д. б. н. (Москва, Россия)
Ю. П. Пивоваров, д. м. н., академик РАН, профессор (Москва, Россия)
А. Г. Платонова, д. м. н. (Киев, Украина)
Н. В. Полунина, член-корр. РАН, д. м. н., профессор (Москва, Россия)
Г. В. Порядин, член-корр. РАН, д. м. н., профессор (Москва, Россия)
А. Ю. Разумовский, член-корр., профессор (Москва, Россия)
О. Ю. Реброва, д. м. н. (Москва, Россия)
А. С. Рудой, д. м. н., профессор (Минск, Белоруссия)
А. К. Рылова, д. м. н., профессор (Москва, Россия)
Г. М. Савельева, академик РАН, д. м. н., профессор (Москва, Россия)
В. Ф. Семиглазов, член-корр. РАН, д. м. н., профессор (Санкт-Петербург, Россия)
Н. А. Скоблина, д. м. н., профессор (Москва, Россия)
Т. А. Славянская, д. м. н., профессор (Москва, Россия)
В. М. Смирнов, д. б. н., профессор (Москва, Россия)
А. Спаллоне, д. м. н., профессор (Рим, Италия)
В. И. Стародубов, академик РАН, д. м. н., профессор (Москва, Россия)
В. А. Степанов, член-корр. РАН, д. б. н., профессор (Томск, Россия)
С. В. Сучков, д. м. н., профессор (Москва, Россия)
Х. П. Тахчиди, академик РАН, д. м. н., профессор (Москва, Россия)
Г. Е. Труфанов, д. м. н., профессор (Санкт-Петербург, Россия)
О. О. Фаворова, д. б. н., профессор (Москва, Россия)
М. Л. Филипенко, к. б. н. (Новосибирск, Россия)
Р. Н. Хазипов, д. м. н. (Марсель, Франция)
М. А. Чундокова, д. м. н., профессор (Москва, Россия)
Н. Л. Шимановский, член-корр. РАН, д. м. н., профессор (Москва, Россия)
Л. Н. Шишкина, д. б. н. (Новосибирск, Россия)
Р. И. Якубовская, д. б. н., профессор (Москва, Россия)

ПОДАЧА РУКОПИСЕЙ <http://vestnikrgmu.ru/login>

ПЕРЕПИСКА С РЕДАКЦИЕЙ editor@vestnikrgmu.ru

СОТРУДНИЧЕСТВО manager@vestnikrgmu.ru

АДРЕС РЕДАКЦИИ ул. Островитянова, д. 1, г. Москва, 117997

Журнал включен в Scopus. CiteScore 2021: 0,5

Журнал включен в WoS. JCR 2021: 0,5

Индекс Хирша (h²) журнала по оценке Google Scholar: 8

Scopus®

SCImago Journal & Country Rank 2020: 0,14

SJR
Scimago Journal & Country Rank

WEB OF SCIENCE™

Журнал включен в Перечень 31.01.2020 (№ 507)



ВЫСШАЯ
АТТЕСТАЦИОННАЯ
КОМИССИЯ (ВАК)

Google
scholar

Здесь находится открытый архив журнала

CYBERLENINKA

DOI выпуска: 10.24075/vrgmu.2022-01

Свидетельство о регистрации средства массовой информации № 012769 от 29 июля 1994 г.

Учредитель и издатель — Российский национальный исследовательский медицинский университет имени Н. И. Пирогова (Москва, Россия)

Журнал распространяется по лицензии Creative Commons Attribution 4.0 International www.creativecommons.org



Подписано в печать 28.02.2022

Тираж 100 экз. Отпечатано в типографии Print.Formula
www.print-formula.ru

REVIEW

5

Molecular biology applications of the red king crab duplex-specific nuclease

Shagin DA, Rebrikov DV

Применение дуплекс-специфичной нуклеазы из камчатского краба в методах молекулярной биологии

Д. А. Шагин, Д. В. Ребриков

ORIGINAL RESEARCH

11

Dynamic changes in the concentration of anti-SARS-CoV-2 antibodies within 12 months after recovery from COVID-19

Mayanskiy NA, Brzhozovskaya EA, Stoyanova SS, Frolov AV, Lebedin YuS

Динамика концентрации антител к SARS-CoV-2 в течение 12 месяцев после перенесенной инфекции COVID-19

Н. А. Маянский, Е. А. Бржозовская, С. С. Стоянова, А. В. Фролков, Ю. С. Лебедин

ORIGINAL RESEARCH

14

Properties of RBD specific IgG from COVID-19 patients and Sputnik V vaccinated individuals

Generalova LV, Grigoriev IV, Vasina DV, Tkachuk AP, Kruzhkova IS, Kolobukhina LV, Burgasova OA, Guschin VA

Свойства антител к RBD у переболевших COVID-19 и вакцинированных препаратом «Спутник V»

Л. В. Генералова, И. В. Григорьев, Д. В. Васина, А. П. Ткачук, И. С. Кружкова, Л. В. Колобухина, О. А. Бургасова, В. А. Гущин

ORIGINAL RESEARCH

22

Gut microbiota alterations and their relationship to the disease severity and some cytokine profile indicators in patients with COVID-19

Gumenyuk LN, Golod MV, Silaeva NV, Sorokina LE, Ilyasov SS, Androschuk NA, Krivosapko OR, Velilyaev AM, Asanova LN

Изменения микробиоты кишечника и их связь с тяжестью заболевания и некоторыми показателями цитокинового профиля у пациентов с COVID-19

Л. Н. Гуменюк, М. В. Голод, Н. В. Силаева, Л. Е. Сорокина, С. С. Ильясов, Н. А. Андрощук, О. Р. Кривошапко, А. М. Велиляев, Л. Н. Асанова

ORIGINAL RESEARCH

30

Meropenem-induced reduction in colistin susceptibility in *Pseudomonas aeruginosa* strain ATCC 27853

Savinova TA, Bocharova YuA, Chaplin AV, Korostin DO, Shamina OV, Mayansky NA, Chebotar IV

Меропенем-индуцированное снижение чувствительности к колистину у *Pseudomonas aeruginosa* ATCC 27853

Т. А. Савинова, Ю. А. Бочарова, А. В. Чаплин, Д. О. Коростин, О. В. Шамина, Н. А. Маянский, И. В. Чеботарь

ORIGINAL RESEARCH

35

Microsatellite instability in colorectal neuroendocrine neoplasms

Meshcheryakova MYu, Kolesnikov EN, Trifanov VS, Timoshkina NN, Snezhko AV, Gvaldin DYu

Микросателлитная нестабильность в нейроэндокринных новообразованиях толстой кишки

М. Ю. Мещерякова, Е. Н. Колесников, В. С. Трифанов, Н. Н. Тимошкина, А. В. Снежко, Д. Ю. Гвалдин

METHOD

41

Sensors for analysis of drugs, drug-drug interactions, and catalytic activity of enzymes

Agafonova LE, Bulko TV, Kuzikov AV, Masamrekh RA, Shumyantseva VV

Сенсоры для анализа лекарственных препаратов, межлекарственных взаимодействий и каталитической активности ферментов

Л. Е. Агафонова, Т. В. Булко, А. В. Кузиков, Р. А. Масамрех, В. В. Шумянцева

ORIGINAL RESEARCH

47

Visual analysis of nigrosome-1 in the differential diagnosis of Parkinson's disease and essential tremor

Moskalenko AN, Filatov AS, Fedotova EYu, Kononov RN, Illarionov SN

Визуальный анализ нигросомы-1 в дифференциальной диагностике болезни Паркинсона и эссенциального тремора

А. Н. Москаленко, А. С. Филатов, Е. Ю. Федотова, Р. Н. Коновалов, С. Н. Илларионов

ORIGINAL RESEARCH

53

Medium-term outcomes of extraarticular corrective osteotomy for slipped capital femoral epiphysis

Egjazaryan KA, Grigoriev AV, Ratiev AP, But-Gusaim AB, Sirotin IV

Среднесрочные результаты внесуставной корригирующей остеотомии бедра при юношеском эпифизеолизе головки бедренной кости

К. А. Егиазарян, А. В. Григорьев, А. П. Ратьев, А. Б. Бут-Гусаим, И. В. Сиротин

ORIGINAL RESEARCH

60

Adherence to treatment in visually impaired individuals

Bikbov MM, Israfilova GZ, Gilmanshin TR, Zainullin RM, Yakupova EM

Приверженность к лечению лиц с нарушением зрения

М. М. Бикбов, Г. З. Исрафилова, Т. Р. Гильманшин, Р. М. Зайнуллин, Э. М. Якупова

MOLECULAR BIOLOGY APPLICATIONS OF THE RED KING CRAB DUPLEX-SPECIFIC NUCLEASE

Shagin DA¹, Rebrikov DV^{1,2} ✉¹ Center for Precision Genome Editing and Genetic Technologies for Biomedicine, Pirogov Russian National Research Medical University, Moscow, Russia² Kulakov National Medical Research Center for Obstetrics, Gynecology and Perinatology, Moscow, Russia

Duplex-specific nuclease (DSN) from hepatopancreas of the craboid *Paralithodes camtschaticus* (red king crab) has a unique combination of properties. Along with thermal stability and a high optimal temperature of catalysis, this enzyme exhibits high substrate selectivity, cleaving only DNA in duplexes (DNA-DNA or DNA-RNA). Accordingly, it digests neither single strands (nor single-stranded regions) of DNA, nor RNA strands with any secondary structure. Such properties make it possible to create unique protocols based on DSN, which is also an important object of fundamental research in the field of nuclease evolution. The review considers diverse applications of the red king crab DSN in modern methods of molecular biology.

Keywords: duplex-specific nuclease, DSN, crab hepatopancreas, *Paralithodes camtschaticus*, red king crab

Funding: the study was supported by the grant no. 075-15-2019-1789, Center for High Precision Genomic Editing and Genetic Technologies for Biomedicine.

Author contribution: DA Shagin — preparation of the manuscript; DV Rebrikov — editing of the manuscript.

✉ **Correspondence should be addressed:** Denis V. Rebrikov
Oparina, 4, Moscow, 117997, Russia; ncagip4@gmail.com

Received: 22.02.2022 **Accepted:** 27.02.2022 **Published online:** 28.02.2022

DOI: 10.24075/brsmu.2022.010

ПРИМЕНЕНИЕ ДУПЛЕКС-СПЕЦИФИЧНОЙ НУКЛЕАЗЫ ИЗ КАМЧАТСКОГО КРАБА В МЕТОДАХ МОЛЕКУЛЯРНОЙ БИОЛОГИИ

Д. А. Шагин¹, Д. В. Ребриков^{1,2} ✉¹ Центр высокоточного редактирования и генетических технологий для биомедицины, Российский национальный исследовательский медицинский университет имени Н. И. Пирогова, Москва, Россия² Национальный медицинский исследовательский центр акушерства, гинекологии и перинатологии имени В. И. Кулакова, Москва, Россия

Дуплекс-специфичная нуклеаза (ДСН) из гепатопанкреаса крабоида *Paralithodes camtschaticus* (камчатский краб) обладает уникальным сочетанием свойств. Наряду с термостабильностью и высокой оптимальной температурой катализа, фермент проявляет высокую субстратную избирательность, расщепляя исключительно ДНК в составе дуплексов (ДНК-ДНК или ДНК-РНК). Соответственно, ни одиночные цепи ДНК, ни одноцепочечные участки ДНК, ни цепи РНК с любой вторичной структурой субстратами ДСН не являются. Такие свойства позволяют создавать уникальные молекулярно-биологические протоколы на основе ДСН, которая также представляет собой важный объект фундаментальных исследований в области эволюции нуклеаз. В обзоре рассматриваются различные применения ДСН из камчатского краба в современных методах молекулярной биологии.

Ключевые слова: дуплекс-специфичная нуклеаза, ДСН, гепатопанкреас краба, *Paralithodes camtschaticus*, камчатский краб

Финансирование: работа выполнена при финансовой поддержке грантом № 075-15-2019-1789, Центр высокоточного редактирования и генетических технологий для биомедицины.

Вклад авторов: Д. А. Шагин — подготовка рукописи; Д. В. Ребриков — редактирование рукописи.

✉ **Для корреспонденции:** Денис Владимирович Ребриков
ул. Академика Опарина, д. 4, г. Москва, 117997, Россия; ncagip4@gmail.com

Статья получена: 22.02.2022 **Статья принята к печати:** 27.02.2022 **Опубликована онлайн:** 28.02.2022

DOI: 10.24075/vrgmu.2022.010

Crab duplex-specific nuclease (DSN) from hepatopancreas of the red king crab was firstly characterized in 2002 [1]. The enzyme with a molecular weight of 41.5 kDa consists of 407 amino acid residues (Genbank AAN86143) and exerts a unique set of functional properties [2, 3]:

DSN exhibits maximum activity at pH 6.6 at 60–65 °C;

DSN remains active after heating at 90°C or incubation at pH within the range of 4–12;

DSN is Mn²⁺, Co²⁺ and Mg²⁺ dependent;

DSN is resistant to proteases (including proteinase K and papain);

DSN cleaves only double-stranded DNA, leaving single strands intact;

DSN shows negligible activity towards RNA of any secondary structure, while effectively cleaving the DNA chain in DNA-RNA hybrids.

The unique properties of DSN, which is also an important object of fundamental research in the field of nuclease evolution [4], inspires creation of molecular protocols on their basis.

This review considers diverse applications of DSN in modern molecular biology.

Single nucleotide polymorphisms (SNP) genotyping

SNP genotyping is used in the diagnosis of genetic predispositions, pharmacogenetics, forensic science, molecular genealogy, population genetics, and other research areas [5–9]. An SNP genotyping protocol known as duplex-specific nuclease preference (DSNP) approach is based on the unique property of DSN to cleave perfect (i.e. fully matched) short double-stranded DNA substrates with much higher efficiency than their imperfect analogs [10].

SNP genotyping by DSNP-analysis requires two specific 10-mer oligonucleotides with a fluorophore at the 5'-end and a quencher at the 3'-end — the so-called FRET-labeled probes (FRET, fluorescence resonance energy transfer). One of the probes corresponds to wild-type allele, the other one corresponds to variant allele. In the case of perfect duplex formed

between the probe and the target DNA, the probe is hydrolyzed by DSN, which results in the fluorophore-quencher uncoupling and emission of fluorescence at a specific wavelength. In the absence of probe hydrolysis, no fluorescence is emitted.

Before DSNP analysis, the studied polymorphic region must be amplified to a high concentration by polymerase chain reaction (PCR) with specific primers. The crude (unpurified) PCR product is mixed with the probes and incubated with DSN at 60°C for 5–10 min. During the incubation, the DNA substrate becomes amplified due to combined activity of DSN and thermostable DNA polymerase; the latter is introduced into the reaction mixture as a component of the crude PCR product used as a template. DSN cleaves double-stranded DNA producing fragments that can serve as primers for DNA polymerase. At the same time, due to the hydrolysis of amplicons, short DNA fragments are formed that are capable of efficient hybridization with the signaling probes. At the final step of the analysis, the reaction mixture is incubated at 30–35°C, which ensures hybridization of the probes with the target DNA and the emission of fluorescence due to DSN activity.

The optimal length of PCR products for DSNP-analysis was tested empirically: fragments of various lengths containing C- or T-variants of the human mitochondrial *COX1* C7028T were hybridized with a T-specific probe. Clear and unambiguous results were obtained for all tested products, proving the possibility of using DSNP analysis for a wide range of amplicon lengths.

Diverse approaches for SNP genotyping have been proposed, based on the difference in physicochemical properties of the variants [11, 12]. With regard to other published protocols, DSNP has several advantages, starting from its overall convenience (the use of crude PCR product, no cleanups/centrifugations, 5 min hands-on and results within 1 hour). Secondly, the protocol allows analysis of both alleles simultaneously in one tube. Thirdly, the specific fluorescence can be recorded using standard laboratory equipment. Finally, the protocol is applicable for virtually any length of the PCR product harboring the polymorphic position.

The study of multiple allelic variants in one tube implies the use of probes with fluorophores that emit at different wavelengths. Effects of different fluorophores on the efficiency of hydrolysis were negligible, unless the mismatches were positioned at the termini. The efficiency of hydrolysis for imperfect duplexes containing an unpaired nucleotide in the midportion did not depend on the type of fluorophores. Importantly, when using probes for different alleles labeled with identical fluorophores, the analysis must be carried out in separate tubes.

DSNP was successfully applied for genotyping of variants involved in a number of diseases or predispositions, including *TP53* C309T; *F2* G20210A, *MTHFR* C677T; *KRAS* G34A, G35T, G35A, and G38A; *NRAS* G34A, G35C, and G35A; *HRAS* G35T; *APOE* C388T; F5 G1698A; and *BRCA1* 5382insC. Allelic status of the studied samples was confirmed by Sanger sequencing.

The results of model experiments showed that DSNP allows reliable differentiation between mutant and wild-type alleles in both homozygous and heterozygous samples. In addition, the example of *BRCA1* 5382insC demonstrates that, apart from point substitutions, the method is also applicable to single-nucleotide indels. The suitability of the same standard reaction conditions for different genomic positions indicates the universality of the approach.

Clustered occurrence of point mutations in certain genomic regions is well described [13]. The majority of available PCR systems cannot afford accurate determination of such closely located mutations by routine genotyping. On an example of *KRAS*, with a mutagenesis hotspot at positions 34 and 35

(G34A, G35A, and G35T [14]), it has been demonstrated that DSNP analysis is suitable for genotyping of closely-spaced point mutations even in multiplex. Simultaneous use of up to four FRET-probes, inclusive, produced specific signal only when the probe was fully complementary to the target.

Occasionally, it may be important not only to detect a variant, but also to measure the allelic ratio for a sample. Such tasks may be relevant for tumor tissue samples or pooled genomic DNA samples from multiple donors [12, 15]. Experiments with *KRAS* G35A as a model proved the possibility of using DSNP for semi-quantitative determination of mutant alleles in complex samples.

Thus, the natural properties of DSN have qualified this enzyme as a basis for a genotyping protocol termed DSNP, fairly simple and automatable. Most prominent advantages of this protocol include

- 1) the use of crude PCR products with arbitrary fragment lengths;
- 2) no purification/separation required;
- 3) rapidity (1 hour, starting from PCR products);
- 4) the allelic ratio assessment option;
- 5) universal applicability: the method is suitable for determination of single-nucleotide substitutions and indels, at clustered positions or not, regardless of the context.

The protocol requires no special equipment apart from that ubiquitously found in the labs. Even fluorescence signals can be assessed with the use of ordinary instruments: for instance, with fluorescein, the signal can be recorded with a conventional UV lamp used in gel-doc systems.

DSNP disadvantages compared with real-time PCR include

- 1) preparative PCR amplification of the target fragment;
- 2) endpoint detection;
- 3) risk of contamination associated with the need to open tubes with amplicons.

cDNA normalization

Heterogeneous gene expression levels in a cell complicate the full-scale analysis of transcriptomes and gene hunting. Normalization of cDNA libraries prior to analysis allows to increase the sensitivity towards rare transcripts.

The classical principle of cDNA normalization involves hybridization kinetics. As hybridization rate is proportional to the squared concentration of molecules in a sample, high-copy fragments renature faster than low-copy fragments [16]. Separation of reassociated double-stranded fragments after denaturation of a complex cDNA sample affords a library with equalized concentrations of abundant and rare transcripts [17–19].

The existing normalization protocols differ by the means of separation of the normalized single-stranded (ss) and double-stranded (ds) fractions. The possibilities include physical separation of fractions using hydroxyapatite chromatography [17, 20] or paramagnetic beads [19, 21], dsDNA digestion with restriction endonucleases [18], and selective amplification of ssDNA using the PCR suppression effect [22]. Unfortunately, these possibilities are hardly adaptable for normalization of cDNA samples enriched with full-length sequences.

The unique properties of DSN enabled a highly efficient and easy-to-perform method, known as DSN-normalization and now a routine at many laboratories in Russia and across the world, universally applicable for normalization of both fragmented and full-length cDNA. Like most its predecessors and counterparts, this method is based on the kinetics of cDNA reassociation, but differs in the way the normalized ssDNA fraction is separated [23].

Table. Representation of repetitive elements in human genomic DNA before and after DSN normalization

Families of repetitive sequences	Control DNA sample (no normalization)			Normalized DNA sample		
	b.p.	%	Mean sequence divergence, %	b.p.	%	Mean sequence divergence, %
Total length	6 643 277	100	–	6 269 460	100	–
LINE L1P	371 253	5.6	9	69 670	1.1	15
ERV-K	20 597	0.3	8	6 575	0.1	12
SSR	68 367	1	10	18 499	0.3	11
Alu	631 112	9.5	12	6 572	0.1	16
Satellite sequences	293 827	4.4	15	7 915	0.1	20
ERV1	165 461	2.5	15	105 155	1.7	17
ERV-L	323 437	4.9	19	245 039	3.9	22
LINE L1M/HAL	496 398	7.5	19	605 965	9.7	21
DNA transposons	161 304	2.4	19	170 331	2.7	21
MIR	118 927	1.8	27	142 060	2.3	27
LINE L2	104 535	1.6	28	147 241	2.3	28
LINE CR1/L3	10 226	0.1	29	13 318	0.2	29
LINE L4-L5	3 508	0.05	33	3 701	0.05	30

After hybridization, the reaction mixture is treated with DSN to remove the non-target fraction of dsDNA. Since DSN is a thermostable enzyme active at 70 °C, the hydrolysis occurs at the same temperature as hybridization. The high temperature affords minimization of non-specific binding and thereby prevents the loss of transcripts prone to formation of secondary structures. The normalized ss cDNA fraction is amplified by PCR.

The method is also applicable to non-amplified first strand cDNA. Abundant transcripts ('majors') are sponged through renaturation of the first strand cDNA with the poly(A)+ RNA that has served as a template for its synthesis. This protocol is applicable with large amounts of biomaterial available so that it is possible to isolate the poly(A)+ RNA fraction from total RNA. It should be noted that in the normalized libraries, the content of clones corresponding to certain highly represented transcripts is sometimes lower than the number of clones corresponding to rare transcripts. Such "supernormalization" can be explained by the continued dominance of major RNA species, which serve as guides for elimination of complementary DNA molecules. Upon the release after DSN-mediated hydrolysis of the complementary DNA strand, major RNAs can form new hybrids with single-stranded DNA molecules, thus promoting their hydrolysis, and so on.

For the subsequent use in a variety of applications, the normalized first strand cDNA must be amplified. For this reason, preparation of first strand cDNA for DSN normalization necessarily involves ligation of adapter sequences, which will provide annealing sites for oligonucleotide PCR primers. As is well-known, in PCR, short fragments are amplified more efficiently than longer fragments. Accordingly, amplification of complex normalized cDNA is fraught with the loss of long transcripts and decreased average length of the library. To preserve the fraction of long cDNA molecules during library preparation, short inverted repeats are included in the design of the adapters. PCR amplification with a primer matching the inverted repeat (albeit shorter) favors amplification of long cDNA molecules against the background of suppressed amplification of short molecules [24]. According to experimental data, normalization of amplified cDNA, although generally less efficient than the first strand cDNA normalization, also provides significant leveling of over-represented transcripts to enable the search for rare mRNA species under circumstances when only total RNA is available.

To date, DSN normalization provides both the simplest and most effective means for cDNA normalization. By contrast with many other protocols, it involves no physical separation of DNA fractions. Furthermore, it can be used to normalize both amplified cDNA and the non-amplified first strand of cDNA enriched with full-length molecules. In addition, DSN-normalization preserves the average lengths as well as the length distributions of cloned cDNA libraries.

Specific enrichment and normalization of genomic DNA libraries

Song et al. (2016) developed a protocol for enrichment with minor alleles (including those with mutations of clinical or biological significance) through selective elimination of wild-type alleles in mixed (pooled) clinical samples, termed Nuclease-Assisted Minor-Allele enrichment using Overlapping Probes, NaME-PrO [25]. The simultaneous removal of the excess of wild-type DNA for a virtually unlimited number of target genomic sequences is performed before amplification. The unique properties of DNS ensure priority cleavage of wild-type DNA regardless of genomic context

For each target sequence, a pair of oligonucleotide probes is designed to bind the target region on opposite strands, with a 10–15 bp overlap between them. The probes are added in excess to the fragmented genomic DNA denatured at 98 °C. When the temperature is lowered to 67 °C, DNA remains single-stranded due to its low concentration and slow reassociation kinetics. The probes anneal to their target sites in DNA, whereby they create pinpoint mismatches on complementary strands upon their contact with mutated DNA, resulting in imperfect duplexes. Upon exposure to DSN, which preferentially cleaves perfect duplexes, the wild-type DNA is cleaved whereas mutant DNA remains substantively intact. Because the two probes match the target sequence on opposite strands, both strands of wild-type DNA undergo preferential cleavage within the region covered by the probes. Thus, if at least one of the DNA strands containing the mutation is preserved after DSN cleavage, then subsequent DNA amplification will lead to exponential amplification providing the multiplex enrichment for all mutated sites simultaneously. This approach abolishes the need for deep sequencing to detect rare mutations.

As demonstrated by the authors, NaME-PrO affords 50 to 200-fold enrichment for a variety of target mutations found in clinical samples (exemplified by KRAS mutations).

In connection with the rapid technological progress, next generation sequencing (NGS), in particular whole-genome sequencing, is becoming an increasingly common approach in basic science and clinical laboratory diagnostics. In eukaryotes, a significant proportion of genomic DNA consists of highly homologous repetitive elements. Their presence not only increases the cost of genome sequencing, but also makes the bioinformatics processing and interpretation of the data extremely difficult.

The problem can be solved by several approaches. In particular, for higher plant genomes, it is possible to employ the pronounced tendency of repetitive sequences to hypermethylation. Yuan et al. (2002) used selective cleavage of hypermethylated regions with restriction endonucleases sensitive to cytosine 5'-methylation [26, 27]. Similarly, Palmer et al. (2003) used the methylation-dependent endonuclease McrBC from the *E. coli* K-12 strain in the construction of maize genomic libraries, thereby limiting the cloning of heavily methylated DNA [28]. Such technical solutions, however, are not applicable to organisms with other methylation patterns that are not selective for repetitive elements.

An alternative solution to the problem, the so-called C0t filtration, is based on the kinetics of DNA renaturation. Genomic DNA is fragmented, heat denatured and cooled. Since low-copy DNA fragments rehybridize slower than repetitive elements, over a certain time the single-stranded fraction becomes enriched with low-copy sequences [29, 30]. Next, the double-stranded fraction containing repetitive elements is separated from the single-stranded fraction (in the classic version, by hydroxyapatite chromatography). Although C0t filtration may work with any complex mixture of heterogeneously represented DNA sequences, its application requires precise knowledge of the reassociation kinetics for a particular genome.

Shagina et al. (2010) investigated the possibility of using DSN normalization to eliminate the highly homologous repetitive elements from genomic sequencing libraries. DNA is subjected to fragmentation, supplemented with adapter sequences through ligation, and denatured by heating. During the renaturation process, the sample is treated with DSN. The preserved single-stranded fraction of genomic DNA enriched in low-copy sequences is amplified with primers corresponding to the adapter sequences [31].

The method was tested in a model experiment on normalization of human genomic DNA before sequencing in a 454 GS FLX system (Roche). To enhance the sponging of non-target sequences, hybridization was carried out in an excess of the Cot-1 fraction of human genomic DNA. For the normalized and control samples, 29,240 and 31,789 reads were obtained with a total coverage of 6,269,460 and 6,643,277 nucleotides, respectively. Representation of diverse repetitive elements in the sequencing data was determined using the Repeat-Masker software available at repeatmasker.org/cgi-bin/WEBRepeatMasker. According to the results, normalization reduced the content of repetitive elements from 40% to 25%.

The Table shows representation of different families of repetitive elements in non-normalized (control) and normalized samples of human genomic DNA. Significant effects can be observed for Alu, LINE L1P, ERV-K, and ERV1 repeats, as well as satellite sequences. At the same time, certain families of repetitive elements show resistance to normalization by this method.

Reciprocally, control samples (no normalization) contained about 10% of sequences sharing 100–91% similarity and about

20% of sequences sharing 90–71% similarity, whereas the remaining 70% of sequences had identical nucleotides in less than 71% positions. DSN normalization reproducibly reduced the content of low-divergent repetitive elements (100–91% identical) 15-fold and medium-divergent repetitive elements (81–90% identical) 2-fold. Concentrations of other sequences in the samples did not decrease with DSN-normalization. Preservation of single-copy genomic sequences during DSN normalization was demonstrated by real-time PCR assay on a panel of 11 unique genes.

These findings indicate that DSN normalization can effectively reduce the content of the evolutionary young low-divergent repetitive sequences in genomic DNA samples. The cut-off threshold can be lowered by using milder reassociation conditions (e.g. by lowering the temperature and/or increasing the cation concentration), albeit with the risk of partial loss of unique sequences due to increased non-specific interactions.

MicroRNA studies

MicroRNA molecules are increasingly considered as promising biomarkers for diagnosis and monitoring of various pathologies, including cancers and autoimmune disorders. They are found in the blood plasma both in a freely circulating form and as part of the exosomal fraction. MicroRNAs are easy to isolate, resistant to degradation, and show reproducible and characteristic expression patterns.

The unique properties of DSN, particularly its indifference to RNA substrates, can be used to create specific chemiluminescent and fluorescent sensors for miRNA [32, 33]. A system developed by Shen et al. (2015) contains biotinylated DNA molecules (probes) labeled with fluorescein and immobilized on magnetic beads. Apart from the target microRNA and the beads, the medium contains DSN, which recognizes and cleaves the duplexes formed upon binding of microRNA with the probe. After the cleavage, the labeled outer fragment of the probe drifts into the medium, while its microRNA partner finds and binds the next immobilized DNA molecule, promotes its cleavage, and so on. The fluorescently labeled cleavage products eventually accumulate in the medium. In the end, the beads with immobilized unreacted probes are separated from the reaction medium with a magnet. The labeled cleavage products remain in the medium for the endpoint detection of fluorescence. The system is sensitive enough to detect femtomolar microRNA concentrations. Noteworthy, in contrast to protocols that use quantitative PCR, amplification of the signal is carried out isothermally at 40 °C, which makes the proposed method even more attractive [33].

CONCLUSION

Duplex-specific nuclease from hepatopancreas of the king crab exerts a unique combination of properties including the exquisite substrate specificity (selectively digests double-stranded DNA without affecting single-stranded DNA or RNA), the high optimal temperature of catalysis (60–65 °C), and the thermal stability (retains activity at 90 °C). Since its original characterization in 2002, the crab nuclease has been featured in diverse molecular protocols, which still evolve and are continually updated. The enzyme has been successfully used in a wide range of applications, including genotyping of single nucleotide polymorphisms (in both experimental and clinical samples), normalization of cDNA and genomic DNA libraries, selective elimination of non-target sequences, and miRNA studies.

References

- Shagin DA, Rebrikov DV, Kozhemyako VB, Altshuler IM, Shcheglov AS, Zhulidov PA, Bogdanova EA, Staroverov DB, Rasskazov VA, Lukyanov S. A novel method for SNP detection using a new duplex-specific nuclease from crab hepatopancreas. *Genome Res.* 2002; 12 (12): 1935–42. DOI: 10.1101/gr.547002.
- Anisimova VE, Rebrikov DV, Shagin DA, Kozhemyako VB, Menzorova NI, Staroverov DB, Ziganshin R, Vagner LL, Rasskazov VA, Lukyanov SA, Shcheglov AS. Isolation, characterization and molecular cloning of duplex-specific nuclease from the hepatopancreas of the Kamchatka crab. *BMC Biochem.* 2008; 9: 14. DOI: 10.1186/1471-2091-9-14.
- Anisimova VE, Rebrikov DV, Zhulidov PA, Staroverov DB, Lukyanov SA, Shcheglov AS. Renaturation, activation, and practical use of recombinant duplex-specific nuclease from Kamchatka crab. *Biochemistry (Mosc).* 2006; 71: 513–9. DOI: 10.1134/s0006297906050075.
- Anisimova VE, Shcheglov AS, Bogdanova EA, Rebrikov DV, Nekrasov AN, Barsova EV, Shagin DA, Lukyanov SA. Is crab duplex-specific nuclease a member of the Serratia family of non-specific nucleases? *Gene.* 2008; 418: 41–8. DOI: 10.1016/j.gene.2008.04.005.
- Vodolazhsky DI, Mayakovskaya AV, Kubyshkin AV, Aliev KA, Fomochkina II. Clinical significance of gene polymorphisms for hereditary predisposition to breast and ovarian cancer (review of literature). *Klin Lab Diagn.* 2021; 66 (12): 760–67. English. DOI: 10.51620/0869-2084-2021-66-12-760-767.
- Yan M, Fan X, Si H, Wang X, Wang Z, Wang Z, Lv X, Yin H, Jia Y, Jiang L, Xia Y, Liu Y. Association between gene polymorphism and adverse effects in cancer patients receiving docetaxel treatment: a meta-analysis. *Cancer Chemother Pharmacol.* 2022; 89 (2): 173–181. DOI: 10.1007/s00280-021-04374-3.
- Haddrill PR. Developments in forensic DNA analysis. *Emerg Top Life Sci.* 2021; 5 (3): 381–393. DOI: 10.1042/ETLS20200304.
- Kling D, Phillips C, Kennett D, Tillmar A. Investigative genetic genealogy: Current methods, knowledge and practice. *Forensic Sci Int Genet.* 2021; 52: 102474. DOI: 10.1016/j.fsigen.2021.102474.
- Borinskaya SA, Gureev AS, Orlova AA, Sanina ED, Kim AA, Gasemianrodsari F, Shirmanov VI, Balanovsky OP, Rebrikov DV, Koshechkin AV, Yankovsky NK. [Allele frequency distributions of -174G/C polymorphism in regulatory region of interleukin 6 gene (IL6) in Russian and worldwide populations]. *Genetika.* 2013; 49 (1): 113–24. Russian. DOI: 10.7868/s0016675813010037.
- Altshuler IM, Zhulidov PA, Bogdanova EA, Mudrik NN, Shagin DA. [Application of the duplex-specific nuclease preference method to the analysis of point mutations in human genes]. *Bioorg Khim.* 2005; 31 (6): 627–36. Russian.
- Syvänen AC. Accessing genetic variation: genotyping single nucleotide polymorphisms. *Nat Rev Genet.* 2001; 2 (12): 930–42. DOI: 10.1038/35103535.
- Syvänen AC, Taylor GR. Approaches for analyzing human mutations and nucleotide sequence variation: a report from the Seventh International Mutation Detection meeting, 2003. *Hum Mutat.* 2004; 23 (5): 401–5. DOI: 10.1002/humu.20031.
- Stewart CA, Horton R, Allcock RJ, Ashurst JL, Atrazhev AM, Coggill P, Dunham I, Forbes S, Halls K, Howson JM, Humphray SJ, Hunt S, Mungall AJ, Osoegawa K, Palmer S, Roberts AN, Rogers J, Sims S, Wang Y, Wilming LG, Elliott JF, de Jong PJ, Sawcer S, Todd JA, Trowsdale J, Beck S. Complete MHC haplotype sequencing for common disease gene mapping. *Genome Res.* 2004; 14 (6): 1176–87. DOI: 10.1101/gr.2188104.
- Mu DQ, Peng YS, Xu QJ. Values of mutations of K-ras oncogene at codon 12 in detection of pancreatic cancer: 15-year experience. *World J Gastroenterol.* 2004; 10 (4): 471–5. DOI: 10.3748/wjg.v10.i4.471.
- Itabashi T, Maesawa C, Uchiyama M, Higuchi T, Masuda T. Quantitative detection of mutant alleles of the K-ras gene with minor groove binder-conjugated fluorogenic DNA probes. *Int J Oncol.* 2004; 24 (3): 687–96.
- Young BD, Anderson MLM. Quantitative analysis of solution hybridisation. In: Hames BD, Higgins SJ, eds. *Nucleic acid hybridisation: a practical approach.* Pp. 47–71. Oxford: IRL Press Limited, 1985.
- Ko MS. An 'equalized cDNA library' by the reassociation of short double-stranded cDNAs. *Nucleic Acids Res.* 1990; 18 (19): 5705–11. DOI: 10.1093/nar/18.19.5705.
- Coche T, Dewez M. Reducing bias in cDNA sequence representation by molecular selection. *Nucleic Acids Res.* 1994 Oct 25; 22 (21): 4545–6. DOI: 10.1093/nar/22.21.4545.
- Carninci P, Shibata Y, Hayatsu N, Sugahara Y, Shibata K, Itoh M, Konno H, Okazaki Y, Muramatsu M, Hayashizaki Y. Normalization and subtraction of cap-trapper-selected cDNAs to prepare full-length cDNA libraries for rapid discovery of new genes. *Genome Res.* 2000; 10 (10): 1617–30. DOI: 10.1101/gr.145100.
- Soares MB, Bonaldo MF, Jelene P, Su L, Lawton L, Efstratiadis A. Construction and characterization of a normalized cDNA library. *Proc Natl Acad Sci U S A.* 1994; 91 (20): 9228–32. DOI: 10.1073/pnas.91.20.9228.
- Sasaki YF, Ayusawa D, Oishi M. Construction of a normalized cDNA library by introduction of a semi-solid mRNA-cDNA hybridization system. *Nucleic Acids Res.* 1994; 22 (6): 987–92. DOI: 10.1093/nar/22.6.987.
- Luk'ianov KA, Gurskaia NG, Matts MV, Khaspekov GL, D'iachenko LB, Chenchik AA, Il'evich-Stuchkov SG, Luk'ianov SA. Metod poluchenii normalizovannykh bibliotek kDNK, osnovannyi na éffekte supressii polimeraznoi tsepnoi reaktcii [A method for obtaining the normalized cDNA libraries based on the effect of suppression of polymerase chain reaction]. *Bioorg Khim.* 1996; 22 (9): 686–90. Russian.
- Zhulidov PA, Bogdanova EA, Shcheglov AS, Vagner LL, Khaspekov GL, Kozhemyako VB, Matz MV, Meleshkevitch E, Moroz LL, Lukyanov SA, Shagin DA. Simple cDNA normalization using kamchatka crab duplex-specific nuclease. *Nucleic Acids Res.* 2004; 32 (3): e37. DOI: 10.1093/nar/gnh031.
- Shagin DA, Lukyanov KA, Vagner LL, Matz MV. Regulation of average length of complex PCR product. *Nucleic Acids Res.* 1999; 27 (18): e23. DOI: 10.1093/nar/27.18.e23.
- Song C, Liu Y, Fontana R, Makrigiorgos A, Mamon H, Kulke MH, Makrigiorgos GM. Elimination of unaltered DNA in mixed clinical samples via nuclease-assisted minor-allele enrichment. *Nucleic Acids Res.* 2016; 44 (19): e146. DOI: 10.1093/nar/gkw650.
- Yuan Y, SanMiguel PJ, Bennetzen JL. Methylation-spanning linker libraries link gene-rich regions and identify epigenetic boundaries in Zea mays. *Genome Res.* 2002; 12 (9): 1345–9. DOI: 10.1101/gr.185902.
- Emberton J, Ma J, Yuan Y, SanMiguel P, Bennetzen JL. Gene enrichment in maize with hypomethylated partial restriction (HMPCR) libraries. *Genome Res.* 2005; 15 (10): 1441–6. DOI: 10.1101/gr.3362105.
- Palmer LE, Rabinowicz PD, O'Shaughnessy AL, Balija VS, Nascimento LU, Dike S, de la Bastide M, Martienssen RA, McCombie WR. Maize genome sequencing by methylation filtration. *Science.* 2003; 302 (5653): 2115–7. DOI: 10.1126/science.1091265.
- Peterson DG, Schulze SR, Sciara EB, Lee SA, Bowers JE, Nagel A, Jiang N, Tibbitts DC, Wessler SR, Paterson AH. Integration of Cot analysis, DNA cloning, and high-throughput sequencing facilitates genome characterization and gene discovery. *Genome Res.* 2002; 12 (5): 795–807. DOI: 10.1101/gr.226102.
- Yuan Y, SanMiguel PJ, Bennetzen JL. High-Cot sequence analysis of the maize genome. *Plant J.* 2003; 34 (2): 249–55. DOI: 10.1046/j.1365-313x.2003.01716.x.
- Shagina I, Bogdanova E, Mamedov IZ, Lebedev Y, Lukyanov S, Shagin D. Normalization of genomic DNA using duplex-specific nuclease. *Biotechniques.* 2010; 48 (6): 455–9. DOI: 10.2144/000113422.
- Deng H, Ren Y, Shen W, Gao Z. An ultrasensitive homogeneous chemiluminescent assay for microRNAs. *Chem Commun (Camb).* 2013; 49 (82): 9401–3. DOI: 10.1039/c3cc44824j.
- Shen W, Yeo KH, Gao Z. A simple and highly sensitive fluorescence assay for microRNAs. *Analyst.* 2015; 140 (6): 1932–8. DOI: 10.1039/c4an02146k.

Литература

- Shagin DA, Rebrikov DV, Kozhemyako VB, Altshuler IM, Shcheglov AS, Zhulidov PA, Bogdanova EA, Staroverov DB, Rasskazov VA, Lukyanov S. A novel method for SNP detection using a new duplex-specific nuclease from crab hepatopancreas. *Genome Res.* 2002; 12 (12): 1935–42. DOI: 10.1101/gr.547002.
- Anisimova VE, Rebrikov DV, Shagin DA, Kozhemyako VB, Menzorova NI, Staroverov DB, Ziganshin R, Vagner LL, Rasskazov VA, Lukyanov SA, Shcheglov AS. Isolation, characterization and molecular cloning of duplex-specific nuclease from the hepatopancreas of the Kamchatka crab. *BMC Biochem.* 2008; 9: 14. DOI: 10.1186/1471-2091-9-14.
- Anisimova VE, Rebrikov DV, Zhulidov PA, Staroverov DB, Lukyanov SA, Shcheglov AS. Renaturation, activation, and practical use of recombinant duplex-specific nuclease from Kamchatka crab. *Biochemistry (Mosc).* 2006; 71: 513–9. DOI: 10.1134/s0006297906050075.
- Anisimova VE, Shcheglov AS, Bogdanova EA, Rebrikov DV, Nekrasov AN, Barsova EV, Shagin DA, Lukyanov SA. Is crab duplex-specific nuclease a member of the Serratia family of non-specific nucleases? *Gene.* 2008; 418: 41–8. DOI: 10.1016/j.gene.2008.04.005.
- Vodolazhsky DI, Mayakovskaya AV, Kubyshkin AV, Aliev KA, Fomochkina II. Clinical significance of gene polymorphisms for hereditary predisposition to breast and ovarian cancer (review of literature). *Klin Lab Diagn.* 2021; 66 (12): 760–67. English. DOI: 10.51620/0869-2084-2021-66-12-760-767.
- Yan M, Fan X, Si H, Wang X, Wang Z, Wang Z, Lv X, Yin H, Jia Y, Jiang L, Xia Y, Liu Y. Association between gene polymorphism and adverse effects in cancer patients receiving docetaxel treatment: a meta-analysis. *Cancer Chemother Pharmacol.* 2022; 89 (2): 173–181. DOI: 10.1007/s00280-021-04374-3.
- Haddrill PR. Developments in forensic DNA analysis. *Emerg Top Life Sci.* 2021; 5 (3): 381–393. DOI: 10.1042/ETLS20200304.
- Kling D, Phillips C, Kennett D, Tillmar A. Investigative genetic genealogy: Current methods, knowledge and practice. *Forensic Sci Int Genet.* 2021; 52: 102474. DOI: 10.1016/j.fsigen.2021.102474.
- Боринская С. А., Гурьев А. С., Орлова А. А., Санина Е. Д., Ким А. А., Гасемианродсари Ф., Ширманов В. И., Балановский О. П., Ребриков Д. В., Кошечкин А. В., Янковский Н. К. Распределение частот аллелей по полиморфизму -174G/C регуляторного участка гена интерлейкина 6 (IL6) в населении России и мира. *Генетика.* 2013; 49 (1): 113–24. DOI: 10.7868/s0016675813010037.
- Альшулер И. М., Жулидов П. А., Богданова Е. А., Мудрик Н. Н., Шагин Д. А. Использование метода DSNP для изучения точечных мутаций генов человека. *Биоорганическая химия.* 2005; 31 (6): 627–36.
- Syvänen AC. Accessing genetic variation: genotyping single nucleotide polymorphisms. *Nat Rev Genet.* 2001; 2 (12): 930–42. DOI: 10.1038/35103535.
- Syvänen AC, Taylor GR. Approaches for analyzing human mutations and nucleotide sequence variation: a report from the Seventh International Mutation Detection meeting, 2003. *Hum Mutat.* 2004; 23 (5): 401–5. DOI: 10.1002/humu.20031.
- Stewart CA, Horton R, Allcock RJ, Ashurst JL, Atrazhev AM, Coggill P, Dunham I, Forbes S, Halls K, Howson JM, Humphray SJ, Hunt S, Mungall AJ, Osogawa K, Palmer S, Roberts AN, Rogers J, Sims S, Wang Y, Wilming LG, Elliott JF, de Jong PJ, Sawcer S, Todd JA, Trowsdale J, Beck S. Complete MHC haplotype sequencing for common disease gene mapping. *Genome Res.* 2004; 14 (6): 1176–87. DOI: 10.1101/gr.2188104.
- Mu DQ, Peng YS, Xu QJ. Values of mutations of K-ras oncogene at codon 12 in detection of pancreatic cancer: 15-year experience. *World J Gastroenterol.* 2004; 10 (4): 471–5. DOI: 10.3748/wjg.v10.i4.471.
- Itabashi T, Maesawa C, Uchiyama M, Higuchi T, Masuda T. Quantitative detection of mutant alleles of the K-ras gene with minor groove binder-conjugated fluorogenic DNA probes. *Int J Oncol.* 2004; 24 (3): 687–96.
- Young BD, Anderson MLM. Quantitative analysis of solution hybridisation. In: Hames BD, Higgins SJ, eds. *Nucleic acid hybridisation: a practical approach.* Pp. 47–71. Oxford: IRL Press Limited, 1985.
- Ko MS. An 'equalized cDNA library' by the reassociation of short double-stranded cDNAs. *Nucleic Acids Res.* 1990; 18 (19): 5705–11. DOI: 10.1093/nar/18.19.5705.
- Coche T, Dewez M. Reducing bias in cDNA sequence representation by molecular selection. *Nucleic Acids Res.* 1994 Oct 25; 22 (21): 4545–6. DOI: 10.1093/nar/22.21.4545.
- Carninci P, Shibata Y, Hayatsu N, Sugahara Y, Shibata K, Itoh M, Konno H, Okazaki Y, Muramatsu M, Hayashizaki Y. Normalization and subtraction of cap-trapper-selected cDNAs to prepare full-length cDNA libraries for rapid discovery of new genes. *Genome Res.* 2000; 10 (10): 1617–30. DOI: 10.1101/gr.145100.
- Soares MB, Bonaldo MF, Jelene P, Su L, Lawton L, Efstratiadis A. Construction and characterization of a normalized cDNA library. *Proc Natl Acad Sci U S A.* 1994; 91 (20): 9228–32. DOI: 10.1073/pnas.91.20.9228.
- Sasaki YF, Ayusawa D, Oishi M. Construction of a normalized cDNA library by introduction of a semi-solid mRNA-cDNA hybridization system. *Nucleic Acids Res.* 1994; 22 (6): 987–92. DOI: 10.1093/nar/22.6.987.
- Лукьянов К. А., Гурская Н. Г., Матц М. В., Хаспеков Г. Л., Дьяченко Л. Б., Ченчик А. А., Ильевич-Стучков С. Г., Лукьянов С. А. Метод получения нормализованных библиотек кДНК, основанный на эффекте супрессии полимеразной цепной реакции. *Биоорганическая химия.* 1996; 22 (9): 686–90.
- Zhulidov PA, Bogdanova EA, Shcheglov AS, Vagner LL, Khaspekov GL, Kozhemyako VB, Matz MV, Meleshkevitch E, Moroz LL, Lukyanov SA, Shagin DA. Simple cDNA normalization using kamchatka crab duplex-specific nuclease. *Nucleic Acids Res.* 2004; 32 (3): e37. DOI: 10.1093/nar/gnh031.
- Shagin DA, Lukyanov KA, Vagner LL, Matz MV. Regulation of average length of complex PCR product. *Nucleic Acids Res.* 1999; 27 (18): e23. DOI: 10.1093/nar/27.18.e23.
- Song C, Liu Y, Fontana R, Makrigiorgos A, Mamon H, Kulke MH, Makrigiorgos GM. Elimination of unaltered DNA in mixed clinical samples via nuclease-assisted minor-allele enrichment. *Nucleic Acids Res.* 2016; 44 (19): e146. DOI: 10.1093/nar/gkw650.
- Yuan Y, SanMiguel PJ, Bennetzen JL. Methylation-spanning linker libraries link gene-rich regions and identify epigenetic boundaries in *Zea mays*. *Genome Res.* 2002; 12 (9): 1345–9. DOI: 10.1101/gr.185902.
- Emberton J, Ma J, Yuan Y, SanMiguel P, Bennetzen JL. Gene enrichment in maize with hypomethylated partial restriction (HMPCR) libraries. *Genome Res.* 2005; 15 (10): 1441–6. DOI: 10.1101/gr.3362105.
- Palmer LE, Rabinowicz PD, O'Shaughnessy AL, Balija VS, Nascimento LU, Dike S, de la Bastide M, Martienssen RA, McCombie WR. Maize genome sequencing by methylation filtration. *Science.* 2003; 302 (5653): 2115–7. DOI: 10.1126/science.1091265.
- Peterson DG, Schulze SR, Sciara EB, Lee SA, Bowers JE, Nagel A, Jiang N, Tibbitts DC, Wessler SR, Paterson AH. Integration of Cot analysis, DNA cloning, and high-throughput sequencing facilitates genome characterization and gene discovery. *Genome Res.* 2002; 12 (5): 795–807. DOI: 10.1101/gr.226102.
- Yuan Y, SanMiguel PJ, Bennetzen JL. High-Cot sequence analysis of the maize genome. *Plant J.* 2003; 34 (2): 249–55. DOI: 10.1046/j.1365-3113x.2003.01716.x.
- Shagina I, Bogdanova E, Mamedov IZ, Lebedev Y, Lukyanov S, Shagin D. Normalization of genomic DNA using duplex-specific nuclease. *Biotechniques.* 2010; 48 (6): 455–9. DOI: 10.2144/000113422.
- Deng H, Ren Y, Shen W, Gao Z. An ultrasensitive homogeneous chemiluminescent assay for microRNAs. *Chem Commun (Camb).* 2013; 49 (82): 9401–3. DOI: 10.1039/c3cc44824j.
- Shen W, Yeo KH, Gao Z. A simple and highly sensitive fluorescence assay for microRNAs. *Analyst.* 2015; 140 (6): 1932–8. DOI: 10.1039/c4an02146k.

DYNAMIC CHANGES IN THE CONCENTRATION OF ANTI-SARS-COV-2 ANTIBODIES WITHIN 12 MONTHS AFTER RECOVERY FROM COVID-19

Mayanskiy NA¹✉, Brzhozovskaya EA¹, Stoyanova SS¹, Frolkov AV¹, Lebedin YuS²

¹ Pirogov Russian National Research Medical University, Moscow, Russia

² XEMA LLC, Moscow, Russia

Generation and maintenance of immunity to SARS-CoV-2 is essential for overcoming the pandemic of the novel coronavirus infection COVID-19. The study was aimed to assess the dynamic changes in the levels of IgG antibodies against the SARS-CoV-2 receptor-binding domain (RBD) with the use of the enzyme-linked immunosorbent assay (ELISA) kits, calibrated using the International Standard for anti-SARS-CoV-2 immunoglobulin (IS-SARS-CoV-2). The concentrations of anti-RBD-IgG were measured in the cohort of individuals, who had recovered from COVID-19, with an interval of a month for 6 months, and at a time point of 12 months, using the ELISA kits, calibrated with the use of IS-SARS-CoV-2; the results were expressed in binding antibody units (BAU) per 1 mL. A total of 97 blood serum samples, obtained from 20 individuals with SARS-CoV-2 infection, confirmed by PCR, were collected. The geometric mean titer (GMT) of anti-RBD-IgG was 433 BAU/mL (range 36-25,900 BAU/mL) within a month after the infection. The concentration of anti-RBD-IgG gradually decreased with time and reached the GMT value of 68 BAU/mL by the 12th month; anti-RBD-IgG persisted in 13 individuals (93%) out of 14, examined 12 months after the infection. The standardized quantitative serological data play a vital part in monitoring the immune response and make it easier to compare the studies, providing the basis for seeking the common serological correlate of the protective immunity to SARS-CoV-2.

Keywords: SARS-CoV-2, anti-RBD IgG, dynamic changes, concentration, BAU/mL

Author contribution: Mayansky NA — concept, data processing, manuscript writing; Brzhozovskaya EA — sample collection, ELISA, data processing, making illustrations; Stoyanova SS — sample collection, data processing, making illustrations; Frolkov AV — data processing, manuscript preparation; Lebedin YuS — concept, ELISA, manuscript editing.

Compliance with ethical standards: the study was approved by the Ethics Committee of the Pirogov Russian National Research Medical University (protocol № 197 dated May 21, 2020).

✉ **Correspondence should be addressed:** Nikolay A. Mayanskiy
Ostrovitianova, str. 1, Moscow, Russia; mayanskiy.nikolay@gmail.com

Received: 01.02.2022 **Accepted:** 14.02.2022 **Published online:** 20.02.2022

DOI: 10.24075/brsmu.2022.007

ДИНАМИКА КОНЦЕНТРАЦИИ АНТИТЕЛ К SARS-COV-2 В ТЕЧЕНИЕ 12 МЕСЯЦЕВ ПОСЛЕ ПЕРЕНЕСЕННОЙ ИНФЕКЦИИ COVID-19

Н. А. Маянский¹✉, Е. А. Бржозовская¹, С. С. Стоянова¹, А. В. Фролков¹, Ю. С. Лебедин²

¹ Российский национальный исследовательский медицинский университет имени Н. И. Пирогова, Москва, Россия

² Общество с ограниченной ответственностью «ХЕМА», Москва, Россия

Формирование и поддержание иммунитета против SARS-CoV-2 является важным условием преодоления пандемии новой коронавирусной инфекции COVID-19. Целью работы было охарактеризовать динамику уровня антител IgG к рецептор-связывающему домену (RBD) SARS-CoV-2 с использованием набора для иммуноферментного анализа (ИФА), откалиброванного при помощи Международного стандарта анти-SARS-CoV-2-иммуноглобулинов (IS-SARS-CoV-2). Концентрацию анти-RBD-IgG измеряли в когорте лиц после выздоровления от COVID-19 с интервалом в месяц в течение 6 месяцев и в точке 12 месяцев с использованием наборов ИФА, откалиброванных IS-SARS-CoV-2; результаты представляли в единицах связывания антител (BAU) на 1 мл. Всего исследовали 97 образцов сыворотки крови от 20 человек с ПЦР-подтвержденной инфекцией SARS-CoV-2. К первому месяцу после заражения средний геометрический титр (GMT) анти-RBD-IgG составил 433 BAU/мл (диапазон 36–25900 BAU/мл). Со временем концентрация IgG против RBD постепенно снижалась, достигая GMT в 68 BAU/мл к 12 месяцу; анти-RBD-IgG сохранялись у 13 из 14 (93%) лиц, обследованных через 12 месяцев после инфицирования. Стандартизированные количественные серологические данные играют важную роль в мониторинге иммунного ответа и облегчают сравнение между исследованиями, создавая основу для поиска общего серологического коррелята иммунной защиты против SARS-CoV-2.

Ключевые слова: SARS-CoV-2, анти-RBD IgG, динамика, концентрация, BAU/мл

Вклад авторов: Н. А. Маянский — концепция, обработка результатов, написание текста; Е. А. Бржозовская — сбор образцов, выполнение ИФА, обработка результатов, подготовка иллюстраций; С. С. Стоянова — сбор образцов, обработка результатов, подготовка иллюстраций; А. В. Фролков — обработка результатов, подготовка рукописи; Ю. С. Лебедин — концепция, выполнение ИФА, редактирование рукописи.

Соблюдение этических стандартов: исследование одобрено этическим комитетом РНИМУ им. Н. И. Пирогова (протокол № 197 от 21 мая 2020 г.).

✉ **Для корреспонденции:** Николай Андреевич Маянский
ул. Островитянова, д. 1. г. Москва, Россия; mayanskiy.nikolay@gmail.com

Статья получена: 01.02.2022 **Статья принята к печати:** 14.02.2022 **Опубликована онлайн:** 20.02.2022

DOI: 10.24075/vrgmu.2022.007

The natural infection and vaccination against COVID-19 result in the production of antibodies against viral antigens, playing a vital part in the immune response monitoring [1]. Although it is expected that the naturally acquired immunity against SARS-CoV-2 would last long [2-3], serological equivalent of antiviral host defense has not yet been discovered. The lack of a standardized approach to laboratory testing is one of the obstacles to defining such correlates, which probably explains

the conflicting literature data on the serological assessment of SARS-CoV-2 infection. The WHO have recently introduced the International Standard for anti-SARS-CoV-2 immunoglobulin (IS-SARS-CoV-2), which makes it possible to unify the results of measuring the levels of anti-SARS-CoV-2 antibodies using the IS-SARS-CoV-2 units, namely the binding antibody units (BAU) [1]. The study was aimed to measure the concentration of IgG against the SARS-CoV-2 receptor-binding domain

(RBD) at different times over the 12-month period in a cohort of healthcare professionals, who have recovered from the SARS-CoV-2 infection, using the enzyme-linked immunosorbent assay (ELISA) kits, calibrated using the IS-SARS-CoV-2.

METHODS

The study, carried out from May 2020 to June 2021, involved the staff members of the Russian Children's Clinical Hospital, Pirogov Russian National Research Medical University. Inclusion criteria: positive PCR test result for COVID-19. There were no exclusion criteria.

In April and May 2020, after returning to work, individuals with positive PCR test results for COVID-19 gave the blood serum samples with an interval of a month for the anti-RBD-IgG measurement. The samples were collected on a monthly basis for 6 months, and the last sample was obtained 12 months after the positive PCR test result; a total of 4–7 samples was obtained from each subject. The samples collected were stored at a temperature of -80°C .

In July 2021, all the samples were assayed in one batch using the ELISA kit for the anti-RBD-IgG quantification (XEMA; Russia) [4], calibrated using the IS-SARS-CoV-2. The analytical measuring range was 15–240 BAU/mL; samples with the anti-RBD-IgG concentration exceeding 240 BAU/mL were further diluted 10–100 times and measured repeatedly in a separate batch. The samples were considered positive when the level of anti-RBD-IgG was 15 BAU/mL.

Statistical processing was performed using the IBM SPSS Statistics 27.0 software package (IBM Corp.; USA).

RESULTS

A total of 97 serum samples were obtained from 20 individuals during the study, including 14 women (70%) with the SARS-CoV-2 infection, confirmed by PCR. The median age was 50 years (Q_1 – Q_3 , 40–57 years). All the subjects had mild to moderate COVID-19, there were no severe cases of the disease.

In three individuals, blood serum samples were obtained a month before the SARS-CoV-2 infection; no anti-RBD-IgG were found in these samples. A month after the positive PCR test result for SARS-CoV-2, anti-RBD-IgG were found in all subjects in a concentration exceeding the threshold value of 15 BAU/mL, with the geometric mean titer (GMT) of 433 BAU/mL (95% CI 123–1,527 BAU/mL; range 36–25,900 BAU/mL) (see Figure). At the time point 2 of the month the median GMT was similar, 456 BAU/mL (95% CI 154–1,353 BAU/mL). Later the concentration of anti-RBD-IgG gradually decreased and reached the median GMT value of 68 BAU/mL (95% CI 35–131 BAU/mL) by the 12th month. All samples were anti-RBD-IgG-positive during the period between the first and the sixth months. Among 14 individuals assessed 12 months after the SARS-CoV-2 infection, 13 individuals (93%) were still seropositive for anti-RBD-IgG with the GMT values exceeding 15 BAU/mL. The median concentration of anti-RBD-IgG was 6.7 times lower (95% CI 4.4–10.3 times) after 12 months compared with the highest median GMT value, defined during the second month after the SARS-CoV-2 infection.

DISCUSSION

To date, the data of only a few studies, involving the standardized values of the amount of antibodies against SARS-CoV-2 after the natural infection and/or vaccination, have been reported

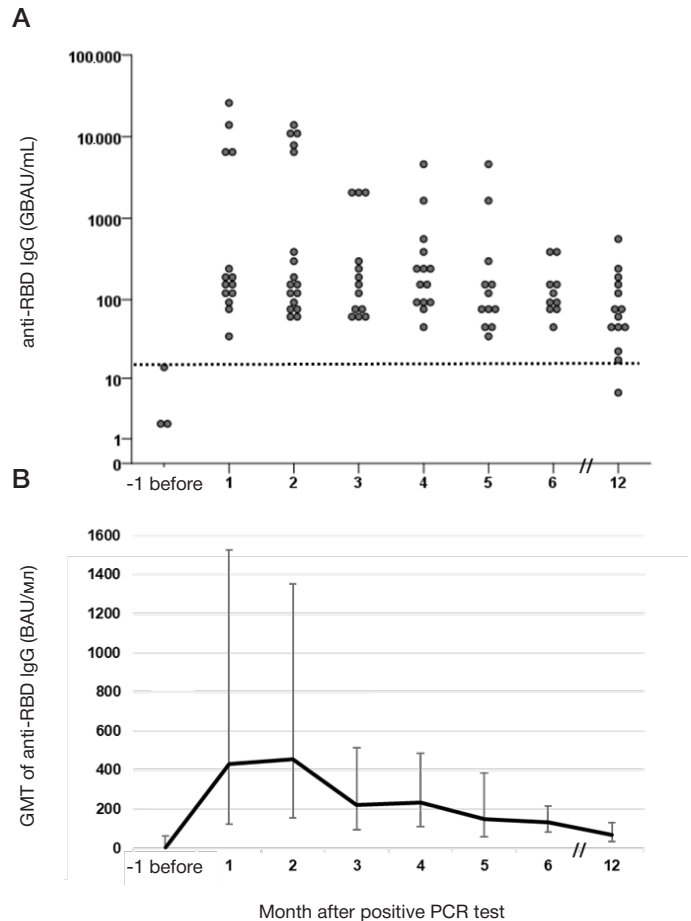


Fig. Concentration of anti-RBD IgG as a function of time after the positive PCR test result for SARS-CoV-2. **(A)** individual values for 97 samples and **(B)** geometric mean titers (GMT) of anti-RBD IgG with the 95% CI, expressed in BAU/mL; dotted line in **(A)** at the level of 15 BAU/mL specifies the positivity threshold

[5–7]. Thus, the live viral neutralization assay showed that anti-RBD-IgG in a concentration of ≥ 100 BAU/mL ensured the complete neutralization of three SARS-CoV-2 variants of concern a year after infection, which reduced the risk of reinfection with these virus strains [5]. Another report mentioned that on day 14 after vaccination, the anti-RBD-IgG GMT in individuals, vaccinated with mRNA vaccine, was 7,756 BAU/mL [6]. Thus, quantitative results provide the basis for seeking the common serological correlate of the protective immunity to SARS-CoV-2. Moreover, these data are important for monitoring the natural immunity and facilitate the comparison of immune responses to various vaccines [1]. Significant differences and systematic error in the numerical results, expressed in BAU/mL, associated with the use of different test systems [7], encourage further efforts to unify serological tests for detection of antibodies against SARS-CoV-2.

CONCLUSIONS

The study analyzes dynamic changes in the antibody response to SARS-CoV-2 infection during the natural immunity production. The use of IS-SARS-CoV-2 for calibration of the ELISA test system made it possible to demonstrate a change in the concentration of anti-RBD IgG over a wide range of 36–25,900 BAU/mL with the widest disparity within two months after the infection. The levels of anti-RBD-IgG gradually decreased with time, however, positive values persisted throughout 12 months of follow-up in the majority of subjects.

References

- Kristiansen PA, Page M, Bernasconi V, Mattiuzzo G, Dull P, Makar K, et al. WHO International Standard for anti-SARS-CoV-2 immunoglobulin. *Lancet*. 2021; 397: 1347–8. DOI: 10.1016/S0140-6736(21)00527-4.
- Wang Z, Muecksch F, Schaefer-Babajew D, Finkin S, Viant C, Gaebler C, et al. Naturally enhanced neutralizing breadth against SARS-CoV-2 one year after infection. *Nature*. 2021; 595: 426–31. DOI: 10.1038/s41586-021-03696-9.
- De Giorgi V, West KA, Henning AN, Chen LN, Holbrook MR, Gross R, et al. Naturally acquired SARS-CoV-2 immunity persists for up to 11 months following infection. *J Infect Dis*. 2021; jjab295. DOI: 10.1093/infdis/jjab295.
- SARS-CoV-2-IgG EIA instruction manual. <https://xema-medica.com/eng/sets/ifu/Archive/>. (kit K153GQIE v2018). (Assessed 20 September 2021).
- Gallais F, Gantner P, Bruel T, Velay A, Planas D, Wendling MJ, et al. Evolution of antibody responses up to 13 months after SARS-CoV-2 infection and risk of reinfection. *EBioMedicine*. 2021; 71: 103561. DOI: 10.1016/j.ebiom.2021.103561.
- Borobia AM, Carcas AJ, Pérez-Olmeda M, Castaño L, Bertran MJ, García-Pérez J, et al. Immunogenicity and reactogenicity of BNT162b2 booster in ChAdOx1-S-primed participants (CombiVacS): a multicentre, open-label, randomised, controlled, phase 2 trial. *Lancet*. 2021; 398: 121–30. DOI: 10.1016/S0140-6736(21)01420-3.
- Kim Y, Lee JH, Ko GY, Ryu JH, Jang JH, Bae H, et al. Quantitative SARS-CoV-2 Spike Antibody Response in COVID-19 Patients Using Three Fully Automated Immunoassays and a Surrogate Virus Neutralization Test. *Diagnostics (Basel)*. 2021; 11: 1496. DOI: 10.3390/diagnostics11081496.

Литература

- Kristiansen PA, Page M, Bernasconi V, Mattiuzzo G, Dull P, Makar K, et al. WHO International Standard for anti-SARS-CoV-2 immunoglobulin. *Lancet*. 2021; 397: 1347–8. DOI: 10.1016/S0140-6736(21)00527-4.
- Wang Z, Muecksch F, Schaefer-Babajew D, Finkin S, Viant C, Gaebler C, et al. Naturally enhanced neutralizing breadth against SARS-CoV-2 one year after infection. *Nature*. 2021; 595: 426–31. DOI: 10.1038/s41586-021-03696-9.
- De Giorgi V, West KA, Henning AN, Chen LN, Holbrook MR, Gross R, et al. Naturally acquired SARS-CoV-2 immunity persists for up to 11 months following infection. *J Infect Dis*. 2021; jjab295. DOI: 10.1093/infdis/jjab295.
- SARS-CoV-2-IgG EIA instruction manual. <https://xema-medica.com/eng/sets/ifu/Archive/>. (kit K153GQIE v2018). (Assessed 20 September 2021).
- Gallais F, Gantner P, Bruel T, Velay A, Planas D, Wendling MJ, et al. Evolution of antibody responses up to 13 months after SARS-CoV-2 infection and risk of reinfection. *EBioMedicine*. 2021; 71: 103561. DOI: 10.1016/j.ebiom.2021.103561.
- Borobia AM, Carcas AJ, Pérez-Olmeda M, Castaño L, Bertran MJ, García-Pérez J, et al. Immunogenicity and reactogenicity of BNT162b2 booster in ChAdOx1-S-primed participants (CombiVacS): a multicentre, open-label, randomised, controlled, phase 2 trial. *Lancet*. 2021; 398: 121–30. DOI: 10.1016/S0140-6736(21)01420-3.
- Kim Y, Lee JH, Ko GY, Ryu JH, Jang JH, Bae H, et al. Quantitative SARS-CoV-2 Spike Antibody Response in COVID-19 Patients Using Three Fully Automated Immunoassays and a Surrogate Virus Neutralization Test. *Diagnostics (Basel)*. 2021; 11: 1496. DOI: 10.3390/diagnostics11081496.

PROPERTIES OF RBD SPECIFIC IGG FROM COVID-19 PATIENTS AND SPUTNIK V VACCINATED INDIVIDUALS

Generalova LV¹, Grigoriev IV², Vasina DV², Tkachuk AP², Kruzhkova IS², Kolobukhina LV², Burgasova OA^{1,2}, Gushchin VA²✉

¹ Peoples' Friendship University of Russia (RUDN University), Moscow, Russia

² Gamaleya National Research Center for Epidemiology and Microbiology, Moscow, Russia

SARS-CoV-2 specific antibody response is a generally accepted measure of postinfection and vaccination-induced immunity assessment. The dynamics of avidity maturation and neutralizing activity of virus-specific immunoglobulins G during the SARS-CoV-2-associated coronavirus infection was studied in cohorts of vaccinated volunteers and COVID-19 patients. 4–6 months after vaccination, neutralization activity was low compared to hospitalized patients (medians 57.4% vs 86.4%). On the opposite, the avidity indices in vaccinated volunteers were significantly higher (median 76.7%) than among hospitalized patients (median 61.4%). During the acute phase of the disease (14–16 days PI), post-vaccination patients have also higher avidity indices than primary patients (medians 43.5% vs 20.4%). Our results suggest that in long-term perspective antibody affinity maturation rate is higher after vaccination than after a natural infection. We demonstrated that Sputnik V vaccination leads to formation of high-avidity IgG, which persists for at least 6 months of observation. These results also indicate the presence of protective efficacy markers for at least 4–6 months after the vaccination or a previous illness and gives grounds for the half-year time period chosen for booster immunization with Sputnik V in Russia.

Keywords: antibody avidity, virus neutralization, SARS-CoV-2, immune memory, vaccination, Sputnik-V

Funding: this research was funded by the Ministry of Health of the Russian Federation, Government assignments number № АААА - А20-120113090054-6, Prof. Olga A. Burgasova was also supported by the RUDN University Strategic Academic Leadership Program.

Author contribution: LV Generalova, IV Grigoriev — research planning, experiments preparation and execution, data interpretation and paper draft preparation; IS Kruzhkova, LV Kolobukhina — data interpretation and paper draft preparation; DV Vasina, AP Tkachuk, OA Burgasova, VA Gushchin — research planning, data interpretation and paper draft preparation.

Compliance with ethical standards: the study was approved by the ethics committee of the First Moscow Infectious Diseases Hospital (protocol № 11/A dated November 16, 2020); informed consent was obtained from all study participants.

✉ **Correspondence should be addressed:** Vladimir A. Gushchin
Gamaleya, 18, str. 9, Moscow, Russia; wowaniada@gmail.com

Received: 23.01.2022 **Accepted:** 08.02.2022 **Published online:** 16.02.2022

DOI: 10.24075/brsmu.2022.005

СВОЙСТВА АНТИТЕЛ К RBD У ПЕРЕБОЛЕВШИХ COVID-19 И ВАКЦИНИРОВАННЫХ ПРЕПАРАТОМ «СПУТНИК V»

Л. В. Генералова¹, И. В. Григорьев², Д. В. Васина², А. П. Ткачук², И. С. Кружкова², Л. В. Колобухина², О. А. Бургасова^{1,2}, В. А. Гушчин²✉

¹ Российский университет дружбы народов, Москва, Россия

² Национальный исследовательский центр эпидемиологии и микробиологии имени Н. Ф. Гамалеи, Москва, Россия

Исследование свойств антител, участвующих в нейтрализации вируса, после перенесенного заболевания COVID-19 и применения профилактических препаратов, остается актуальной задачей, от которой зависит выработка стратегий первичной и повторной иммунизации. Измерение уровня антител к антигенам SARS-CoV-2 — один из основных способов оценки иммунитета, однако не дает достаточной информации о количественных и качественных показателях иммунного ответа. Целью работы было исследовать свойства антител IgG к RBD у переболевших COVID-19 и вакцинированных препаратом «Спутник V». На когортах пациентов (18–80 лет; соотношение мужчин и женщин — 47 : 53), переболевших COVID-19, и вакцинированных добровольцев изучена динамика созревания аффинности и изменения нейтрализующей активности IgG к RBD. Нейтрализующая активность сывороток крови у добровольцев через 4–6 месяцев после вакцинации снизилась по сравнению с образцами переболевших пациентов (медианы — 57,4 и 86,4% соответственно). Индекс avidности у вакцинированных добровольцев, напротив, был значительно выше, чем у перенесших COVID-19 (76,7 и 61,4% соответственно). В острую фазу заболевания (14–16 дней от появления симптомов) ранее вакцинированные пациенты имели более высокий индекс avidности, чем первичные пациенты (43,5 и 20,4% соответственно). В долгосрочной перспективе степень созревания аффинности вирусспецифических IgG после вакцинации может быть выше, чем после естественно перенесенной инфекции. Показано, что вакцинация «Спутником V» приводит к формированию высокоавидных IgG, сохраняющихся по крайней мере 6 месяцев. Продемонстрировано наличие уровней антител, коррелирующих с протективным иммунитетом, на протяжении 4–6 месяцев после вакцинации или перенесенной инфекции.

Ключевые слова: avidность антител, вирус-нейтрализация, SARS-CoV-2, иммунная память, вакцинация, Спутник V

Финансирование: исследование проведено при поддержке гранта Министерства здравоохранения РФ, № АААА - А20-120113090054-6, профессору О. А. Бургасовой было выделено финансирование по программе стратегического академического лидерства РУДН.

Вклад авторов: Л. В. Генералова и И. В. Григорьев — планирование исследования, подготовка и проведение экспериментов, интерпретация данных и написание статьи; И. С. Кружкова и Л. В. Колобухина — интерпретация данных, написание статьи; Д. В. Васина, А. П. Ткачук, О. А. Бургасова, В. А. Гушчин — планирование исследования и написание статьи.

Соблюдение этических стандартов: исследование одобрено этическим комитетом Первой московской инфекционной больницы (протокол № 11/A от 16 ноября 2020 г.); всеми участниками исследования было подписано информированное согласие.

✉ **Для корреспонденции:** Владимир Алексеевич Гушчин
ул. Гамалеи, 18, стр. 9, г. Москва, Россия; wowaniada@gmail.com

Статья получена: 23.01.2022 **Статья принята к печати:** 08.02.2022 **Опубликована онлайн:** 16.02.2022

DOI: 10.24075/vrgmu.2022.005

SARS-CoV-2 specific antibody response is a generally accepted measure of postinfection and vaccination-induced immunity assessment. However, the protective efficacy of virus specific antibodies and their ability to withstand the individual's reinfection may be influenced not only by antibody quantity but also their quality including neutralizing activity, binding affinity, isotypes spectrum etc., which are not characterized well enough. In general, SARS-CoV-2 antibody avidity (% of antibodies with high affinity) correlated with duration of infection and higher neutralizing titers [1]. Indeed, high avidity antibodies but not the level of spike-binding antibodies has been previously associated with positive clinical outcomes [2]. At the moment there is no published information about the antibody affinity maturation after the Sputnik V vaccination and in recovered patients, as well as antibodies functional transformations during the prolonged period of observation. This study aims to provide the longitudinal assessment of antibody responses dynamics in patients recovered from COVID-19 and Sputnik V vaccinated individuals with or without further infection and to characterize the patterns of sustaining long-term immunity.

METHODS

Study participants

During the study we enrolled 41 participants divided into 3 groups (Table 1): 23 patients, hospitalized in Moscow with different disease severity, were sampled upon the admission to the hospital (acute phase) and 4–6 months after the hospital discharge; 9 vaccinated patients sampled during their hospitalization and 9 healthy vaccinated volunteers at different times from the complete vaccination. Median symptom durations in hospitalized patients before the first sampling were 14 days among unvaccinated individuals and 10 days among vaccinated individuals. For vaccinated volunteers, the absence of COVID-19 was confirmed by the lack of anti-Nc IgG seroconversion.

We characterized antibodies from the three groups of participants. The group of inpatient volunteers was recruited in November through December 2020 at the First Moscow Infectious Diseases Hospital (Moscow, Russia); vaccinated patients were hospitalized and enrolled in March through April 2021 in the same source. Healthy volunteers vaccinated with Sputnik V vaccine were recruited in September through December 2020. Eligible volunteers were adults aged 18–80 years.

All patients were either diagnosed with SARS-CoV-2 infection by RT-PCR of nasopharyngeal swabs or confirmed with CT scanning. Disease severity in hospitalized patients was

determined in accordance with NEWS [3]. Group of vaccinated patients included hospitalized participants diagnosed with SARS-CoV-2 infection who received a second vaccine dose at least two weeks before the infection. The vaccinated healthy volunteers received two doses of Sputnik, free of symptoms of COVID-19 for at least 14 days before the sampling. No statistical methods were used to predetermine sample size.

Blood sample processing and storage

Blood samples were collected by venipuncture to vacutainers with clot activator and shipped to the laboratory at +4 °C. Centrifugation at 3000 rpm for 10 minutes was applied to obtain serum, which was further aliquoted and stored at –30 °C.

Anti-nucleocapsid and anti-RBD IgG antibody detection

The anti-nucleocapsid (Nc) and anti-RBD IgG antibodies were measured using in house ELISA test-systems and expressed in positivity index (p.i., S/CO). Briefly, for antibody detection we used recombinant receptor-binding domain fragment of S1 SARS-CoV-2 Spike protein (RBD № 8COV1; HyTest, Russia), expressed in eukaryotic cells and recombinant SARS-CoV-2 Nucleocapsid (Nc) protein, expressed in *Escherichia coli* and purified in our laboratory.

To perform anti-RBD and anti-Nc ELISAs, 96 well high binding plates (Costar 2592; Corning, USA) were coated overnight with 100 µl of 1 µg/mL recombinant protein solution in PBS. Next day the plates were blocked for 2 hours at room temperature with a blocking buffer, containing 0,5% casein. Serum samples were diluted 1 : 100 with universal ELISA buffer S011 (XEMA; Russia). Sera of PCR+ reconvalescent was used as a positive control and a pool of pre-COVID samples, collected in 2019, was used as negative control. ELISA plates with 100 µl of diluted samples were incubated 1 hour at 37 °C and washed 3 times with PBS, containing 0,1% Tween-20. After washing, wells were incubated with 100 µl of HRP-conjugated anti-human IgG (Novex A18823; USA) for 1 hour at 37 °C and washed 6 times. After adding 100 µl of the HRP substrate solution, containing 3,3',5,5'-Tetramethylbenzidine (R055; XEMA, Russia) per well, the colour reaction was developed for 10 minutes at room temperature and then stopped by 10% HCl. Optical density (OD) was measured at 450 nm using Multiscan FC (Thermo Scientific; USA).

Neutralization assay (Inhibiting assay)

Detection of IgG neutralizing antibodies was performed with commercial "SARS-CoV-2-anti-RBD-ELISA" kit (MT-

Table 1. Study Cohorts. Values are reported as the medians with the range in parentheses

Characteristics	Patients (n = 23)	Vaccinated volunteers (n = 9)	Volunteers (n = 9)
Age median years, IQR	59 (54–65)	72 (69–79)	34 (33–39)
Sex, %	52% male, 48% female	33% male, 67% female	56% male, 44% female
Time from symptom onset to Visit 1 (Me days min-max)	14 (9–17)	10 (5–19)	NA
Time from symptom onset to Visit 2 (Me days min-max)	135 (116–159)	16 (11–24)	NA
Time from initial vaccination to Visit 1 (Me days min-max)	NA	62 (30–88)	147 (100–263)
Time from initial vaccination to Visit 2 (Me days min-max)	NA	68 (35–95)	261 (161–349)

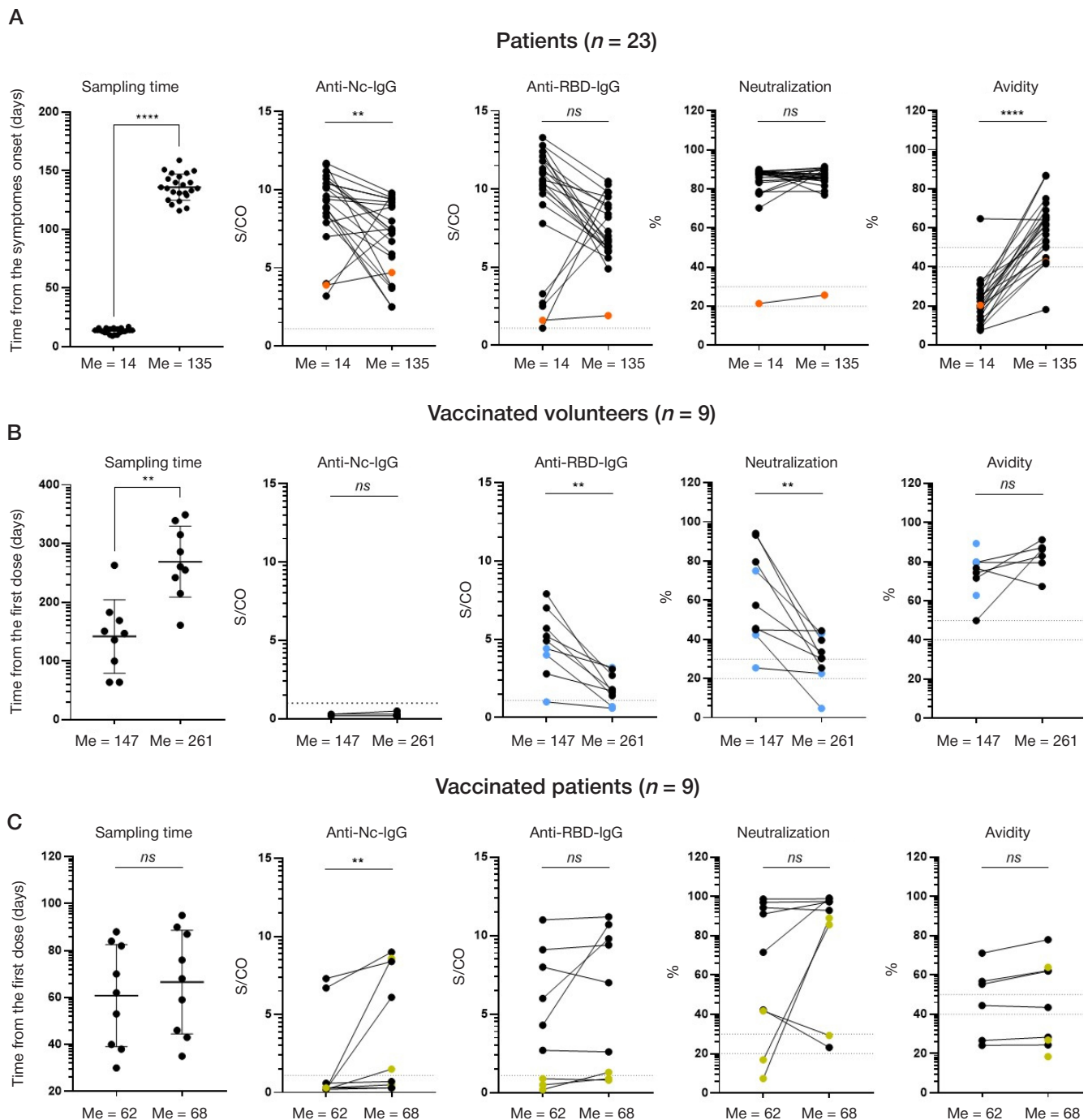


Fig. 1. Immune responses to SARS-CoV-2 in the studied groups. **(A)** Cohort of hospitalized patients **(B)** Cohort of vaccinated patients **(C)** Cohort of healthy vaccinated volunteers. Significant differences are shown as asterisks (Wilcoxon signed-rank test). Me — median time of sampling in groups from the symptoms onset or the initial vaccination as indicated in the axis

I-C1-04.192; MedipalTech, Russia) in accordance with manufacturer's instructions. Briefly, serum samples were mixed with biotinylated recombinant human ACE-2 receptor and added to the ELISA plate, precoated with recombinant RBD. After incubation and wash, streptavidin-conjugated HRP was added to the wells. Reaction was visualized by adding an HRP-substrate solution. Optical density in wells was inversely proportional to the concentration of antibodies, able to block ACE-2 binding to RBD. Inhibition coefficient (IC) was calculated as ratio of sample OD to negative control OD, subtracted from 1. $IC = (1 - OD_{sample}/ON_{neg}) - 100\%$. The antibody neutralization criteria were assessed as high neutralizing if serum sample inhibited binding of soluble RBD to ACE-2 on plate by $> 30\%$; intermediate one, if the inhibition

rate was between 20 and 30%; and a low level for samples with inhibition $< 20\%$.

Avidity assay

The IgG avidity assay targeted the spike protein RBD of SARS-CoV-2 was performed with "SARS-CoV-2-ELISA-IgG plus" kit (No MT-I-C1-03.192; MedipalTech, Russia) in accordance with manufacturer's instructions. Briefly, duplicate anti-RBD IgG positive serum samples were incubated in wells of ELISA plates, precoated with recombinant RBD. Then either PBS (non-denaturing conditions) or urea solution (denaturing agent, DA) was added to the wells. After washing, HRP-conjugated anti-human IgG was added and, finally, reaction was visualized by

Table 2. Antibody levels and characteristics in cohorts of patients with different disease severity

		Patients			
		Total (<i>n</i> = 23)	Mild (<i>n</i> = 10)	Moderate (<i>n</i> = 6)	Severe (<i>n</i> = 7)
Visit 1, median (IQR)					
1	RBD-specific IgG, S/CO	10.5 (7.8–11.8)	10.4 (7.6–11.9)	8.9 (1.5–11.5)	11.3 (10.2–12.8)
	Negative, <i>n</i> (%)	1 (4.3)	0 (0)	1 (20)	0 (0)
	Reactive, <i>n</i> (%)	22 (95.6)	10 (100)	5 (80)	7 (100)
2	N-specific IgG, S/CO	9.4 (7.9–10.7)	9.9 (8.8–11.3)	7.45 (3.7–8.55)	10.4 (8.8–10.7)
	Negative, <i>n</i> (%)	0 (0)	0 (0)	0 (0)	0 (0)
	Reactive, <i>n</i> (%)	23 (100)	10 (100)	6 (100)	7 (100)
3	Neutralization, %	87.7 (83.3–88.7)	87.5 (78.4–88.9)	87.1 (58.1–88.5)	87.8 (87.3–89.0)
	Low, <i>n</i> (%)	1 (4.3)	0 (0)	1 (20)	0 (0)
	High, <i>n</i> (%)	22 (95.6)	10 (100)	5 (80)	7 (100)
4	Avidity, %	20.4 (14.6–26.3)	19.5 (15.28–25.7)	22.2 (17.4–25.95)	22.4 (8.7–31.6)
	Low, <i>n</i> (%)	22 (95.6)	9 (90)	6 (100)	7 (100)
	High, <i>n</i> (%)	1 (4.3)	1 (10)	0 (0)	0 (0)
Visit 2, median (IQR)					
1	RBD-specific IgG, S/CO	6.8 (6.1–9.0)	6.5 (6.1–8.7)	6.6 (4.7–9.2)	7.3 (6.8–9.8)
	Negative, <i>n</i> (%)	0 (0)	0 (0)	0 (0)	0 (0)
	Reactive, <i>n</i> (%)	23 (100)	10 (100)	6 (100)	7 (100)
2	N-specific IgG, S/CO	7.4 (4.7–9.2)	7.3 (3.5–9.3)	6.7 (5.5–9.1)	7.4 (3.8–9.4)
	Negative, <i>n</i> (%)	0 (0)	0 (0)	0 (0)	0 (0)
	Reactive, <i>n</i> (%)	23 (100)	10 (100)	6 (100)	7 (100)
3	Neutralization, %	86.4 (84.3–89.5)	86.2 (80.9–88.8)	87.1 (69.7–90.1)	85.8 (85.3–89.5)
	Low, <i>n</i> (%)	1 (4.3)	0 (0)	1 (20)	0 (0)
	High, <i>n</i> (%)	22 (95.6)	10 (100)	5 (80)	7 (100)
4	Avidity, %	61.4 (50.0–66.2)	64.7 (52.3–70.0)	55.7 (42.4–62.6)	59.0 (42.2–75.0)
	Low, <i>n</i> (%)	6 (26.1)	1 (10)	3 (50)	2 (28.6)
	High, <i>n</i> (%)	17 (73.9)	9 (90)	3 (50)	5 (71.4)

adding HRP-substrate solution. Avidity index (a.i.), proportional to antibody denaturation resistance, was calculated as ratio of OD-450 in DA and PBS wells. The antibody avidity criteria were as follows: avidity index (a.i.) > 50% — high avidity; between 40 and 50% — intermediate avidity; < 40% — low avidity.

Data analysis

The results are reported as medians with min-max range and the parameters were compared between groups by the Mann-Whitney nonparametric *t* test and at different time points using the paired Wilcoxon rank test. *P* value < 0.05 was considered statistically significant.

RESULTS

All antibody assays were provided for 100% of samples. Samples of 23 hospitalized patients with confirmed COVID-19 demonstrated a common Ab dynamics pattern. Two weeks after the symptoms onset all samples became IgG positive for both RBD (Me S/CO 10.5, min-max, 1.1–13.3) and Nc (Me, 9.4, min-max 3.2–11.7) (Fig. 1, Table 2). Twenty two out of 23 samples (95.6%) demonstrated high neutralization activity in ACE2-RBD binding inhibition assay and low avidity with median 20% (min-max 7.5%–37.3%) of anti-RBD IgG antibodies. Only 1 sample in this cohort had a.i. of 64.7%, probably due to previous unregistered antigen exposure. As expected, these results propose the presence of unmaturing virus-specific IgG [4]. To analyze the longevity of humoral immunity to SARS-CoV-2

in convalescent patients, blood samples were collected 4–6 months later. All samples remained positive for anti-RBD and anti-Nc IgG (Fig. 2, Table 2). Median anti-RBD p.i. dropped from 10.5 to 6.8 S/CO and median anti-Nc p.i. — from 9.4 to 7.4 S/CO. Samples with low anti-RBD IgG levels (S/CO <5) at the first time point were obtained after 10–12 days after the symptom's onset, thus, they had not enough time to reach peak of serum antibody concentrations due to heterogeneity of SARS-CoV-2 incubation period and variability in the individual dynamics of Ab production. However, four months later all patients with one exception had similar levels of anti-RBD IgG (Me S/CO 6.8, IQR 6.3–8.9).

Although we detected a 1.5-fold decrease of anti-RBD IgG levels of this cohort, the neutralization activity remained at high level without significant difference between first and second time points which indicates that the quantity of antibodies is not the only determinant of the neutralizing activity. Preservation of high neutralization effects can be due to the compensation of decreased antibody concentration by improved quality (specificity and affinity) during this period. On the other hand, the observed effect may be due to the peculiarities of the test system used in the study. Since the measured values are near the limit of quantification of the system it does not allow to reliably assess the changes in neutralizing activity. Additional experiments are required to access neutralization dynamics more precisely. During the same observation period anti-RBD IgG avidity increased significantly, reaching a high avidity level (>50%) in 78% of patients. Median avidity at the second time point was 61.4% (min-max 18.2–86.9%). Remaining

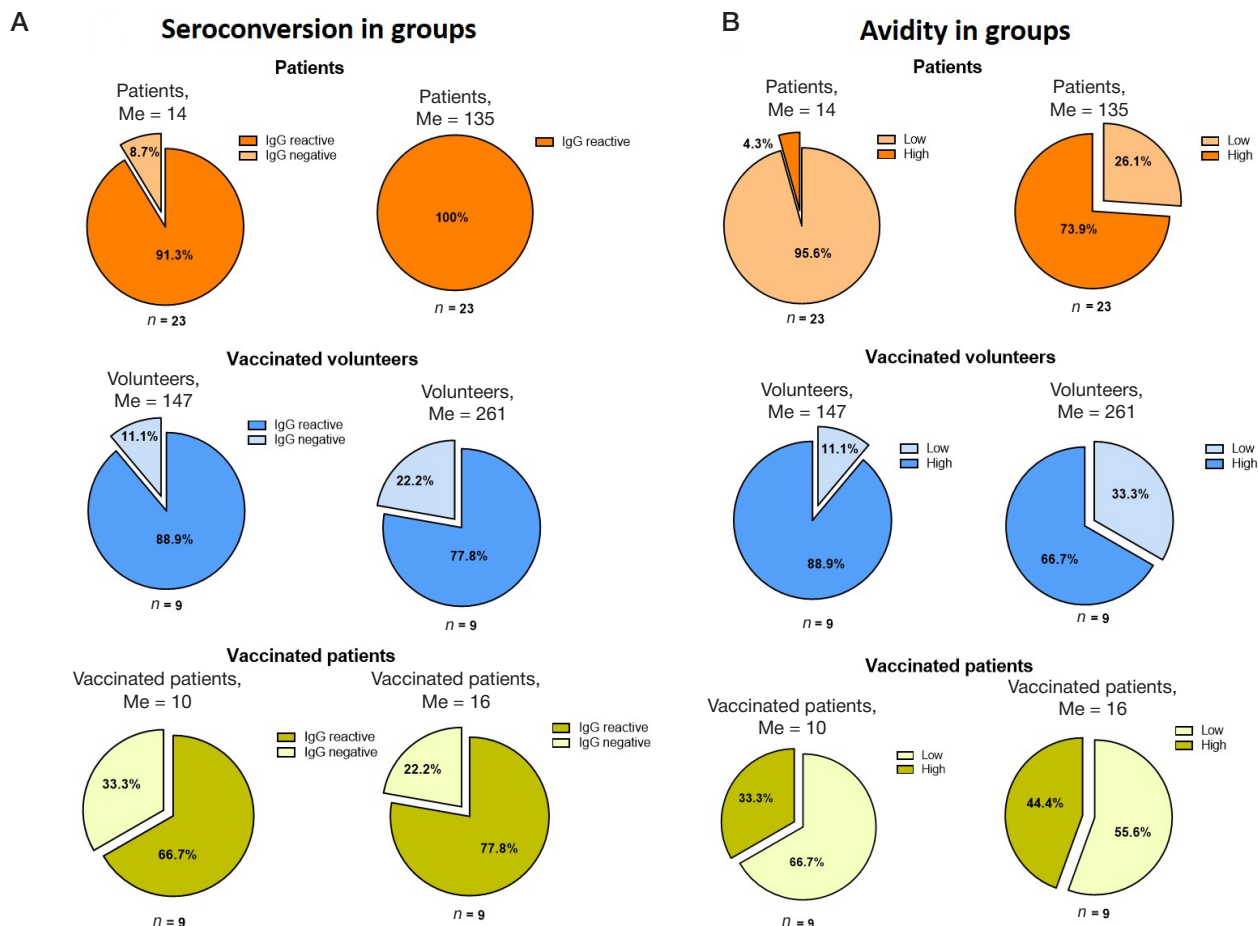


Fig. 2. Anti-RBD IgG conversion (A) and avidity dynamics (B) in the studied groups

6 patients (22%) had intermediate (40–50%, "maturation zone") or low (<40%) anti-RBD IgG avidity. Importantly, five of low- and intermediate-avidity patients had moderate or severe disease (Fig. 3). One patient (Fig 1A, orange circles) had low levels of anti-RBD IgG and neutralization activity at both time points, but his anti-RBD IgG avidity increased from 20.4 to 42.7%. To the end of the hospitalization period most patients possessed strong IgG response to SARS-CoV-2 antigens and their antibodies were effective at preventing RBD binding to human ACE-2. During the next months affinity maturation of anti-RBD IgG response occurred and overall concentration of anti-RBD and anti-Nc IgG decreased, neutralization activity remained at high level.

In a group of healthy Sputnik V vaccinated volunteers (Fig. 1B) 8 out of 9 samples were positive for anti-RBD IgG at the first time point (median of 147 days after the initial vaccination) with 4.9 S/CO (min-max 1–7.9). Four months later (261 days post initial vaccination), the median anti-RBD IgG p.i. dropped significantly to a median level 1.7 S/CO although 7 out of 9 volunteers still remained positive for anti-RBD IgG. None of the volunteers had detectable IgG to Nc, indicating there were no cases of infection with SARS-CoV-2 in this group. The neutralization correlated the IgG dynamics and decreased significantly in all samples from median 57.4% in the first time point to median 30.6% in the second time point. On the opposite, the avidity remained at the same high level indicating that at the first time point (147 days post vaccination), antibody maturation occurred in all vaccinated volunteers. However, for 3 samples (33%) at the second time point it was impossible to estimate the avidity as the level of anti-RBD IgG was too low (Fig. 1B, highlighted in blue).

In a group of Sputnik V vaccinated patients with confirmed COVID-19 (Fig 1C, Table 1) the median time from receiving a first vaccine dose was 62 days (ranging from 30 to 88 days) and the median time of sampling from symptoms onset was 10 days (5 to 19 days). At that time 6 out of 9 samples were positive for anti-RBD IgG with median 4.3 S/CO and only two were positive for anti-Nc IgG. All anti-RBD positive samples and one negative sample were positive in the neutralization ELISA (median 71.6%, min-max 7.4%–98.6%). Most of the samples (66.7%) demonstrated low avidity antibodies with median a.i. 27.6% (min-max 0%–71.1%). The second sampling time point in this group was around the 16th day after the symptoms onset. One week after the first sampling, the median S/CO of anti-RBD IgG in general did not change significantly (median 7 S/CO, min-max 0.8–11.2), however, 7 out of nine patients were seropositive after the infection and/or vaccination. The neutralization did not significantly change compared to the first time point (median 92.9%, min-max 23.2%–99.2%), the same was observed for avidity. Neutralization activity in two samples with low levels of anti-RBD IgG increased significantly to 85 and 89%, probably due to anti-RBD IgM production. (Fig. 1, yellow dots)

DISCUSSION

In COVID-19 patients, neutralizing antibody titers correlate with the severity of the infection [5, 6] and can be achieved even at low somatic hypermutation [7, 8]. The RBD region is found to be immunodominant and it is the target of approximately 90% of the neutralizing antibodies presented in the sera of SARS-CoV-2-infected people. Furthermore, it has been determined that

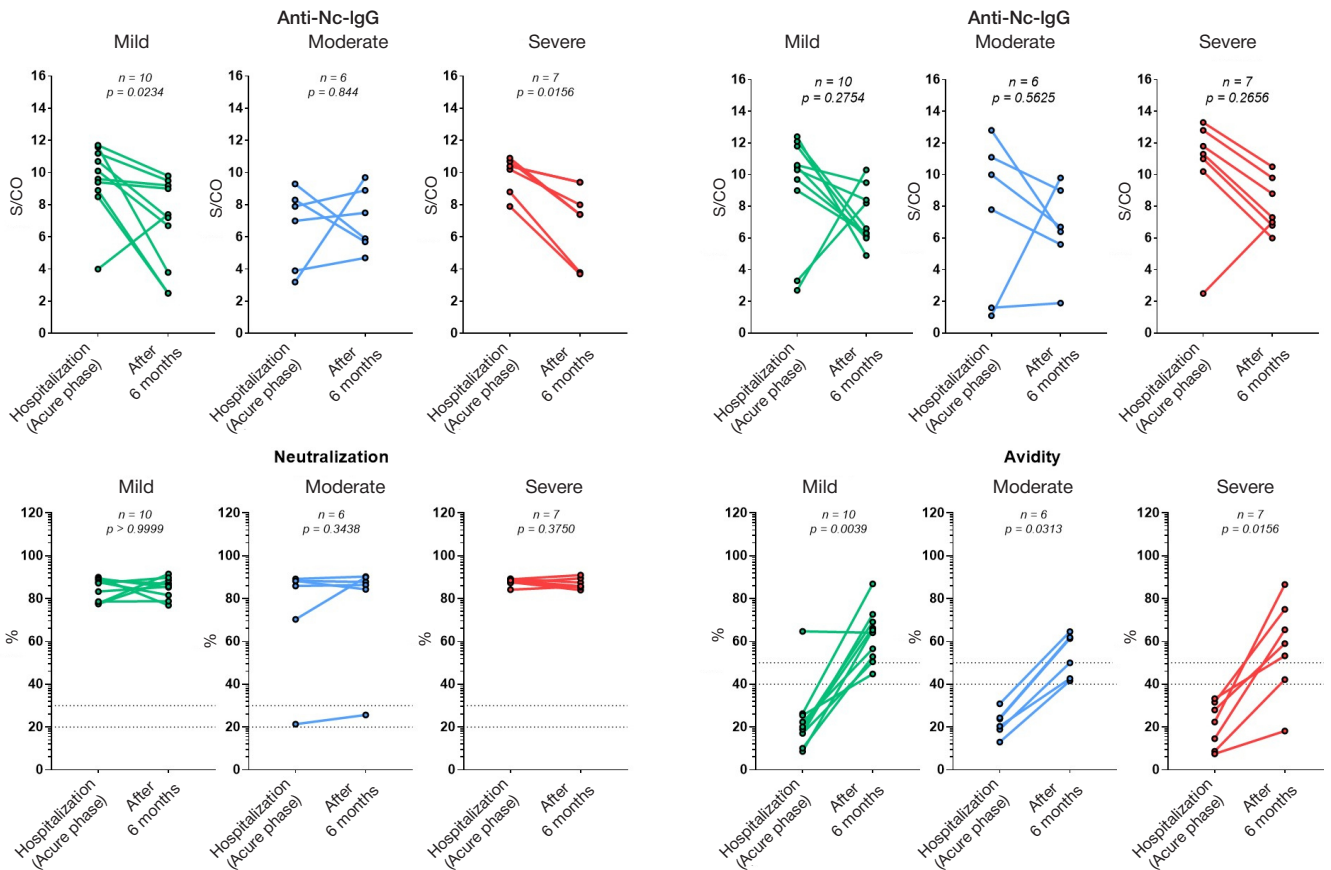


Fig. 3. Antibody levels in patients with different disease severity

anti-RBD IgG titers decrease with time post symptom onset, presenting a half-life of approximately 49 days. Importantly, antibody avidity increases over time due to increased maturation (somatic hypermutation, followed by selection in germinal centers). In the serum of hospitalized COVID-19 patients, there is a higher number of IgG against S protein and RBD, compared with that in non-serious and asymptomatic patients [9]. It was previously shown that antibody avidity increased over duration of infection and remained elevated [1]. In convalescent donors' plasma higher neutralizing titer had a stronger positive correlation with anti-spike IgG avidity than with anti-nucleocapsid IgG avidity proposing the anti-RBD IgG to be the main source of neutralizing activity.

Comparing samples of hospitalized patients and vaccinated volunteers 4–6 months after the infection or the vaccination, vaccinated volunteers had significantly lower levels of anti-RBD IgG and neutralization activity, but significantly higher anti-RBD IgG avidity (Fig. 4A, C). All hospitalized patients remained positive for anti-RBD IgG, while in one of the vaccinated volunteers antibody levels dropped below baseline (Fig. 4C).

When comparing the groups of Sputnik V fully vaccinated patients and unvaccinated patients samples, collected during the acute phase of infection (2–3 weeks after symptoms onset) it was shown that, in vaccinated patients antibody levels to both RBD and Nc antigens were significantly lower, than in unvaccinated patients (Fig. 4B). Anti-RBD IgG avidity was significantly higher in vaccinated patients indicating that despite low antibody levels, vaccination did induce primary immune response and formation of memory B-cells and their antibody production during the infection demonstrates signs of secondary immune response. In the long-term perspective antibody affinity maturation rate is higher after vaccination than after natural infection. Although it is proposed that antibody

maturation increases their neutralization potency [10], here we observe no significant correlation between these parameters.

Our study is under certain significant limitations. First of all, it is based on a small number of samples. Patients in this study had a limited spectrum of COVID-19 clinical manifestations. Particularly, our research does not include asymptomatic and outpatient individuals with a mild course of disease, which represent the most of COVID-19 cases in comparison with other disease manifestations. Second, we could not estimate the peaks of antibody production and maturation as only two timepoints were analyzed in each group.

CONCLUSIONS

We observed the anticipated dynamics of Ab levels in convalescent patients with the peak at acute phase followed by gradual decrease in the subsequent months. But despite the loss of anti-RBD antibodies concentrations, serum neutralization activity remained at high/sufficient level, probably due to improved Ab specificity and increased avidity. Here, we demonstrated the formation and persistence of high avidity IgG for at least 6 months after Sputnik V immunization. It indicates that protectivity markers remain at sufficient levels for at least 4-6 months after the infection or the vaccination. These results give rounds for the half-year period chosen for booster immunization with Sputnik V in Russia. Based on our data one can't estimate the proportion and characteristics of patients requiring earlier revaccination due to drop of vaccine-induced protection before the 6 months period. We propose that low anti-RBD IgG avidity two months after vaccination could be one of the potential markers for preliminary revaccination. Possibly this may indicate that estimation of RBD-specific antibodies avidity can serve not only as a prognostic marker of

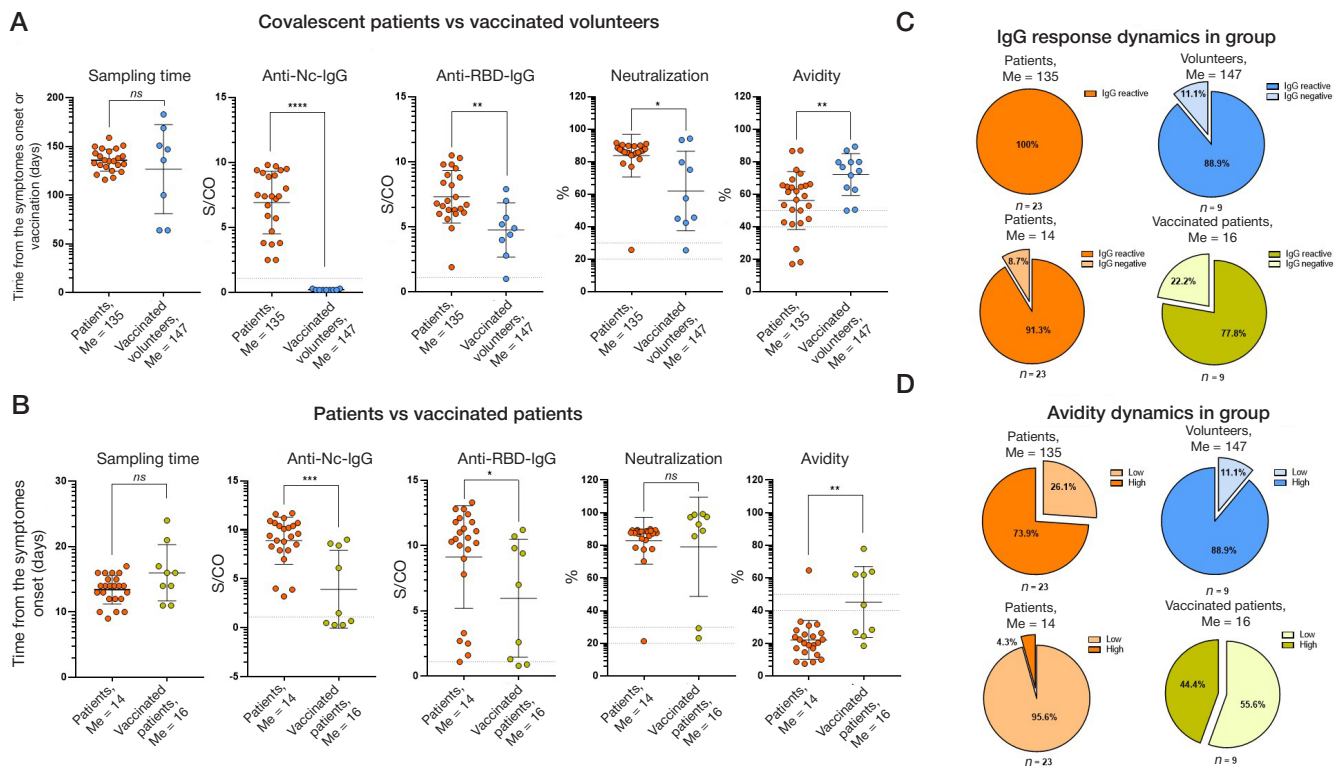


Fig. 4. Comparison of immune responses in different groups. **(A)** Comparison of unvaccinated coalescent patients and healthy vaccinated volunteers 4–6 months after the infection/vaccination. **(B)** Comparison of vaccinated and unvaccinated patients in the acute phase of infection (2–3 weeks from symptoms onset). **(C)** Comparison of anti-RBD IgG conversion in the studied groups. **(D)** Comparison of sera avidity dynamics in the studied groups. Significant differences are shown as asterisks (Mann–Whitney U test)

disease severity, but also to determine individuals, who require revaccination earlier than 6 months after receiving the initial

dose. Further study on larger samples is needed to verify this hypothesis.

References

1. Benner SE, Patel EU, Laeyendecker O, et al. SARS-CoV-2 antibody avidity responses in COVID-19 patients and convalescent plasma donors. *J Infect Dis.* 2020; 222: 1974–84.
2. Tang J, Grubbs G, Lee Y, et al. Impact of convalescent plasma therapy on SARS-CoV-2 antibody profile in COVID-19 patients. *Clin Infect Dis.* 2021; ciab317.
3. Baker KF, Hanrath AT, Schim van der Loeff I, et al. National Early Warning Score 2 (NEWS2) to identify inpatient COVID-19 deterioration: a retrospective analysis. *Clin Med (Lond).* 2021; 21 (2): 84–89.
4. Paul KS Chan, Pak-Leong Lim, Esther YM Liu, et al. Antibody Avidity Maturation during Severe Acute Respiratory Syndrome–Associated Coronavirus Infection. *J Infect Dis.* 2005; 192 (1): 166–9.
5. Wang C, Li W, Drabek D, et al. A human monoclonal antibody blocking SARS-CoV-2 infection. *Nat Commun.* 2020; 11 (1): 2251.
6. Long Q, Liu B, Deng H, et al. Antibody responses to SARS-CoV-2 in patients with COVID-19. *Nat Med.* 2020; 26 (6): 845–8.
7. Kreer C, Zehner M, Weber T, et al. Longitudinal isolation of potent near-germline SARS-CoV-2-neutralizing antibodies from COVID-19 patients. *Cell.* 2020; 182 (4): 843–54.
8. Chi X, Yan R, Zhang J, et al. A neutralizing human antibody binds to the N-terminal domain of the spike protein of SARS-CoV-2. *Science.* 2020; 369 (6504): 650–5.
9. Piccoli L, Park Y, Tortorici M, et al. Mapping neutralizing and immunodominant sites on the SARS-CoV-2 Spike Receptor-Binding Domain by structure-guided high-resolution serology. *Cell.* 2020; 183 (4): 1024–42.
10. Gaebler C, Wang Z, Lorenzi JCC, et al. Evolution of antibody immunity to SARS-CoV-2. *Nature.* 2021; 591, 639–44.

Литература

1. Benner SE, Patel EU, Laeyendecker O, et al. SARS-CoV-2 antibody avidity responses in COVID-19 patients and convalescent plasma donors. *J Infect Dis.* 2020; 222: 1974–84.
2. Tang J, Grubbs G, Lee Y, et al. Impact of convalescent plasma therapy on SARS-CoV-2 antibody profile in COVID-19 patients. *Clin Infect Dis.* 2021; ciab317.
3. Baker KF, Hanrath AT, Schim van der Loeff I, et al. National Early Warning Score 2 (NEWS2) to identify inpatient COVID-19 deterioration: a retrospective analysis. *Clin Med (Lond).* 2021; 21 (2): 84–89.
4. Paul KS Chan, Pak-Leong Lim, Esther YM Liu, et al. Antibody Avidity Maturation during Severe Acute Respiratory Syndrome–Associated Coronavirus Infection. *J Infect Dis.* 2005; 192 (1): 166–9.
5. Wang C, Li W, Drabek D, et al. A human monoclonal antibody blocking SARS-CoV-2 infection. *Nat Commun.* 2020; 11 (1): 2251.
6. Long Q, Liu B, Deng H, et al. Antibody responses to SARS-CoV-2 in patients with COVID-19. *Nat Med.* 2020; 26 (6): 845–8.
7. Kreer C, Zehner M, Weber T, et al. Longitudinal isolation of potent near-germline SARS-CoV-2-neutralizing antibodies from COVID-19 patients. *Cell.* 2020; 182 (4): 843–54.
8. Chi X, Yan R, Zhang J, et al. A neutralizing human antibody binds to the N-terminal domain of the spike protein of SARS-CoV-2. *Science.* 2020; 369 (6504): 650–5.

- to the N-terminal domain of the spike protein of SARS-CoV-2. *Science*. 2020; 369 (6504): 650–5.
9. Piccoli L, Park Y, Tortorici M, et al. Mapping neutralizing and immunodominant sites on the SARS-CoV-2 Spike Receptor-Binding Domain by structure-guided high-resolution serology. *Cell*. 2020; 183 (4): 1024–42.
 10. Gaebler C, Wang Z, Lorenzi JCC, et al. Evolution of antibody immunity to SARS-CoV-2. *Nature*. 2021; 591, 639–44.

GUT MICROBIOTA ALTERATIONS AND THEIR RELATIONSHIP TO THE DISEASE SEVERITY AND SOME CYTOKINE PROFILE INDICATORS IN PATIENTS WITH COVID-19

Gumenyuk LN, Golod MV, Silaeva NV, Sorokina LE [✉], Ilyasov SS, Androschuk NA, Krivoshapko OR, Velilyaev AM, Asanova LN

Vernadsky Crimean Federal University, Simferopol, Russia

Gut microbiota is an essential element of maintaining the immune homeostasis, including in individuals with COVID-19. The study was aimed to assess taxonomic changes in the gut microbiota and their relationship with the disease severity and the levels of IL6, IL10, IL17, and TNF α in patients with COVID-19. A total of 110 patients with COVID-19 (index group) and 98 individuals with no COVID-19 (control group) were enrolled to the comparative cross-sectional study. The gut microbiota composition was determined by shotgun sequencing. Blood serum levels of IL6, IL10, IL17, and TNF α were assessed by enzyme-linked immunosorbent assay. The following significant changes in the gut microbiota composition were observed in patients with COVID-19 in contrast to controls: decreased abundance of *B. adolescentis* ($p = 0.048$), *E. rectale* ($p = 0.036$), *F. prausnitzii* ($p = 0.0002$), *B. dorei* ($p < 0.001$), and increased abundance of *R. gnavus* ($p = 0.012$), *Cl. hathewayi* ($p = 0.003$), *E. faecium* ($p = 0.0003$). Correlations were established between the abundance of *B. dorei* and the IL6 levels ($r = 0.49$; $p = 0.034$), the abundance of *F. prausnitzii* and the levels of IL10, IL17 ($r = 0.44$; $p = 0.001$ and $r = -0.52$; $p < 0.001$, respectively). The abundance of *R. gnavus* correlated with the TNF α levels, and the abundance of *E. faecium* was related to the levels of IL6 ($r = 0.47$; $p = 0.002$) and TNF α ($r = 0.56$; $p = 0.001$). The relationship between the abundance of *B. dorei*, *F. prausnitzii*, *E. faecium* and the higher SHOKS-COVID clinical assessment scale scores was also revealed ($r = -0.54$; $p = 0.001$, $r = -0.60$; $p < 0.001$ and $r = 0.67$; $p = 0.005$, respectively). Targeted correction of gut microbiota may improve the COVID-19 treatment efficacy.

Keywords: COVID-19, SARS-CoV-2, gut microbiota, cytokine status

Author contribution: Gumenyuk LN, Sorokina LE — significant contribution to the study concept and design; Golod MV, Silaeva NV, Androschuk NA — data acquisition, analysis, and interpretation; Ilyasov SS — statistical data processing; Krivoshapko OR, Velilyaev AM, Asanova LN — manuscript writing.

Compliance with ethical standards: the study was approved by the Ethics Committee of the S.I. Georgievsky Medical Academy, V.I. Vernadsky Crimean Federal University (protocol № 11 dated November 23, 2021), planned and conducted in accordance with the Declaration of Helsinki. The informed consent was obtained from all study participants.

✉ **Correspondence should be addressed:** Leya E. Sorokina
Bulvar Lenina, 5/7, Simferopol, 295006, Republic of Crimea; leya.sorokina@mail.ru

Received: 18.01.2022 **Accepted:** 02.02.2022 **Published online:** 19.02.2022

DOI: 10.24075/brsmu.2022.006

ИЗМЕНЕНИЯ МИКРОБИОТЫ КИШЕЧНИКА И ИХ СВЯЗЬ С ТЯЖЕстью ЗАБОЛЕВАНИЯ И НЕКОТОРЫМИ ПОКАЗАТЕЛЯМИ ЦИТОКИНОВОГО ПРОФИЛЯ У ПАЦИЕНТОВ С COVID-19

Л. Н. Гуменюк, М. В. Голод, Н. В. Силаева, Л. Е. Сорокина [✉], С. С. Ильясов, Н. А. Андрощук, О. Р. Кривошапко, А. М. Велиляев, Л. Н. Асанова

Крымский федеральный университет имени В. И. Вернадского, Симферополь, Россия

Важной составляющей поддержания иммунного гомеостаза в том числе при COVID-19 является микробиота кишечника. Целью работы было изучить изменения таксономического состава микробиоты кишечника и характер их взаимосвязи с тяжестью заболевания, содержанием IL6, IL10, IL17 и TNF α у пациентов с COVID-19. В одномоментном сравнительном исследовании приняли участие 110 пациентов с COVID-19 (основная группа) и 98 лиц, не инфицированных COVID-19 (контрольная группа). Оценка состава микробиоты кишечника проводили методом шотган-секвенирования. Уровень IL6, IL10, IL17 и TNF α в сыворотке крови определяли с помощью твердофазного иммуноферментного анализа. Обнаружены статистически значимые изменения в составе кишечной микробиоты у пациентов с COVID-19 в отличие от контрольной группы: снижение численности *B. adolescentis* ($p = 0,048$), *E. rectale* ($p = 0,036$), *F. prausnitzii* ($p = 0,0002$), *B. dorei* ($p < 0,001$) и повышение численности *R. gnavus* ($p = 0,012$), *Cl. hathewayi* ($p = 0,003$), *E. faecium* ($p = 0,0003$). Установлена корреляция численности *B. dorei* с показателем IL6 ($r = 0,49$; $p = 0,034$), численности *F. prausnitzii* и показателей IL10, IL17 ($r = 0,44$; $p = 0,001$ и $r = -0,52$; $p < 0,001$ соответственно). Численность *R. gnavus* коррелировала с показателем TNF α , а численность *E. faecium* — с IL6 ($r = 0,47$; $p = 0,002$) и TNF α ($r = 0,56$; $p = 0,001$). Также выявлена сопряженность численности *B. dorei*, *F. prausnitzii* и *E. faecium* с более высокими баллами по шкале оценки клинического состояния ШОКС-КОВИД ($r = -0,54$; $p = 0,001$, $r = -0,60$; $p < 0,001$ и $r = 0,67$; $p = 0,005$ соответственно). Направленная коррекция кишечной микробиоты может улучшить эффективность лечения COVID-19.

Ключевые слова: COVID-19, SARS-CoV-2, микробиота кишечника, цитокиновый статус

Вклад авторов: Л. Н. Гуменюк, Л. Е. Сорокина — существенный вклад в замысел и дизайн исследования; М. В. Голод, Н. В. Силаева, Н. А. Андрощук — сбор, анализ и интерпретация данных; С. С. Ильясов — статистическая обработка данных; О. Р. Кривошапко, А. М. Велиляев, Л. Н. Асанова — подготовка рукописи.

Соблюдение этических стандартов: исследование одобрено этическим комитетом Крымской медицинской академии им. С. И. Георгиевского ФГАОУ ВО «Крымский федеральный университет им. В. И. Вернадского» (протокол № 11 от 23 ноября 2021 г.), спланировано и проведено в соответствии с Хельсинской декларацией. Все лица, включенные в исследование, подписали добровольное информированное согласие.

✉ **Для корреспонденции:** Лея Евгеньевна Сорокина
бул. Ленина, 5/7, г. Симферополь, 295006, Республика Крым; leya.sorokina@mail.ru

Статья получена: 18.01.2022 **Статья принята к печати:** 02.02.2022 **Опубликована онлайн:** 19.02.2022

DOI: 10.24075/vrgmu.2022.006

World Health Organization declared the pandemic in response to the novel coronavirus infection, caused by the SARS-CoV-2 virus, which was named COVID-19 [1]. Severe forms of this disorder are associated with progressive viral pneumonia and acute respiratory distress syndrome (ARDS). The increasing systemic inflammation plays a vital part in the COVID-19 pathophysiology. Excessive cytokine production, which is

caused by SARS-CoV-2 and known as cytokine storm, is closely related to the disease severity [2]. High levels of interleukins IL1 α , IL1RA, IL6, IL8, IL9, IL10, IL17, C-reactive protein (CRP), tumor necrosis factor (TNF α), are found in patients with COVID-19 [3–5].

Accumulated data of the *in vitro* and *in vivo* studies show that gastrointestinal tract (GIT) is also susceptible to COVID-19. For

example, studying the *in vitro* model, simulating the cellular and spatial intestinal structure, showed the SARS-CoV-2 capability of infecting enterocytes [6]. The frequency of gastrointestinal symptoms in patients with COVID-19 reaches 20% [7]. This is caused by the SARS-CoV-2 ability to enter cells by binding to the angiotensin-converting enzyme 2 (ACE2) receptor, which is intensively expressed on the enterocyte surface in the ileum and colon. The latter results in gastrointestinal symptoms due to the virus-induced immune-mediated damage [8]. Moreover, viral RNA of SARS-CoV-2 can be detected in fecal samples more than 30 days after the disease onset [9]. In this regard the role played by gut microbiota is actively discussed in literature. As is known, gut microbiota is an essential element of maintaining the immune homeostasis. For its part, gut microbiota dysbiosis is directly related to numerous inflammatory disorders [10]. Strong evidence of quantitative changes in the gut microbiota of patients with COVID-19 is provided [11]. In general, a downward trend in the bacterial species diversity is observed in patients with COVID-19, together with the depletion of beneficial commensals and enrichment in pathobionts [12]. However, information about the species composition of gut microbiota is fragmented and conflicting. Taking into account the potential of interactions, realized through the gut-lung axis, to increase the host susceptibility to viral infections and reduce the functional activity of immune cells, thus contributing to systemic hyperinflammation and cytokine storm syndrome, further investigation of the gut microbiota alterations and their relationship with the cytokine status indicators in patients with COVID-19 is relevant.

The study was aimed to assess taxonomic changes in the gut microbiota and their relationship with the disease severity and the levels of IL6, IL10, IL17, and TNF α in patients with COVID-19.

METHODS

A total of 110 patients with COVID-19 (66 females (60.0%), 44 males (40.0%); the average age was 28.6 ± 8.4 years), who had been admitted to hospitals, working in the Obligatory Medical Insurance system in Simferopol (index group, IG), and 98 healthy volunteers with no COVID-19 (61 females (62.2%), 37 males (37.8%); the average age was 29.2 ± 7.6 years), who had their annual health examination at the Gemokod medical center, Simferopol (control group, CG), were enrolled to the comparative cross-sectional study by continuous sampling.

Inclusion criteria for the IG: age 18–45 years; COVID-19, confirmed by positive polymerase chain reaction (PCR) test for the SARS-CoV-2 RNA and/or the typical multislice computed tomography (CT) findings of viral pneumonia; mild, moderate or severe COVID-19.

Exclusion criteria for the IG: extremely severe COVID-19; type 1 or 2 diabetes mellitus; obesity; myocardial infarction, severe cardiac arrhythmias, heart failure; history of hypertensive disease, stroke, transient ischemic attack; acute cerebrovascular disease (within six months before the beginning of the study); severe or decompensated concomitant somatic diseases, which could make it more difficult for the patient to participate in the study and affect the study results;

irritable bowel syndrome; chronic gastrointestinal and liver diseases; hematological and oncological diseases; history of mental disorders, alcoholism or drug addiction; taking antibiotics, probiotics, prebiotics, antiviral drugs, symbiotics or acid-suppression medications within three months before the beginning of the study; taking medications, affecting the passage of stool, within a month before the beginning of the study; refusal to participate in research.

Inclusion criteria for healthy volunteers: age 18–45 years; no COVID-19, confirmed by PCR test for the SARS-CoV-2 RNA; no chronic disorders or allergic reactions; no infectious or acute disorders within two months before the study; no history of mental disorders, alcoholism or drug addiction; no abnormal passage of stool (constipation/diarrhea); taking no antibiotics, probiotics, prebiotics, antiviral drugs or symbiotics within three months before the beginning of the study; taking no medications, affecting the passage of stool, within a month before the beginning of the study.

Exclusion criteria for healthy volunteers: body temperature above 36.9 °C; refusal to participate in research.

Characteristics of patients with COVID-19 and healthy volunteers are presented in Table 1. The groups were comparable in gender ($p = 0.96$; χ^2), age ($p = 0.92$; χ^2), and body mass index ($p = 0.054$; χ^2).

Clinical characteristics of patients with COVID-19 are provided in Table 2. Individuals with moderate COVID-19 (80 patients (72.7 \pm 0.68%)) predominated among patients. Fever (103 patients (94.2%)) and cough (96 patients (86.9 \pm 0.61%)) were the most common symptoms of the disease. According to CT images, viral pneumonia was diagnosed in 95 patients (67.1 \pm 0.38%).

In all patients, the diagnosis of COVID-19 was confirmed by PCR test for SARS-CoV-2 (specimens were obtained from nasopharyngeal and oropharyngeal swabs) and/or typical multislice CT findings of viral pneumonia. The diagnosis and severity of COVID-19, as well as the extent of pneumonia on CT images, were assessed in accordance with the Temporary Guidelines on Prevention, Diagnosis and Treatment of Novel Coronavirus Infection (COVID-19) of the Ministry of Health of the Russian Federation, versions 6–9.

The original Clinical Assessment Scale for patients with coronavirus infection (SHOKS-COVID) was used to objectify the severity of clinical manifestations [13].

In order to analyze the taxonomic composition of the patients' gut microbiota, fecal samples were collected on the first day of hospital stay (in the morning, 8 a.m. to 10 a.m.). The samples were frozen and stored in disposable plastic containers at a temperature of -80 °C before the metagenomic analysis. Total DNA was isolated by the phenol-based extraction. Nucleotide sequence of the DNA isolated was determined by shotgun sequencing using the SOLiD 5500 Wildfire system for high-throughput sequencing (AppliedBiosystems; USA) [14].

QIIME software version 1.9.1 was used to filter the reads based on their quality and perform taxonomic classification [15]. The approach, involving the use of two taxonomic databases, was applied to perform the taxonomic assignment of the reads. At the first stage, the reference set of the bacterial

Table 1. Characteristics of patients with COVID-19 and healthy volunteers

Indicators	Index group ($n = 110$)	Control group ($n = 98$)
Females / males ($n, \%$)	66 (60.0) / 44 (40.0)	61 (62.2) / 37 (37.8)
Average age years ($M \pm CD$)	28.6 ± 8.4	29.2 ± 7.6
Body mass index, kg/m^2 ($M \pm CD$)	23.4 ± 4.2	23.7 ± 3.6

Table 2. Clinical characteristics of patients with COVID-19

Indicator	Index group (n = 110)
Mild course (n, %)	7 (6.3)
Moderate course (n, %)	80 (72.7)
Severe course (n, %)	23 (21.0)
Fever	103 (94.2)
Sore throat	68 (61.8)
Cough	96 (86.9)
Shortness of breath	63 (56.9)
Nausea	37 (33.6)
Diarrhea	24 (22.1)
Temperature, median [25%; 75%]	37.8 [36.7; 37.9]
RR per minute, median [25%; 75%]	20.0 [17.0; 22.0]
HR, beats/min (m ± CD)	89.9 ± 16.1
SBP, mm Hg, median [25%; 75%]	120 [120; 132]
SO ₂ , %, median [25%; 75%]	96.0 [94.0; 98.0]
Severity of the condition, SHOKS-COVID score, points, Me [25%; 75%]	3.4 [1.6; 6.1]
CT stage — 0 (n, %)	25 (22.6)
CT stage CT-1 (n, %)	41 (37.4)
CT stage CT-2 (n, %)	32 (29.1)
CT stage CT-3 (n, %)	12 (10.9)

Note: RR — respiratory rate, HR — heart rate, SBP — systolic blood pressure, SO₂ — oxygen saturation, CT — computed tomography.

operational taxonomic units (OTUs) was selected based on the comparison of the 16s rRNA gene reads obtained with the GreenGenes database, version 13.5 [16]. At the second stage, taxonomic assignment of these OTUs was performed using the RDP algorithm based on the custom human intestinal database, HITdb [17].

Qualitative and quantitative assessment of the gut microbiota composition involved identification of species, genera, and phyla of microorganisms. Assessment of α -diversity by calculating the Chao1 index, number of the taxa observed (Sobs), and the indicator of species richness (ACE), was performed with the Mothur v.1.22.0 software (<http://www.mothur.org>).

IL6, IL10, IL17 and TNF α were selected as the cytokine profile markers, which was due to their key role in the pathogenesis of cytokine storm and ARDS [3–5].

Blood samples were collected from peripheral vein during the first day of hospital stay. Blood was taken in the morning (between 7 and 9 a.m.) in a fasting state at rest (for at least 15 min). Test tubes containing blood serum were frozen and stored at a temperature of –20 °C. Serum levels of IL6, IL10, IL17, and TNF α were assessed using the enzyme-linked immunosorbent assay (ELISA) test system (Vector-Best; Vector-Best; Novosibirsk, Russia) with the Elisys Quattro automated ELISA analyzer (Human GmbH; Germany).

Statistical data processing was performed using the STATISTICA 8.0 software package (StatSoft. Inc.; USA). In case of normal distribution, the mean and the standard deviation were defined, and in case of non-normal distribution, the median, 25th and 75th percentiles were calculated. Distributions were tested for normality using the Gaussian distribution. Percentage and absolute values were defined for qualitative traits. Comparative analysis for the normal distribution of quantitative traits was performed using the parametric Student's *t*-test. In case of non-normal distribution it was performed using the Mann–Whitney *U* test, and comparative analysis of quantitative traits was carried out using the chi-squared test (χ^2). Spearman's correlation coefficient was used to assess the relationship between the traits. The differences were considered significant

when $p < 0.05$. Correlation analysis and multiple rank correlation were also applied, and the correlations' significance was tested with the contingency tables.

RESULTS

Assessing the taxonomic composition of gut microbiota revealed a significant decrease in the α -diversity of the bacterial community (Chao1 index; $p = 0.016$) in patients with COVID-19 compared to controls. The ACE and Sobs indices were also slightly decreased in the group of patients with COVID-19 compared to the CG, however, no significant differences were observed ($p = 0.054$; $p = 0.052$, respectively) (Fig. 1).

Comparison of the species composition of gut microbiota revealed a significant decrease in the abundance of *Bifidobacterium adolescentis* SPM1005-A ($p = 0.048$), *Eubacterium rectale* ATCC 33656 ($p = 0.036$), *Faecalibacterium prausnitzii* A2-165 ($p = 0.0002$), *Bacterioides dorei* DSM 17855 ($p = 0.001$) in patients with COVID-19 compared to controls, together with the increased abundance of *Ruminococcus gnavus* ATCC 29149 ($p = 0.012$), *Clostridium hathewayi* DSM-13479 ($p = 0.003$), and *Enterococcus faecium* W54 ($p = 0.0003$) (Fig. 2).

Serum levels of IL6, IL10, IL17, and TNF α were significantly higher in patients with COVID-19 compared to the CG (Table 3).

Clarification of the relationship between the gut microbiota alterations and some cytokine profile indicators in patients with COVID-19 revealed significant correlations between the abundance of *B. dorei* and the IL6 levels ($r = -0.49$; $p = 0.034$), abundance of *F. prausnitzii* and the IL10, IL17 levels ($r = -0.44$; $p = 0.001$ and $r = -0.52$; $p < 0.001$, respectively). The abundance of *R. gnavus* correlated with the levels of TNF α ($r = 0.51$; $p = 0.036$), and the abundance of *E. faecium* was related to the levels of IL6 ($r = 0.47$; $p = 0.002$) and TNF α ($r = 0.56$; $p = 0.001$). Correlation analysis also revealed the relationship between the abundance of *B. dorei*, *F. prausnitzii*, *E. faecium*, and the higher SHOKS-COVID scores ($r = -0.54$ and $p = 0.001$; $r = -0.60$ and $p < 0.001$; $r = 0.67$ and $p = 0.005$, respectively).

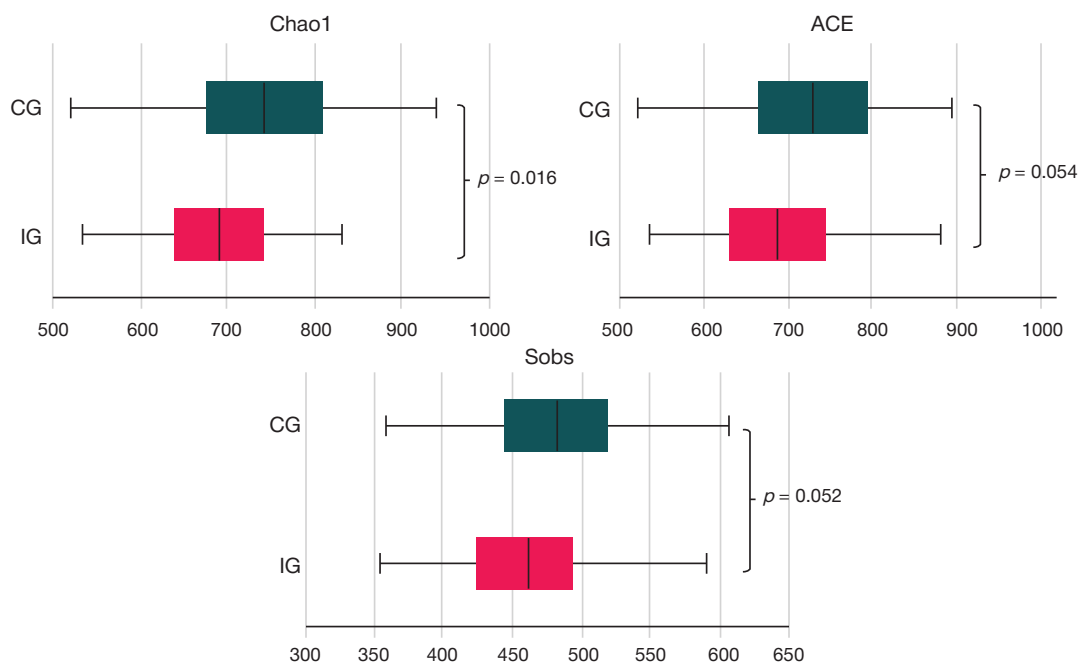


Fig. 1. Comparative analysis of the gut microbiota phylogenetic composition in patients with COVID-19 and healthy volunteers. IG — index group, CG — control group

DISCUSSION

In a number of previous studies, alterations in the composition of gut microbiota in patients with COVID-19 have been reported [7, 11, 12]. Our findings have also shown significant differences in the composition of gut microbiota between patients with COVID-19 and individuals with no COVID-19. According to our data, patients with COVID-19 have a lower bacterial α -diversity compared to individuals with no COVID-19, which is confirmed by the significantly lower Chao1 index and is consistent with the results of previous studies [11]. In patients with COVID-19, gut dysbiosis is characterized by the decreased abundance of bacteria having the immunomodulatory potential, the type

representatives *B. adolescentis*, *E. rectale*, *F. prausnitzii*, *B. dorei*, that are known to be the main butyrate-producing bacteria (butyrate is a powerful anti-inflammatory metabolite). At the same time, we have revealed the increased abundance of potential pathobionts: the bacteria *R. gnavus*, *Cl. hathewayi*, and *E. faecium*. Among them, *E. faecium* is noteworthy, the presence of which in fecal samples of patients with COVID-19 has been previously reported by Italian researchers [18]. High levels of *E. faecium* in the gut microbiota of critically ill patients could be of some clinical significance due to the *E. faecium* pathogenic potential, resistance to common antimicrobial drugs, and the ability to rapidly acquire genetic material or alter gene expression, allowing the bacteria to acquire the

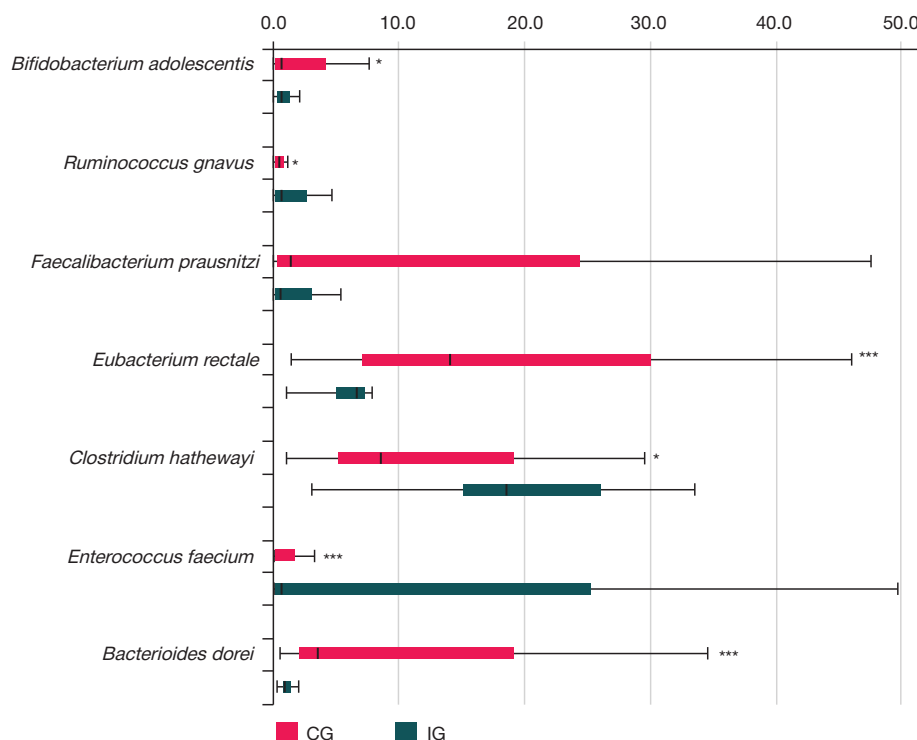


Fig. 2. Comparative analysis of the genus-level gut microbiota composition in patients with COVID-19 and healthy volunteers. IG — index group, CG — control group

Table 3. Comparative analysis of cytokine profile in patients with COVID-19 and healthy volunteers ($m \pm CD$)

Indicator	Index group $n = 110$	Control group $n = 98$	p
IL6, pg/mL	10.5 \pm 6.6	3.8 \pm 1.8	$p = 0.036$
IL10, pg/mL	9.3 \pm 5.4	2.9 \pm 1.1	$p = 0.021$
IL17, pg/mL	4.9 \pm 2.2	2.4 \pm 1.1	$p = 0.046$
TNF α , pg/mL	17.9 \pm 8.6	5.2 \pm 2.4	$p = 0.012$

resistance determinants to almost all antibacterial agents [19, 20]. Independently from the strain of the genus *Enterococcus*, gut microbiota of patients with COVID-19 can therefore function as a reservoir of the potentially antibiotic-resistant opportunistic pathogens, able to migrate through the damaged epithelial barrier into the systemic circulation, as has already been shown in the context of other disorders [20]. Our findings are to some extent consistent with the previously reported research data. For example, in one of the studies, patients with COVID-19 were characterized by the decreased abundance of *B. dorei*, and the increased abundance of *E. faecium* [18]. In another study, patients with COVID-19 were characterized by the decreased abundance of *B. adolescentis*, *E. rectale*, *F. prausnitzii*, and the increased abundance of bacteria *R. gnavus* [21]. The contrasting data patterns could be due to the fact, that the studies were carried out in different geographic regions with the use of different inclusion criteria. The groups varied considerably in age: 28.6 \pm 8.4 years in our study vs. 73.0 [59.0; 85.0] in the previously reported study [18], and 36.4 \pm 18.7 years in the study [21]. Moreover, in contrast to the listed above researchers, we did not study patients with somatic comorbidities and patients, taking antibacterial and/or antiviral medications, in order to mitigate their influence on the study results.

Despite the fact that some bacteria identified could be common to a number of other disorders, both gastrointestinal and systemic, the determined relationship between the decreased levels of *B. dorei*, *F. prausnitzii*, increased levels of *E. faecium* and the higher SHOKS-COVID scores suggests that changes in the abundance of these bacteria may be typical for this cohort of patients with COVID-19. We have compared the associations determined with the results of earlier studies. Thus, depletion of members of the genus *Bacteroides* was observed in patients, admitted to the intensive care unit [18]. It is interesting that in another study [7], the abundance of *B. dorei* negatively correlated with the SARS-CoV-2 load in the faeces of patients with COVID-19. The researchers noted that, taking into account the association of this bacterium with the decreased ACE2 receptor expression in the murine colon, *B. dorei* could potentially provide protection against the SARS-CoV-2 virus. Data are presented on the negative correlation between the bacterium *F. prausnitzii*, known for its anti-inflammatory effect, and the COVID-19 severity [7]. At the same time, higher abundance of strains of the genus *Enterococcus* ($p = 0.0001$) was observed in patients with COVID-19, admitted to the intensive care units, compared to patients, admitted to the general medicine units [18]. It can be assumed that therapeutic upscaling of *B. dorei*, *F. prausnitzii* together with the *E. faecium* downscaling is effective for mitigation of the disease severity. However, further research with appropriate design is required to confirm this hypothesis. Some authors point out that prebiotics and/or probiotics may be used as a potential (additional) vector of the COVID-19 therapy to reduce the disease severity and minimize the risk of secondary bacterial infections [22, 23].

A number of studies have proven the impact of gut microbiota on the susceptibility to infectious and noncommunicable diseases [24]. It has been specified that the intestinal flora

immunomodulatory effect is realized through activation of genes, encoding a number of cytokines in the immune and epithelial cells, which determines heterogeneity of their immunomodulatory properties [25]. It has been reported that heterogeneity of the immunoregulatory effects is typical for both dominant and associative microsymbionts [26]. Thus, cumulative effects of the normal bacterial flora representatives on the secretion of cytokines by human immune cells in the conditions of eubiosis ensure the cytokine balance, characterized by moderate levels of pro-inflammatory cytokines (IL6, TNF α) and regulated by the suppressing effects of anti-inflammatory cytokines. Thus, in the context of increasing antigen load in dysbiosis through activation of toll-like receptors, the increased production of a whole range of pro-inflammatory cytokines is observed. These cytokines promote both local inflammation and the effector immune response in the gut-associated lymphoid tissue, protecting the body from pathogens [27].

As previously reported, COVID-19 infection is associated with the increased levels of cytokines IL6, IL10, IL17, and TNF α [4]. In our study, significant differences in the levels of IL6, IL10, IL17, and TNF β between patients with COVID-19 and healthy volunteers were also observed.

It is assumed that the COVID-19 severity results from the cytokine storm [4]. It is noteworthy that some of the listed above cytokines correlate with the gut microbiota pattern, the specific profile of which is capable of inducing the cytokine storm. Our study revealed the correlation between the abundance of bacteria *B. dorei* and the levels of IL6 in patients with COVID-19.

We have revealed the relationship between the abundance of bacteria *F. prausnitzii* and the levels of IL10, which could be mediated by the decreased secretion of metabolites, blocking the NF- κ B transcription factor activation and the IL8 production. For example, the in vivo study showed that activation of the peripheral blood mononuclear cells by *F. prausnitzii* resulted in the significantly reduced secretion of IL12 and TNF α , together with the increased secretion of IL10 [28]. Furthermore, the abundance of bacteria *F. prausnitzii* negatively correlated with the IL17 levels. When performing literature analysis, we have found no publications on studying the relationship between gut microbiota and IL17 in patients with COVID-19. At the same time, it has been shown that *F. prausnitzii* inhibits IL17 production in rats [29]. Studying the experimental colitis model has demonstrated that bacteria *F. prausnitzii* exert their anti-inflammatory effects due to production of butyrate, which maintains the balance between the pro-inflammatory T helper 17 cells (Th17) and immunoregulatory T cells (Treg) via inhibition of histone deacetylase 1. In turn, imbalance between Th17 and Treg promotes autoimmune inflammation [30].

We have also revealed the relationship between the abundance of the bacteria *Ruminococcus gnavus* and the TNF α levels. These data are consistent with the previously reported research results [31], showing that higher levels of *R. gnavus* in patients with COVID-19 correlate with the surge of pro-inflammatory cytokines IFN γ and TNF α , resulting in the cytokine storm and activation of the type 1 helper T cells.

We have discovered that the abundance of bacteria *E. faecium* correlates with the levels of IL6 and TNF α . We

have found the reports of similar correlations in patients with ulcerative colitis [32] and AIDS/HIV [33].

Thus, in the context of the COVID-19-associated gut dysbiosis, orientation of immunoregulatory effects towards pro- and anti-inflammatory cytokines is limited in the normal flora representatives, which contributes to the impaired homeostasis and the development of inflammatory and autoimmune responses.

CONCLUSIONS

The relationship between the decreased levels of bacteria *B. dorei*, *F. prausnitzii* together with the increased levels of bacteria *E. faecium* and the higher SHOKS-COVID scores has been defined in patients with COVID-19, which is indicative of

the pathognomonic nature of these taxonomic alterations of intestinal microflora in individuals, infected with SARS-CoV-2. Significant correlations between the abundance of gut bacteria *B. dorei*, *F. prausnitzii*, *R. gnavus*, *E. faecium* and the levels of IL6, IL10, IL17, TNF α have been found in the SARS-CoV-2-infected patients, which confirms the gut microbiota capability of being involved in systemic inflammation and maintaining the immune tolerance in COVID-19. Our findings in combination with the data reported in literature demonstrate the key role in the COVID-19 pathogenesis played by microbiota. The more systematic and detailed research in this area would enable the development of new approaches, as well as selective probiotics for microbiota correction in patients with COVID-19 and treatment of post-COVID effects.

References

- Statement on the second meeting of the International Health Regulations Emergency Committee regarding the outbreak of novel coronavirus (2019-nCoV). World Health Organization (WHO), 2020. Available from: [https://www.who.int/news-room/detail/30-01-2020-statement-on-the-second-meeting-of-the-international-health-regulations-\(2005\)-emergency-committee-regarding-the-outbreak-of-novel-coronavirus-\(2019-ncov\)](https://www.who.int/news-room/detail/30-01-2020-statement-on-the-second-meeting-of-the-international-health-regulations-(2005)-emergency-committee-regarding-the-outbreak-of-novel-coronavirus-(2019-ncov)) (assessed Dec 15, 2021).
- Tao W, Zhang G, Wang X, et al. Analysis of the intestinal microbiota in COVID-19 patients and its correlation with the inflammatory factor IL18. *Med Microecol.* 2020; 5: 100023. DOI:10.1016/j.medmic.2020.100023.
- Tay MZ, Poh CM, Rénia L, MacAry PA, Ng LFP. The trinity of COVID-19: immunity, inflammation and intervention. *Nat Rev Immunol.* 2020; 20 (6): 363–74. DOI: 10.1038/s41577-020-0311-8.
- Costela-Ruiz VJ, Illescas-Montes R, Puerta-Puerta JM, Ruiz C, Melguizo-Rodríguez L. SARS-CoV-2 infection: The role of cytokines in COVID-19 disease. *Cytokine Growth Factor Rev.* 2020; 54: 62–75. DOI: 10.1016/j.cytogfr.2020.06.001.
- Zhou F, Yu T, Du R, et al. Clinical course and risk factors for mortality of adult inpatients with COVID-19 in Wuhan, China: a retrospective cohort study. *Lancet.* 2020; 395: 1054–62. DOI: 10.1016/S0140-6736(20)30566-3.
- Lamers MM, Beumer J, van der Vaart J, et al. SARS-CoV-2 productively infects human gut enterocytes. *Science.* 2020; 369 (6499): 50–54. DOI: 10.1126/science.abc1669.
- Zuo T, Zhang F, Lui GCY, et al. Alterations in Gut Microbiota of Patients With COVID-19 During Time of Hospitalization. *Gastroenterology.* 2020; 159 (3): 944–55.e8. DOI:10.1053/j.gastro.2020.05.048.
- Guan WJ, Ni ZY, Hu Y, et al. Clinical Characteristics of Coronavirus Disease 2019 in China. *N Engl J Med.* 2020; 382 (18): 1708–20. DOI: 10.1056/NEJMoa2002032.
- Chan KH, Poon LL, Cheng VC, et al. Detection of SARS coronavirus in patients with suspected SARS. *Emerg Infect Dis.* 2004; 10 (2): 294–9. DOI: 10.3201/eid1002.030610.
- Wu HJ, Wu E. The role of gut microbiota in immune homeostasis and autoimmunity. *Gut Microbes.* 2012; 3 (1): 4–14. DOI: 10.4161/gmic.19320.
- Gu S, Chen Y, Wu Z, et al. Alterations of the Gut Microbiota in Patients With Coronavirus Disease 2019 or H1N1 Influenza. *Clin Infect Dis.* 2020; 71 (10): 2669–78. DOI: 10.1093/cid/ciaa709.
- Zuo T, Liu Q, Zhang F, et al. Depicting SARS-CoV-2 faecal viral activity in association with gut microbiota composition in patients with COVID-19. *Gut.* 2021; 70 (2): 276–84. DOI: 10.1136/gutjnl-2020-322294.
- Mareev VYu, Begrambekova YuL, Mareev YuV. Kak ocenivat' rezul'taty lechenija bol'nyh s novoj koronavirusnoj infekciej (COVID-19)? Shkala Ocenki Klinicheskogo Sostojanija (ShOKS-KOVID). *Kardiologija.* 2020; 60 (11): 35–41. Russian.
- Mitra S, Forster-Fromme K, Damms-Machado A, et al. Analysis of the intestinal microbiota using SOLiD16S rRNA gene sequencing and SOLiD shotgun sequencing. *BMC Genomics.* 2013; 14 (5): 16.
- Caporaso JG, Kuczynski J, Stombaugh J, et al. QIIME allows analysis of high-throughput community sequencing data. *Nat Methods.* 2010; 7 (5): 335–6. DOI: 10.1038/nmeth.f.303.
- DeSantis, TZ, Hugenholtz P, Larsen N. Greengenes, a chimera-checked 16S rRNA gene database and workbench compatible with ARB. *Appl Environ Microbiol.* 2006; 72: 5069–72.
- Ritari J, Salojärvi J, Lahti L, de Vos WM. Improved taxonomic assignment of human intestinal 16S rRNA sequences by a dedicated reference database. *BMC Genomics.* 2015; 16 (1): 1056. DOI: 10.1186/s12864-015-2265-y.
- Gaibani P, D'Amico F, Bartoletti M, et al. The Gut Microbiota of Critically Ill Patients With COVID-19. *Front Cell Infect Microbiol.* 2021; 11: 670424. DOI: 10.3389/fcimb.2021.670424.
- Gilmore MS, Clewell DB, Ike Y, Shankar N, eds. *Enterococci: From Commensals to Leading Causes of Drug Resistant Infection.* Boston: Massachusetts Eye and Ear Infirmary, 2014.
- Tamburini FB, Andermann TM, Tkachenko E, Senchyna F, Banaei N, Bhatt AS. Precision identification of diverse bloodstream pathogens in the gut microbiome. *Nat Med.* 2018; 24 (12): 1809–14. DOI: 10.1038/s41591-018-0202-8.
- Yeoh YK, Zuo T, Lui GC, et al. Gut microbiota composition reflects disease severity and dysfunctional immune responses in patients with COVID-19. *Gut.* 2021; 70 (4): 698–06. DOI: 10.1136/gutjnl-2020-323020.
- Danilenko VN, Devyatkin AV, Marsova MV, et al. Common inflammatory mechanisms in COVID-19 and Parkinson's diseases: the role of microbiome, probiotics and postbiotics in their prevention. *Journal of Inflammation Research.* 2021; 14, 6349–81. DOI: 10.2147/JIR.S333887.
- Poluektova E, Yunes R, Danilenko V. The Putative Antidepressant Mechanisms of Probiotic Bacteria: Relevant Genes and Proteins. *Nutrients.* 2021; 13 (5): 1591. DOI: 10.3390/nu13051591.
- West CE, Renz H, Jenmalm MC, et al. The gut microbiota and inflammatory noncommunicable diseases: associations and potentials for gut microbiota therapies. *J Allergy Clin Immunol.* 2015; 135 (1): 3–14. DOI: 10.1016/j.jaci.2014.11.012.
- Sun Z, Song ZG, Liu C, et al. Gut microbiome alterations and gut barrier dysfunction are associated with host immune homeostasis in COVID-19 patients. *BMC Med.* 2022; 24: 20. DOI: 10.1186/s12916-021-02212-0.
- Buharin OV, Chajnikova IN, Ivanova EV, i dr. Immunoreguljatornyj profil' mikrosimbiontov kischechnogo biotopa cheloveka. *Zhurnal mikrobiologii, jepidemiologii i immunobiologii.* 2018; 4: 42–51. Russian.
- Hursitoglu M, Isiksacan N, Erismis B, et al. In-vitro cytokine production and nasopharyngeal microbiota composition in the early stage of COVID-19 infection. *Cytokine.* 2022; 149: 155757. DOI: 10.1016/j.cyto.2021.155757.

28. Sokol H, Pigneur B, Watterlot L, et al. Faecalibacterium prausnitzii is an anti-inflammatory commensal bacterium identified by gut microbiota analysis of Crohn disease patients. *Proc Natl Acad Sci USA*. 2008; 105 (43): 16731–6. DOI: 10.1073/pnas.0804812105.
29. Zhang M, Qiu X, Zhang H, et al. Faecalibacterium prausnitzii inhibits interleukin-17 to ameliorate colorectal colitis in rats. *PLoS One*. 2014; 9 (10): e109146. DOI: 10.1371/journal.pone.0109146.
30. Zhou L, Zhang M, Wang Y, et al. Faecalibacterium prausnitzii Produces Butyrate to Maintain Th17/Treg Balance and to Ameliorate Colorectal Colitis by Inhibiting Histone Deacetylase 1. *Inflamm Bowel Dis*. 2018; 24 (9): 1926–40. DOI: 10.1093/ibd/izy182.
31. van der Lelie D, Taghavi S. COVID-19 and the Gut Microbiome: More than a Gut Feeling. *mSystems*. 2020; 5 (4): e00453-20. DOI: 10.1128/mSystems.00453-20.
32. Li L, Zhong Q. Correlation of intestinal microflora with cytokines and Toll-like receptors expression in patients with ulcerative colitis. *Infect Dis Inf*. 2017; 30 (6): 361–4. DOI: 10.3969/j.issn.1007-8134.2017.06.012.
33. Lu J, Ma SS, Zhang WY, Duan JP. Changes in peripheral blood inflammatory factors (TNF α and IL6) and intestinal flora in AIDS and HIV-positive individuals. *J Zhejiang Univ Sci B*. 2019; 20 (10): 793–802. DOI: 10.1631/jzus.B1900075.

Литература

1. Statement on the second meeting of the International Health Regulations Emergency Committee regarding the outbreak of novel coronavirus (2019-nCoV). World Health Organization (WHO), 2020. Available from: [https://www.who.int/news-room/detail/30-01-2020-statement-on-the-second-meeting-of-the-international-health-regulations-\(2005\)-emergency-committee-regarding-the-outbreak-of-novel-coronavirus-\(2019-ncov\)](https://www.who.int/news-room/detail/30-01-2020-statement-on-the-second-meeting-of-the-international-health-regulations-(2005)-emergency-committee-regarding-the-outbreak-of-novel-coronavirus-(2019-ncov)) (assessed Dec 15, 2021).
2. Tao W, Zhang G, Wang X, et al. Analysis of the intestinal microbiota in COVID-19 patients and its correlation with the inflammatory factor IL18. *Med Microecol*. 2020; 5: 100023. DOI:10.1016/j.medmic.2020.100023.
3. Tay MZ, Poh CM, Rénia L, MacAry PA, Ng LFP. The trinity of COVID-19: immunity, inflammation and intervention. *Nat Rev Immunol*. 2020; 20 (6): 363–74. DOI: 10.1038/s41577-020-0311-8.
4. Costela-Ruiz VJ, Illescas-Montes R, Puerta-Puerta JM, Ruiz C, Melguizo-Rodríguez L. SARS-CoV-2 infection: The role of cytokines in COVID-19 disease. *Cytokine Growth Factor Rev*. 2020; 54: 62–75. DOI: 10.1016/j.cytogfr.2020.06.001.
5. Zhou F, Yu T, Du R, et al. Clinical course and risk factors for mortality of adult inpatients with COVID-19 in Wuhan, China: a retrospective cohort study. *Lancet*. 2020; 395: 1054–62. DOI: 10.1016/S0140-6736(20)30566-3.
6. Lamers MM, Beumer J, van der Vaart J, et al. SARS-CoV-2 productively infects human gut enterocytes. *Science*. 2020; 369 (6499): 50–54. DOI: 10.1126/science.abc1669.
7. Zuo T, Zhang F, Lui GCY, et al. Alterations in Gut Microbiota of Patients With COVID-19 During Time of Hospitalization. *Gastroenterology*. 2020; 159 (3): 944–55.e8. DOI:10.1053/j.gastro.2020.05.048.
8. Guan WJ, Ni ZY, Hu Y, et al. Clinical Characteristics of Coronavirus Disease 2019 in China. *N Engl J Med*. 2020; 382 (18): 1708–20. DOI: 10.1056/NEJMoa2002032.
9. Chan KH, Poon LL, Cheng VC, et al. Detection of SARS coronavirus in patients with suspected SARS. *Emerg Infect Dis*. 2004; 10 (2): 294–9. DOI: 10.3201/eid1002.030610.
10. Wu HJ, Wu E. The role of gut microbiota in immune homeostasis and autoimmunity. *Gut Microbes*. 2012; 3 (1): 4–14. DOI: 10.4161/gmic.19320.
11. Gu S, Chen Y, Wu Z, et al. Alterations of the Gut Microbiota in Patients With Coronavirus Disease 2019 or H1N1 Influenza. *Clin Infect Dis*. 2020; 71 (10): 2669–78. DOI: 10.1093/cid/ciaa709.
12. Zuo T, Liu Q, Zhang F, et al. Depicting SARS-CoV-2 faecal viral activity in association with gut microbiota composition in patients with COVID-19. *Gut*. 2021; 70 (2): 276–84. DOI: 10.1136/gutjnl-2020-322294.
13. Мареев В. Ю., Беграмбекова Ю. Л., Мареев Ю. В. Как оценивать результаты лечения больных с новой коронавирусной инфекцией (COVID-19)? Шкала Оценки Клинического Состояния (ШОКС–КОВИД). *Кардиология*. 2020; 60 (11): 35–41.
14. Mitra S, Forster-Fromme K, Damms-Machado A, et al. Analysis of the intestinal microbiota using SOLiD16S rRNA gene sequencing and SOLiD shotgun sequencing. *BMC Genomics*. 2013; 14 (5): 16.
15. Caporaso JG, Kuczynski J, Stombaugh J, et al. QIIME allows analysis of high-throughput community sequencing data. *Nat Methods*. 2010; 7 (5): 335–6. DOI: 10.1038/nmeth.f.303.
16. DeSantis, TZ, Hugenholtz P, Larsen N. Greengenes, a chimeric-checked 16S rRNA gene database and workbench compatible with ARB. *Appl Environ Microbiol*. 2006; 72: 5069–72.
17. Ritari J, Salojärvi J, Lahti L, de Vos WM. Improved taxonomic assignment of human intestinal 16S rRNA sequences by a dedicated reference database. *BMC Genomics*. 2015; 16 (1): 1056. DOI: 10.1186/s12864-015-2265-y.
18. Gaibani P, D'Amico F, Bartoletti M, et al. The Gut Microbiota of Critically Ill Patients With COVID-19. *Front Cell Infect Microbiol*. 2021; 11: 670424. DOI: 10.3389/fcimb.2021.670424.
19. Gilmore MS, Clewell DB, Ike Y, Shankar N, eds. *Enterococci: From Commensals to Leading Causes of Drug Resistant Infection*. Boston: Massachusetts Eye and Ear Infirmary, 2014.
20. Tamburini FB, Andermann TM, Tkachenko E, Senchyna F, Banaei N, Bhatt AS. Precision identification of diverse bloodstream pathogens in the gut microbiome. *Nat Med*. 2018; 24 (12): 1809–14. DOI: 10.1038/s41591-018-0202-8.
21. Yeoh YK, Zuo T, Lui GC, et al. Gut microbiota composition reflects disease severity and dysfunctional immune responses in patients with COVID-19. *Gut*. 2021; 70 (4): 698–06. DOI: 10.1136/gutjnl-2020-323020.
22. Danilenko VN, Devyatkin AV, Marsova MV, et al Common inflammatory mechanisms in COVID-19 and Parkinson's diseases: the role of microbiome, pharmabiotics and postbiotics in their prevention. *Journal of Inflammation Research*. 2021; 14, 6349–81. DOI: 10.2147/JIR.S333887.
23. Poluektova E, Yunes R, Danilenko V. The Putative Antidepressant Mechanisms of Probiotic Bacteria: Relevant Genes and Proteins. *Nutrients*. 2021; 13 (5): 1591. DOI: 10.3390/nu13051591.
24. West CE, Renz H, Jenmalm MC, et al. The gut microbiota and inflammatory noncommunicable diseases: associations and potentials for gut microbiota therapies. *J Allergy Clin Immunol*. 2015; 135 (1): 3–14. DOI: 10.1016/j.jaci.2014.11.012.
25. Sun Z, Song ZG, Liu C, et al. Gut microbiome alterations and gut barrier dysfunction are associated with host immune homeostasis in COVID-19 patients. *BMC Med*. 2022; 24: 20. DOI: 10.1186/s12916-021-02212-0.
26. Бухарин О. В., Чайникова И. Н., Иванова Е. В. и др. Иммунорегуляторный профиль микросимбионтов кишечного биотопа человека. *Журнал микробиологии, эпидемиологии и иммунобиологии*. 2018; 4: 42–51.
27. Hursitoglu M, Isiksacan N, Erisimis B, et al. In-vitro cytokine production and nasopharyngeal microbiota composition in the early stage of COVID-19 infection. *Cytokine*. 2022; 149: 155757. DOI: 10.1016/j.cyto.2021.155757.
28. Sokol H, Pigneur B, Watterlot L, et al. Faecalibacterium prausnitzii is an anti-inflammatory commensal bacterium identified by gut microbiota analysis of Crohn disease patients. *Proc Natl Acad Sci USA*. 2008; 105 (43): 16731–6. DOI: 10.1073/pnas.0804812105.
29. Zhang M, Qiu X, Zhang H, et al. Faecalibacterium prausnitzii inhibits interleukin-17 to ameliorate colorectal colitis in rats. *PLoS One*. 2014; 9 (10): e109146. DOI: 10.1371/journal.pone.0109146.
30. Zhou L, Zhang M, Wang Y, et al. Faecalibacterium prausnitzii Produces Butyrate to Maintain Th17/Treg Balance and to Ameliorate Colorectal Colitis by Inhibiting Histone Deacetylase 1. *Inflamm Bowel Dis*. 2018; 24 (9): 1926–40. DOI: 10.1093/ibd/

31. van der Lelie D, Taghavi S. COVID-19 and the Gut Microbiome: More than a Gut Feeling. *mSystems*. 2020; 5 (4): e00453-20. DOI: 10.1128/mSystems.00453-20.
32. Li L, Zhong Q. Correlation of intestinal microflora with cytokines and Toll-like receptors expression in patients with ulcerative colitis. *Infect Dis Inf*. 2017; 30 (6): 361–4. DOI: 10.3969/j.issn.1007-8134.2017.06.012.
33. Lu J, Ma SS, Zhang WY, Duan JP. Changes in peripheral blood inflammatory factors (TNF α and IL6) and intestinal flora in AIDS and HIV-positive individuals. *J Zhejiang Univ Sci B*. 2019; 20 (10): 793–802. DOI: 10.1631/jzus.B1900075.

MEROPENEM-INDUCED REDUCTION IN COLISTIN SUSCEPTIBILITY IN *PSEUDOMONAS AERUGINOSA* STRAIN ATCC 27853

Savinova TA ✉, Bocharova YuA, Chaplin AV, Korostin DO, Shamina OV, Mayansky NA, Chebotar IV

Pirogov Russian National Research Medical University, Moscow, Russia

Antibiotic-resistant strains of *Pseudomonas aeruginosa* are a global threat to public health. The knowledge of mechanisms underlying antibiotic resistance is essential to counter *P. aeruginosa* infections. This study describes the phenomenon of meropenem-induced cross-resistance to colistin in the ATCC 27853 strain of *P. aeruginosa*. The study was conducted in the specimens of *P. aeruginosa* grown from the reference ATCC 27853 strain in the medium containing meropenem gradients. Susceptibility of the isolates to carbapenems and colistin was assessed using the agar dilution method; susceptibility to colistin was assessed using the broth microdilution method. A total of 93 *P. aeruginosa* isolates were analyzed; of them two demonstrated reduced susceptibility to carbapenems (meropenem, imipenem) and colistin. Whole-genome sequencing of the isolates was performed on a MGISEQ-2000 platform. Missense mutations in the *oprD* and *mexD* genes and a nonsense mutation in the *phoQ* gene were detected. We conclude that exposure of *P. aeruginosa* to meropenem can lead to cross-resistance to colistin, a last resort drug for *P. aeruginosa* infections.

Keywords: antibiotic resistance, *Pseudomonas aeruginosa*, meropenem, colistin

Funding: the study was supported by the Russian Science Foundation (Project 20-15-00235).

Acknowledgements: the authors thank the Center of Precision Genome Editing and Genetic Technologies for Biomedicine of Pirogov Russian National Research Medical University for their advice on the methodology of the study.

Author contribution: Savinova TA — formal analysis of sequencing data, manuscript preparation; Bocharova YuA — methodology, formal analysis; Chaplin AV — formal analysis of sequencing data; Korostin DO — methodology, data validation; Shamina OV — methodology; Mayansky NA, Chebotar IV — concept; manuscript editing.

✉ **Correspondence should be addressed:** Tatiana A. Savinova
Ostrovityanova, 1, Moscow, 117997, Russia; taniyasavinova@gmail.com

Received: 27.12.2021 **Accepted:** 10.01.2022 **Published online:** 19.01.2022

DOI: 10.24075/brsmu.2022.001

МЕРОПЕНЕМ-ИНДУЦИРОВАННОЕ СНИЖЕНИЕ ЧУВСТВИТЕЛЬНОСТИ К КОЛИСТИНУ У *PSEUDOMONAS AERUGINOSA* ATCC 27853

Т. А. Савинова ✉, Ю. А. Бочарова, А. В. Чаплин, Д. О. Коростин, О. В. Шамина, Н. А. Маянский, И. В. Чеботарь

Российский национальный исследовательский медицинский университет имени Н. И. Пирогова, Москва, Россия

Нечувствительные к антибиотикам штаммы *Pseudomonas aeruginosa* представляют собой глобальную проблему в здравоохранении. Исследование механизмов возникновения резистентности лежит в основе разработки способов борьбы с *P. aeruginosa*. Целью работы было исследовать возникновение кросс-резистентности у *P. aeruginosa* в процессе адаптации к популярному антибиотику меропенему. Объектами исследования были образцы *P. aeruginosa*, полученные при росте референтного штамма *P. aeruginosa* ATCC 27853 на среде с возрастающей концентрацией меропенема. Чувствительность изолятов к карбапенемам и колистину определяли при помощи разведения в агаре, чувствительность к колистину оценивали методом серийных разведений. Было получено 93 изолята *P. aeruginosa*, два из которых имели сниженную чувствительность одновременно к карбапенемам (меропенем, имипенем) и колистину. Геномы изолятов секвенировали на полногеномном секвенаторе MGISEQ-2000; обнаружены миссенс-мутации в генах *oprD* и *mexD* и нонсенс-мутация в *phoQ*. Полученные результаты показывают, что при воздействии меропенема на штаммы *P. aeruginosa* может развиваться кросс-резистентность к колистину — препарату резерва для лечения синегнойной инфекции.

Ключевые слова: антибиотики, резистентность, *Pseudomonas aeruginosa*, меропенем, колестин

Финансирование: работа выполнена при поддержке гранта Российского научного фонда (проект № 20-15-00235).

Благодарности: авторы благодарят Центр высокоточного редактирования и генетических технологий для биомедицины ФГАОУ ВО РНИМУ им. Н. И. Пирогова Минздрава РФ за консультации по методической части исследования.

Вклад авторов: Т. А. Савинова — формальный анализ данных секвенирования, подготовка рукописи; Ю. А. Бочарова — методология, формальный анализ; А. В. Чаплин — формальный анализ данных секвенирования; Д. О. Коростин — методология, валидация данных; О. В. Шамина — методология; Н. А. Маянский, И. В. Чеботарь — концептуализация, редактирование рукописи.

✉ **Для корреспонденции:** Татьяна Александровна Савинова
ул. Островитянова, д. 1, г. Москва, 117997, Россия; taniyasavinova@gmail.com

Статья получена: 27.12.2021 **Статья принята к печати:** 10.01.2022 **Опубликована онлайн:** 19.01.2022

DOI: 10.24075/vrgmu.2022.001

Pseudomonas aeruginosa is a significant opportunistic pathogen and a serious burden to public health and economy [1]. Especially dangerous are carbapenem-resistant strains of *P. aeruginosa* regarded by WHO as critical priority pathogens [2]. This breeds the need for understanding mechanisms underlying bacterial resistance to carbapenems. Research into the molecular genetic underpinnings of carbapenem resistance focuses mostly on β -lactamase-associated mechanisms that are determined by plasmid genes and therefore can be acquired through horizontal gene transfer. However, there

is another contributor whose role should not be overlooked: induced mutations in the core genome of *P. aeruginosa* resulting in high-level carbapenem resistance [3]. There are two approaches to the study of mutations conferring resistance to carbapenems. The first involves the analysis of drug-resistant isolates obtained from clinical, agricultural or environmental sources. In the second approach, the evolution of antibiotic resistance is modeled *in vitro*. For that, bacteria are grown in antibiotic concentration gradients. A smart method for studying mutational resistance has been proposed in [4]. Its authors

created a spatiotemporal model that enabled migration of *Escherichia coli* in trimethoprim and ciprofloxacin gradients and generated a variety of mutants for further analysis. Interestingly, some of the *E. coli* clones carried mutations that were not linked to trimethoprim or ciprofloxacin resistance [4]. So, we became curious to explore the direction and implications of such mutations. Specifically, we were interested in the clinically significant phenomenon of cross-resistance, in which a mutation induced by exposure to an antibiotic could confer resistance to other antibiotics [5, 6]. The aim of this study was to test the hypothesis that *P. aeruginosa* can develop cross-resistance to other antibiotics while adapting to meropenem.

METHODS

Bacteriological study

In our experiment, we used the spatiotemporal model of antibiotic resistance in motile bacteria [4]. The reference ATCC 27853 strain of *P. aeruginosa* was precultured in semi-solid LB agar (0.28% agarose) in a Petri dish at 37 °C for 24 h. After 24 h, the cells were harvested from the propagating colony front and seeded onto another Petri dish with semi-solid LB agar. The procedure was repeated 3 times. Then, 10 µl of the grown bacterial culture was picked up with an inoculation loop and introduced into the top layer (semi-solid agar) of the culture medium contained in a device shown in the Figure. The medium had a sandwich composition. The bottom layer was LB Miller broth (Becton Dickinson; USA) supplemented with 1.6% agarose, 30 µg/ml kanamycin sulfate, 100 µg/ml cycloheximide, and meropenem taken at one of the concentrations shown in the Figure. The optimum thickness of the bottom layer equaled three-fifths of the total medium thickness (~2.0 cm). The bottom layer was distributed into 5 isolated compartments of the dish containing different concentrations of meropenem. The middle layer (one-fifth of the total medium thickness) was LB Miller broth supplemented with 2.0% agarose, 30 µg/ml kanamycin sulfate, 100 µg/ml cycloheximide, and ink (4.0 ml per 1 L culture medium) added as a contrasting background for photography purposes. The middle layer spread over the bottom layer was solid. The top layer (one-fifth of the total medium thickness) was semi-solid agar (Miller LB broth) with

0.3% agarose, 30 µg/ml kanamycin sulfate and 100 µg/ml cycloheximide.

The cells were incubated in air at 37 °C for 216 h. Every 12 h, *P. aeruginosa* samples were collected from the propagating colony front and reseeded on Mueller–Hinton agar (Becton Dickinson; USA) to obtain a sufficient amount of bacteria for the subsequent analysis of their phenotypic traits (antibiotic resistance profiles) and genomic changes.

Resistance to meropenem and imipenem was tested using the agar dilution method described in [7]. Resistance to colistin was assessed using the broth microdilution method following the guidelines of the Clinical and Laboratory Standards Institute (CLSI) [8].

Bacterial DNA was isolated from the 24-h culture of *P. aeruginosa* grown on Mueller–Hinton agar (Becton Dickinson; USA) using a QIAamp DNA Mini Kit (Qiagen; Germany) according to the manufacturer's protocol. The obtained DNA samples were stored at –20 °C.

To prepare genomic DNA libraries, 400 g of the isolated bacterial DNA was sheared in an ultrasonicator (Covaris; USA). The fragments were then end-repaired and ligated to MGI adapters (MGI; China). The libraries were purified on Agencourt AMPure XP beads (Beckman; USA). Concentrations of the bacterial DNA and DNA libraries were measured using a Qubit 4 fluorometer (Thermo Fisher Scientific; USA).

Whole-genome sequencing was performed using the MGISEQ-2000 platform (MGI; China). Read length was 250 bp.

The quality of the raw sequence data was tested in FASTQC; the reads were trimmed in Trimmomatic v.0.38. Bacterial genomes were assembled de novo using SPAdes 3.14 [9]. The assembled sequences were tested for contamination using Contest16S. The obtained genome assemblies were evaluated in QUAST 5.0 [10]. Genetic similarity between the assembled genomes was assessed in MUMmer [11]. The genomes were annotated using RAST [12] and Prokka software [13]. To detect the presence of single nucleotide polymorphisms (SNPs), the short reads were mapped to the reference genome in Snippy [14]. ATCC 27853 was used as a reference genome. The detected variants were annotated and their influence on the genes was predicted in SnpEff [15]. The search for antibiotic resistance genes in the genomes assembled de novo, their analysis and validation of the detected SNPs were all carried

Table. Characteristics of carbapenem-resistant strains of *P. aeruginosa* with reduced susceptibility to colistin

Methodology		Characteristic	<i>P. aeruginosa</i> ATCC 27853, reference	<i>P. aeruginosa</i> , isolate E62	<i>P. aeruginosa</i> , isolate E74
Phenotypic antibiotic susceptibility assessment	Agar dilution method, susceptibility to	meropenem	0.25 µg/ml, S	16 µg/ml, R	16 µg/ml, R
		imipenem	0.001 µg/ml, S	128 µg/ml, R	256 µg/ml, R
	Broth microdilution method, susceptibility to	colistin	0.5 µg/ml, I*	2 µg/ml, I*	4 µg/ml, R
Changes in genome	Carbapenem resistance genes	<i>oprD</i>	wt	Mutation resulting in G307D	Mutation resulting in G307D
		<i>mexD</i>	wt	Mutation resulting in E89K	Mutation resulting in E89K
	Colistin resistance gene	<i>phoQ</i>	wt	Nonsense mutation resulting in Y290stop	Nonsense mutation resulting in Y290stop
	Polymorphism	SNP	—	134	177

Note: S — susceptible; I — intermediate; R — resistant; wt — wild type, matches the reference genome; SNP — single nucleotide polymorphism; * — according to the CLSI criteria, the term “susceptible” cannot be applied to describe the susceptibility of *P. aeruginosa* to colistin; all *P. aeruginosa* strains for which colistin MIC ≤ 2 µg/ml are classified as susceptible at increased exposure.

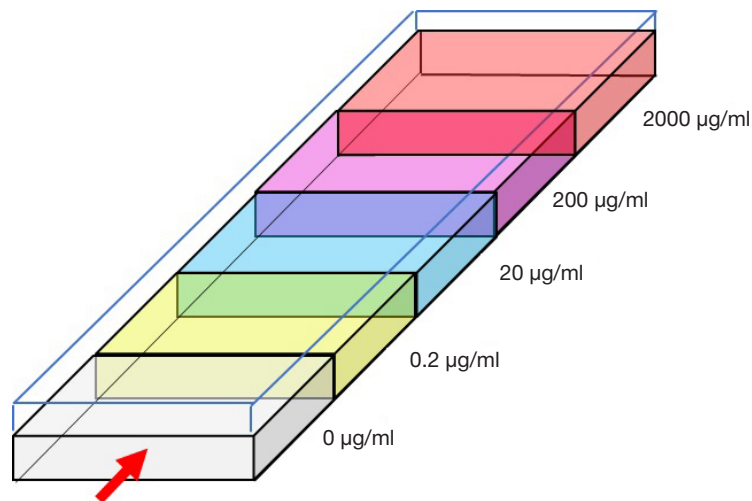


Fig. A device (MEGA-plate, 40 × 20 cm) for spatiotemporal modeling of meropenem resistance in *P. aeruginosa*. The bottom of the device is divided into 5 sections separated by 2.5-cm walls. The culture medium in the MEGA plate has a sandwich composition. The bottom layer contains solid LB agar (the description is provided in the article) distributed into the sections. Each of the sections contains different concentrations of meropenem (shown on the right). The middle layer is LB agar without meropenem. The top layer is semi-solid LB agar (Miller). The arrow indicates the inoculation site and the direction in which *P. aeruginosa* propagates along the surface of semi-solid agar.

out in BLASTn. The analysis of resistance determinants was aided by ResFinder and the AMRFinderPlus algorithm included in the NCBI Pathogen Detection pipeline [16, 17]

RESULTS

A total of 93 *P. aeruginosa* mutants with various phenotypic traits (colony color, antibiotic resistance profile, mucoid/non-mucoid phenotype) were harvested during 216 h of incubation. Among those isolates, two strains (E62 obtained at 192 h of incubation and E74 obtained at 216 h of incubation) demonstrated significantly reduced (four- to eightfold) susceptibility to colistin and high resistance to meropenem and imipenem. Phenotypic and genotypic characteristics of these 2 strains are shown in the Table.

For E62, meropenem and imipenem MICs were 16 µg/ml and 128 µg/ml, respectively; for E74, they were 16 µg/ml and 256 µg/ml, respectively, which satisfied the CLSI criteria for antibiotic resistance. According to CLSI criteria, the E62 isolate was characterized as susceptible to colistin at increased exposure; for this strain, colistin MIC was 4 times higher than for the baseline strain. According to the CLSI criteria, the E74 strain was characterized as resistant to colistin (MIC: 4 µg/ml).

Both strains carried a mutation in the porin gene (*oprD*) resulting in the substitution of glycine with aspartic acid at position 307 of the protein. Besides, both isolates had a missense mutation in the *mexD* gene (this gene encodes the subunit of the MexCD-OprJ efflux pump). Also, both E62 and E74 had a nonsense mutation in the *phoQ* gene resulting in the premature termination of protein synthesis (289 out of 448 amino acids).

DISCUSSION

P. aeruginosa strains with simultaneous resistance to carbapenems and polymyxins are not rare. For example, among multidrug resistant *P. aeruginosa* representatives, 22.2% of meropenem-resistant isolates were unsusceptible to colistin [18]. The evolution of such isolates is rarely described in the literature. It is possible that they acquire their resistance profiles through consecutive or simultaneous therapeutic exposure to carbapenems and colistin. The phenomenon observed in our study proves that *P. aeruginosa* can reduce their susceptibility

to colistin following exposure to meropenem. The hypothetical mechanisms underlying induction of cross-resistance to colistin by meropenem fall into the “all roads lead to resistance” concept, meaning that in *P. aeruginosa* any stressor causes hypermutability and leads to the emergence of multiple clones with novel properties [3]. Such a mutational explosion can lead to the emergence of persisting mutations disrupting synthesis of lipopolysaccharides, the primary target of colistin.

Genomes of the E62 and E74 isolates carried mutations that can explain their resistance to meropenem/imipenem and reduced susceptibility to colistin. The missense mutation in the *oprD* gene reported in this study may have caused a structural change in the OprD porin, which transports meropenem and imipenem inside the bacterial cell [19]. The search of GeneBank (<https://www.ncbi.nlm.nih.gov/genbank>) identified only one clinical isolate with a similar amino acid sequence of the OprD porin (GCA_003194245.1). Similar to our mutant, this isolate obtained in 2013 was also resistant to meropenem and imipenem (MIC > 32 µg/ml). Another mutation that could have reduced susceptibility to carbapenems was the missense mutation in the *mexD* gene encoding the subunit of the MexCD-OprJ efflux pump. The MexCD-OprJ system is involved in the efflux of β-lactams; its hyperexpression is correlated with carbapenem resistance in *P. aeruginosa* [20]. The *phoQ* gene codes for the sensor histidine kinase, which is part of the two-component regulatory PhoPQ system. Mutations in *phoQ* were reported to cause resistance to polymyxins in *P. aeruginosa*, including specimens isolated from patients with cystic fibrosis [21, 22].

Thus, all phenotypic characteristics of carbapenem-resistant isolates of *P. aeruginosa* with reduced susceptibility to colistin observed in our study were associated with mutations.

CONCLUSIONS

The phenomenon of cross-resistance described in this paper may be due to the fact that the rate of point mutations in *P. aeruginosa*, specifically in the genes implicated in antimicrobials resistance, increases under stress conditions. Our findings prove that exposure to meropenem can lead to resistance not only to other β-lactams but also to colistin used as a last resort drug for *P. aeruginosa* infections, which seriously complicates the treatment strategy and limits its options.

References

- Bou R, Lorente L, Aguilar A, Perpignan J, Ramos P, Peris M, et al. Hospital economic impact of an outbreak of *Pseudomonas aeruginosa* infections. *J Hosp Infect.* 2009; 71 (2): 138–42. Available from: <https://doi.org/10.1016/j.jhin.2008.07.018>.
- World Health Organization (WHO). Global Priority List of Antibiotic-Geneva, Switzerland: 2017. Available at: http://www.who.int/medicines/publications/WHO-PPL-Short_Summary_25Feb-ET_NM_WHO.pdf (accessed November 2021).
- Breidenstein EB, de la Fuente-Nunez C, Hancock RE. *Pseudomonas aeruginosa*: all roads lead to resistance. *Trends Microbiol.* 2011; 19 (8): 419–26. Available from: <https://doi.org/10.1016/j.tim.2011.04.005>
- Baym M, Lieberman TD, Kelsic ED, Chait R, Gross R, Yelin I, et al. Spatiotemporal microbial evolution on antibiotic landscapes. *Science.* 2016; 353 (6304): 1147–51. Available from: <https://doi.org/10.1126/science.aag0822>.
- Pal C, Papp B, Lazar V. Collateral sensitivity of antibiotic-resistant microbes. *Trends Microbiol.* 2015; 23 (7): 401–40. Available from: <https://doi.org/10.1016/j.tim.2015.02.009>.
- Gnanadhas DP, Marathe SA, Chakravorty D. Biocides–resistance, cross-resistance mechanisms and assessment. *Expert Opin Investig Drugs.* 2013; 22 (2): 191–06. Available from: <https://doi.org/10.1517/13543784.2013.748035>.
- European Committee for Antimicrobial Susceptibility Testing (EUCAST) of the European Society of Clinical Microbiology and Infectious Diseases (ESCMID). Determination of minimum inhibitory concentrations (MICs) of antibacterial agents by agar dilution. *Clin Microbiol Infect.* 2000; 6 (9): 509–15. Available from: <https://doi.org/10.1046/j.1469-0691.2000.00142.x>.
- Clinical and Laboratory Standards Institute (CLSI). Performance Standards for Antimicrobial Susceptibility Testing. Available from: <http://em100.edaptivedocs.net/dashboard.aspx> (accessed November 2021).
- Bankevich A, Nurk S, Antipov D, Gurevich AA, Dvorkin M, Kulikov AS et al. SPAdes: a new genome assembly algorithm and its applications to single-cell sequencing. *J Comput Biol.* 2012; 19: 455–77. Available from: <https://doi.org/10.1089/cmb.2012.0021>.
- Gurevich A, Saveliev V, Vyahhi N, Tesler G. QUASt: quality assessment tool for genome assemblies. *Bioinformatics.* 2013; 29 (8): 1072–5. Available from: <https://doi.org/10.1093/bioinformatics/btt086>.
- Marcais G, Delcher AL, Phillippy AM, Coston R, Salzberg SL, Zimin A. MUMmer4: A fast and versatile genome alignment system. *PLoS Comput Biol.* 2018; 14 (1): e1005944. Available from: <https://doi.org/10.1371/journal.pcbi.1005944>.
- Overbeek R, Olson R, Pusch GD, Olsen GJ, Davis JJ, Disz T, et al. The SEED and the Rapid Annotation of microbial genomes using Subsystems Technology (RAST). *Nucleic Acids Res.* 2014; 42: D206–14. Available from: <https://doi.org/10.1093/nar/gkt1226>.
- Seemann T. Prokka: rapid prokaryotic genome annotation. *Bioinformatics.* 2014; 30 (14): 2068–9. Available from: <https://doi.org/10.1093/bioinformatics/btu153>.
- Seemann T. Snippy: fast bacterial variant calling from NGS reads. *GitHub.* 2015. Available from: <https://github.com/tseemann/snippy> (accessed November 2021).
- Cingolani P, Platts A, Wang LL, Coon M, Nguyen T, Wang L, et al. A program for annotating and predicting the effects of single nucleotide polymorphisms, SnpEff: SNPs in the genome of *Drosophila melanogaster* strain w1118; iso-2; iso-3. *Fly.* 2012; 6 (2): 80–92. Available from: <https://doi.org/10.4161/fly.19695>.
- Feldgarden M, Brover V, Haft DH, Prasad AB, Slotta DJ, Tolstoy I, et al. Validating the AMRFinder Tool and Resistance Gene Database by Using Antimicrobial Resistance Genotype-Phenotype Correlations in a Collection of Isolates. *Antimicrob Agents Chemother.* 2019; 63 (11): e00483-19. Available from: <https://doi.org/10.1128/AAC.00483-19>.
- Bortolaia V, Kaas RS, Ruppe E, Roberts MC, Schwarz S, Cattoir V, et al. ResFinder 4.0 for predictions of phenotypes from genotypes. *J Antimicrob Chemother.* 2020; 75 (12): 3491–500. Available from: <https://doi.org/10.1093/jac/dkaa345>.
- Sader HS, Huband MD, Castanheira M, Flamm RK. *Pseudomonas aeruginosa* antimicrobial susceptibility results from four years (2012 to 2015) of the international network for optimal resistance monitoring program in the United States. *Antimicrob Agents Chemother.* 2017; 61 (3): e02252–16. Available from: <https://doi.org/10.1128/AAC.02252-16>.
- Chevalier S, Bouffartigues E, Bodilis J, Maillot O, Lesouhaitier O, Feuilloley MGJ, et al. Structure, function and regulation of *Pseudomonas aeruginosa* porins. *FEMS Microbiol Rev.* 2017; 41 (5): 698–722. Available from: <https://doi.org/10.1093/femsre/fux020>.
- Zahedi Bialvaei A, Rahbar M, Hamidi-Farahani R, Asgari A, Esmailkhani A, Mardani Dashti Y, et al. Expression of RND efflux pumps mediated antibiotic resistance in *Pseudomonas aeruginosa* clinical strains. *Microbial Pathog.* 2021; 153: 104789. Available from: <https://doi.org/10.1016/j.micpath.2021.104789>.
- Barrow K, Kwon DH. Alterations in two-component regulatory systems of phoPQ and pmrAB are associated with polymyxin B resistance in clinical isolates of *Pseudomonas aeruginosa*. *Antimicrob Agents Chemother.* 2009; 53 (12): 5150–4. Available from: <https://doi.org/10.1128/AAC.00893-09>.
- Miller AK, Brannon MK, Stevens L, Johansen HK, Selgrade SE, Miller SI, et al. PhoQ mutations promote lipid A modification and polymyxin resistance of *Pseudomonas aeruginosa* found in colistin-treated cystic fibrosis patients. *Antimicrob Agents Chemother.* 2011; 55 (12): 5761–9. Available from: <https://doi.org/10.1128/AAC.05391-11>.

Литература

- Bou R, Lorente L, Aguilar A, Perpignan J, Ramos P, Peris M, et al. Hospital economic impact of an outbreak of *Pseudomonas aeruginosa* infections. *J Hosp Infect.* 2009; 71 (2): 138–42. Available from: <https://doi.org/10.1016/j.jhin.2008.07.018>.
- World Health Organization (WHO). Global Priority List of Antibiotic-Geneva, Switzerland: 2017. Available at: http://www.who.int/medicines/publications/WHO-PPL-Short_Summary_25Feb-ET_NM_WHO.pdf (accessed November 2021).
- Breidenstein EB, de la Fuente-Nunez C, Hancock RE. *Pseudomonas aeruginosa*: all roads lead to resistance. *Trends Microbiol.* 2011; 19 (8): 419–26. Available from: <https://doi.org/10.1016/j.tim.2011.04.005>
- Baym M, Lieberman TD, Kelsic ED, Chait R, Gross R, Yelin I, et al. Spatiotemporal microbial evolution on antibiotic landscapes. *Science.* 2016; 353 (6304): 1147–51. Available from: <https://doi.org/10.1126/science.aag0822>.
- Pal C, Papp B, Lazar V. Collateral sensitivity of antibiotic-resistant microbes. *Trends Microbiol.* 2015; 23 (7): 401–40. Available from: <https://doi.org/10.1016/j.tim.2015.02.009>.
- Gnanadhas DP, Marathe SA, Chakravorty D. Biocides–resistance, cross-resistance mechanisms and assessment. *Expert Opin Investig Drugs.* 2013; 22 (2): 191–06. Available from: <https://doi.org/10.1517/13543784.2013.748035>.
- European Committee for Antimicrobial Susceptibility Testing (EUCAST) of the European Society of Clinical Microbiology and Infectious Diseases (ESCMID). Determination of minimum inhibitory concentrations (MICs) of antibacterial agents by agar dilution. *Clin Microbiol Infect.* 2000; 6 (9): 509–15. Available from: <https://doi.org/10.1046/j.1469-0691.2000.00142.x>.
- Clinical and Laboratory Standards Institute (CLSI). Performance Standards for Antimicrobial Susceptibility Testing. Available from: <http://em100.edaptivedocs.net/dashboard.aspx> (accessed November 2021).
- Bankevich A, Nurk S, Antipov D, Gurevich AA, Dvorkin M, Kulikov AS et al. SPAdes: a new genome assembly algorithm and its applications to single-cell sequencing. *J Comput Biol.* 2012; 19: 455–77. Available from: <https://doi.org/10.1089/cmb.2012.0021>.
- Gurevich A, Saveliev V, Vyahhi N, Tesler G. QUASt: quality

- assessment tool for genome assemblies. *Bioinformatics*. 2013; 29 (8): 1072-5. Available from: <https://doi.org/10.1093/bioinformatics/btt086>.
11. Marcais G, Delcher AL, Phillippy AM, Coston R, Salzberg SL, Zimin A. MUMmer4: A fast and versatile genome alignment system. *PLoS Comput Biol*. 2018; 14 (1): e1005944. Available from: <https://doi.org/10.1371/journal.pcbi.1005944>.
 12. Overbeek R, Olson R, Pusch GD, Olsen GJ, Davis JJ, Disz T, et al. The SEED and the Rapid Annotation of microbial genomes using Subsystems Technology (RAST). *Nucleic Acids Res*. 2014; 42: D206–14. Available from: <https://doi.org/10.1093/nar/gkt1226>.
 13. Seemann T. Prokka: rapid prokaryotic genome annotation. *Bioinformatics*. 2014; 30 (14): 2068–9. Available from: <https://doi.org/10.1093/bioinformatics/btu153>.
 14. Seemann T. Snippy: fast bacterial variant calling from NGS reads. GitHub. 2015. Available from: <https://github.com/tseemann/snippy> (accessed November 2021).
 15. Cingolani P, Platts A, Wang LL, Coon M, Nguyen T, Wang L, et al. A program for annotating and predicting the effects of single nucleotide polymorphisms, SnpEff: SNPs in the genome of *Drosophila melanogaster* strain w1118; iso-2; iso-3. *Fly*. 2012; 6 (2): 80–92. Available from: <https://doi.org/10.4161/fly.19695>.
 16. Feldgarden M, Brover V, Haft DH, Prasad AB, Slotta DJ, Tolstoy I, et al. Validating the AMRFinder Tool and Resistance Gene Database by Using Antimicrobial Resistance Genotype-Phenotype Correlations in a Collection of Isolates. *Antimicrob Agents Chemother*. 2019; 63 (11): e00483-19. Available from: <https://doi.org/10.1128/AAC.00483-19>.
 17. Bortolaia V, Kaas RS, Ruppe E, Roberts MC, Schwarz S, Cattoir V, et al. ResFinder 4.0 for predictions of phenotypes from genotypes. *J Antimicrob Chemother*. 2020; 75 (12): 3491–500. Available from: <https://doi.org/10.1093/jac/dkaa345>.
 18. Sader HS, Huband MD, Castanheira M, Flamm RK. *Pseudomonas aeruginosa* antimicrobial susceptibility results from four years (2012 to 2015) of the international network for optimal resistance monitoring program in the United States. *Antimicrob Agents Chemother*. 2017; 61 (3): e02252–16. Available from: <https://doi.org/10.1128/AAC.02252-16>.
 19. Chevalier S, Bouffartigues E, Bodilis J, Maillot O, Lesouhaitier O, Feuilloley MGJ, et al. Structure, function and regulation of *Pseudomonas aeruginosa* porins. *FEMS Microbiol Rev*. 2017; 41 (5): 698–722. Available from: <https://doi.org/10.1093/femsre/flux020>.
 20. Zahedi Bialvaei A, Rahbar M, Hamidi-Farahani R, Asgari A, Esmailkhani A, Mardani Dashti Y, et al. Expression of RND efflux pumps mediated antibiotic resistance in *Pseudomonas aeruginosa* clinical strains. *Microbial Pathog*. 2021; 153: 104789. Available from: <https://doi.org/10.1016/j.micpath.2021.104789>.
 21. Barrow K, Kwon DH. Alterations in two-component regulatory systems of phoPQ and pmrAB are associated with polymyxin B resistance in clinical isolates of *Pseudomonas aeruginosa*. *Antimicrob Agents Chemother*. 2009; 53 (12): 5150–4. Available from: <https://doi.org/10.1128/AAC.00893-09>.
 22. Miller AK, Brannon MK, Stevens L, Johansen HK, Selgrade SE, Miller SI, et al. PhoQ mutations promote lipid A modification and polymyxin resistance of *Pseudomonas aeruginosa* found in colistin-treated cystic fibrosis patients. *Antimicrob Agents Chemother*. 2011; 55 (12): 5761–9. Available from: <https://doi.org/10.1128/AAC.05391-11>.

MICROSATELLITE INSTABILITY IN COLORECTAL NEUROENDOCRINE NEOPLASMS

Meshcheryakova MYu [✉], Kolesnikov EN, Trifanov VS, Timoshkina NN, Snezhko AV, Gvaldin DYu

National Medical Research Center of Oncology, Rostov-on-Don, Russia

Microsatellite instability (MSI) characterizes a special molecular genetic subtype of malignancies and is associated with the deficiency of mismatched DNA repair. There are no reliable data on the frequency of MSI in colorectal neuroendocrine neoplasms due to the relative rarity of this cancer type. The prognostic significance of MSI is debatable. The aim of this study was to investigate the frequency of the MSI phenotype among colorectal neuroendocrine neoplasms (NENs) with different primary location, grade and stage. Twenty-nine patients (15 men and 14 women, mean age: 62.5 years) included in the study underwent surgery for colorectal neuroendocrine tumors between 2015 and 2018. The mean follow-up period was 3.8 years. Colorectal NENs were grouped by primary location and stage. The majority of the patients (52%) had stage III cancer at diagnosis. The microsatellite stability (MSS) phenotype was confirmed in 24 patients (83%), whereas the MSI phenotype was observed in 5 patients (17%). All MSI-positive tumors were stage I well-differentiated grade G1 or G2 neuroendocrine tumors (NETs) of the rectum. Overall survival was 50% for patients with stage II MSS-positive NENs of the colon and rectum, 33% for stage III and 0% for stage IV. For patients with stage I MSI-positive NENs of the rectum, overall survival was 100%. Thus, the frequency of MSI-positive colorectal NENs was estimated.

Keywords: colorectal neuroendocrine neoplasms, microsatellite instability, overall survival, prognosis

Author contributions: Kolesnikov EN — data collection, analysis and interpretation; manuscript editing; Trifanov VS — study design; data collection, manuscript editing; Timoshkina NN — data analysis and interpretation; manuscript preparation; Snezhko AV — data acquisition; Gvaldin DYu — data analysis and interpretation; Meshcheryakova MYu — literature analysis; manuscript preparation.

Compliance with ethical standards: the study was approved by the Ethics Committee of the National Medical Research Centre for Oncology (Protocol № 3 dated February 9, 2021); informed consent was obtained from all study participants.

✉ **Correspondence should be addressed:** Milana Yu. Meshcheryakova
14 liniya, 63, Rostov-on-Don; meshcheryakovamilana@mail.ru

Received: 12.01.2022 **Accepted:** 27.01.2022 **Published online:** 14.02.2022

DOI: 10.24075/brsmu.2022.004

МИКРОСАТЕЛЛИТНАЯ НЕСТАБИЛЬНОСТЬ В НЕЙРОЭНДОКРИННЫХ НОВООБРАЗОВАНИЯХ ТОЛСТОЙ КИШКИ

М. Ю. Мещерякова [✉], Е. Н. Колесников, В. С. Трифанов, Н. Н. Тимошкина, А. В. Снежко, Д. Ю. Гвалдин

Национальный медицинский исследовательский центр онкологии, Ростов-на-Дону, Россия

С нарушением работы системы репарации неспаренных оснований ДНК связано понятие о микросателлитной нестабильности (MSI), характеризующей особый молекулярно-биологический подтип злокачественных опухолей. Достоверные данные о частоте встречаемости MSI в нейроэндокринных новообразованиях толстой кишки отсутствуют, что связано с относительно небольшим числом пациентов. Сведения о прогностической значимости MSI также противоречивы. Целью исследования было изучение частоты встречаемости MSI в нейроэндокринных новообразованиях (НЭН) толстой кишки в зависимости от локализации, степени дифференцировки опухоли и стадии заболевания. Включенные в исследование 29 пациентов были прооперированы в период с 2015 по 2018 г. по поводу нейроэндокринных новообразований толстой кишки (мужчины — 15 человек, женщины — 14 человек, средний возраст постановки диагноза — 62,5 лет). Средний срок наблюдения составил 3,8 лет. НЭН толстой кишки были распределены по локализациям, а также по стадиям заболевания. У большинства пациентов, включенных в исследование, была диагностирована III стадия заболевания (52%). Статус микросателлитной стабильности (MSS) был подтвержден у 24 пациентов (83%), тогда как MSI-статус — у пяти (17%) соответственно. Все случаи MSI-позитивных новообразований соответствовали высокодифференцированным G1 и G2 нейроэндокринным опухолям прямой кишки на I стадии заболевания. Общая выживаемость пациентов с MSS-позитивными НЭН толстой кишки составила на II стадии — 50%, на III — 33%, на IV стадии — 0%. Общая выживаемость пациентов с MSI-позитивными НЭН прямой кишки на I стадии составила 100%. Таким образом, была определена частота встречаемости MSI-позитивных НЭН толстой кишки.

Ключевые слова: нейроэндокринные новообразования толстой кишки, микросателлитная нестабильность, общая выживаемость, прогноз

Вклад авторов: Е. Н. Колесников — получение, анализ и интерпретация данных, редактирование статьи; В. С. Трифанов — дизайн исследования, редактирование статьи; Н. Н. Тимошкина — анализ и интерпретация полученных данных, написание текста статьи; А. В. Снежко — получение данных для анализа; Д. Ю. Гвалдин — анализ и интерпретация полученных данных; М. Ю. Мещерякова — обзор публикаций, написание текста статьи.

Соблюдение этических стандартов: исследование одобрено этическим комитетом НМИЦ онкологии (протокол № 3 от 09 февраля 2021 г.); все участники подписали информированное согласие на участие в исследовании.

✉ **Для корреспонденции:** Милана Юрьевна Мещерякова
ул.14-линия, д. 63, г. Ростов-на-Дону; meshcheryakovamilana@mail.ru

Статья получена: 12.01.2022 **Статья принята к печати:** 27.01.2022 **Опубликована онлайн:** 14.02.2022

DOI: 10.24075/vrgmu.2022.004

DNA mismatch repair is a unique biological mechanism for repairing DNA damage occurring during cell division [1]. Proteins involved in DNA mismatch repair are encoded by 6 key genes: *MSH2*, *MLH1*, *PMS2*, *MSH3*, *MSH6*, and *MLH3*. Inherited or sporadic mutations, as well as other epigenetic events like *MLH1* promoter hypermethylation, can inactivate any of these genes and disrupt the normal functioning of the entire mechanism [2]. This results in the accumulation of multiple unrepaired mutations in the genome and changes to

the length of microsatellites, which are 2–9 bp-long sequences in the euchromatin portion of the genome [3]. Consequently, if the microsatellite is located within an intron region, a reading frame shift may occur in the coding sequence, followed by the inactivation of various genes. Thus, defects in the DNA mismatch repair mechanism give rise to a genomic phenotype known as microsatellite instability (MSI) [1].

MSI-positive tumors are less aggressive than those that do not have the MSI phenotype, presumably due to a high

mutation rate resulting in increased neoantigen load, which stimulates antitumor immune response. Logically, tumors with the MSI phenotype should respond better to checkpoint inhibitor (CPI) immunotherapy. This hypothesis has been confirmed for melanoma, gastric cancer and colorectal cancer (CRC). However, the prognostic significance of the MSI status in the late (IV) stages of CRC remains controversial [4].

Today, MSI is recognized as an important predictor of tumor response to immunotherapy regardless of the primary tumor site [1].

Due to the versatility of this marker, which expands indications for CPI therapy, testing for the patient's MSI status is becoming an essential diagnostic procedure approved unanimously by the leading cancer research communities, including ASCO, ESMO, NCCN, and RUSSCO [2]. The MSI status affects the choice of treatment strategy for patients with early-stage CRC, which is being reflected in contemporary clinical guidelines [5].

So far, there have been no randomized clinical trials evaluating the effectiveness of different immunotherapy regimens for colorectal neuroendocrine neoplasms (NENs). Besides, the prevalence of MSI-positive colorectal and gastrointestinal NENs remains understudied, as is the impact of the MSI status on the clinical outcome.

We hypothesize that MSI-positive colorectal NENs are a separate group of tumors with a different clinical presentation and prognosis. Colorectal NENs are relatively rare, so enrolling a large number of patients in the clinical trial may pose a problem. In the largest molecular genetic studies of colorectal NENs conducted so far, the average number of patients did not exceed 100. In earlier publications estimating the frequency of the MSI phenotype among neuroendocrine carcinomas (NECs; $n = 53$) and mixed gastrointestinal adenoneuroendocrine carcinomas ($n = 36$), 12.4% of the tumors (11/89), including NECs of the colon, stomach and the duodenum, were MSI-positive [6]. The authors of the publication identified a few clinicopathological and molecular genetic features of MSI-positive tumors. Briefly, MSI-positive carcinomas had higher methylation levels than MSI-negative tumors (40.6% vs 20.2%); the most frequently methylated genes were *MLH1*, *p16*, *PAX6*, *PAX5*, *THBS1*, *TP73*, *DAPK1*, *MGMT*, *PYCARD*, *CDH13*, *HIC1*, and *TIMP3*. The MSI status was correlated to the presence of mutations in the *BRAF* gene [6]. These findings show that the MSI-status of the tumor is associated with a specific set of its molecular characteristics, which, in our opinion, may hold promise for future research. The aim of our study was to evaluate the MSI status in

colorectal NENs with different primary tumor location, grade and stage.

METHODS

The study included 29 patients undergoing surgical treatment for colorectal NENs at the National Medical Research Centre for Oncology (Rostov-on-Don) between 2015 and 2018. Of them, 15 were men and 14 were woman. The mean age at diagnosis was 62.5 years. The mean follow-up period was 3.8 years. The following inclusion criteria were applied: expression of neuroendocrine differentiation markers (chromogranin A, synaptophysin) confirmed by immunohistochemistry; informed consent to participate in the study. All tissue specimens were analyzed using the 2019 WHO classification criteria.

DNA was isolated from the paraffinized tissue samples obtained during surgery. Briefly, 10 slices were prepared from the paraffin-embedded tumor or seemingly healthy tissue using a microtome; then, they were deparaffinized in xylol. The samples were incubated with a lysis buffer in the presence of proteinase K at 58 °C for 6–12 h until complete tissue lysis. After that, total DNA was isolated and purified using a DNA-sorb-B kit (AmpliSens; Russia) following the manufacturer's protocol. DNA concentrations were measured with a Qubit 2.0 fluorometer (LifeTechnologies; USA).

Five monomorphic microsatellite loci (NR21, NR24, NR27, BAT25 and BAT26) were tested for their MSI status by means of fragment analysis. Each of the obtained total DNA templates were PCR-amplified in 5 reactions. Each 20 μ l PCR reaction contained 10–20 ng of DNA, 0.175 μ M of each primer, 2 mM of dNTP, 15 mM of $MgCl_2$ and 0.5 un. of Taq-polymerase. The following PCR protocol was applied: initial denaturation at 94 °C for 5 min, followed by 40 cycles of denaturation at 94 °C for 30 s, primer annealing at 59 °C, extension at 72 °C and final extension at 72 °C for 45 s. The size of the PCR product ranged from 50 to 350 pn.

Detection of the fluorescently tagged PCR products was performed by means of fragment analysis. Briefly, 1 μ l of the obtained PCR products was combined with 19 μ l of Hi-Di formamide and 0.5 μ l of GeneScan™ 600 LIZ® Size Standard (Thermo Fisher; USA). The samples were incubated in a CH-100 heating/cooling dry block thermostat (Biosan; USA) at 95 °C for 5 min and processed in an ABI PRISM 3500 genetic analyzer (Applied Biosystems; USA) following the manufacturer's protocol. The obtained data were analyzed in GeneMapper Software (Thermo Fisher; USA). The peak detection value was set to 50 relative fluorescence units (RFU). MSI was concluded

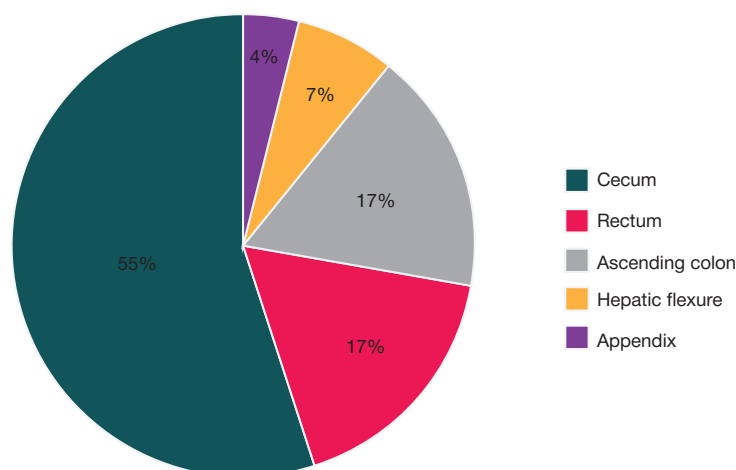


Fig. 1. Distribution of colorectal NENs by primary tumor location

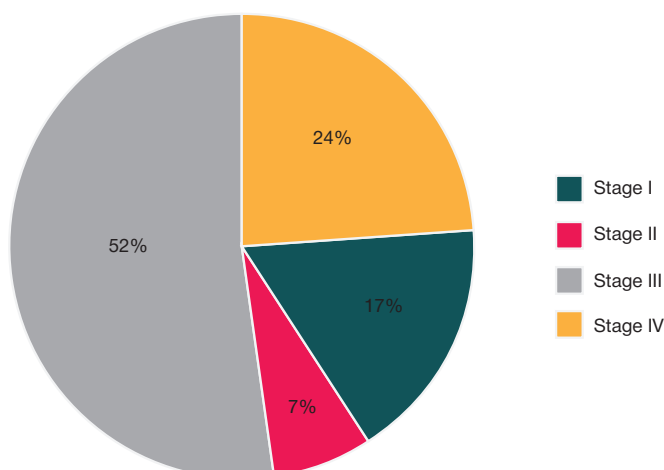


Fig. 2. Distribution of colorectal NENs by stage

if 2 or more of the studied loci were polymorphic. The level of MLH1 methylation was determined by bisulfate-converted DNA pyrosequencing using a PyroMark Q24 CpG MLH1 assay according to the manufacturer's protocol (QIAGEN; Germany).

Statistical analysis was carried out in Statsoft Statistica 10.0 (StatSoft; USA) for Windows 10. Primary data analysis was performed using descriptive statistics (central tendencies and measures of variability).

RESULTS

Colorectal NENs were grouped by primary location. Of them, 55% ($n = 16$) were cecal, 17% ($n = 5$) were NENs of the rectum, 17% ($n = 5$) were tumors of the ascending colon, 7% ($n = 2$) were localized to the right hepatic flexure, and 4% ($n = 1$) were appendiceal (Fig. 1).

The majority of the patients included in the study had stage III cancer (52%, $n = 15$) (Fig. 2).

In our cohort of patients, NENs of the colon occurred more frequently than other histological subtypes (55%, $n = 16$), and their frequency was directly correlated with the stage of the disease. Patient distribution by the histological subtype and stage of cancer is shown in Fig. 3.

Microsatellite stability (MSS) was confirmed in 83% of cases ($n = 24$); 17% ($n = 5$) of the tumors were MSI-positive. All MSI-positive tumors were well or moderately differentiated stage I cancers: two of them were G1 and 3 were G2 neuroendocrine

neoplasms of the rectum. All of those 5 tumors had microsatellite instability in all of the 5 studied STR loci.

MLH1 was hypermethylated in all MSI-positive specimens (Me = 20%, range: 14–42%) and hypomethylated in all samples with the MSS phenotype (Me = 4%, range: 4–14%). Based on the obtained data, we concluded that the leading cause of the MSI-status in colorectal NENs was inhibition of transcription of the key mismatch repair system genes caused by hypermethylation of their promoter. In the literature, this mechanism was previously described for sporadic colorectal adenocarcinomas.

The distribution of colonic NENs with the confirmed MSS phenotype by primary location and stage is shown in Fig. 4 and 5.

For our patients with MSS-positive NENs of the colon, the three-year survival rate was 50% for stage II, 33% for stage III, and 0% for stage IV. For the patients with stage I MSI-H NENs of the rectum, the three-year survival rate was 100%.

DISCUSSION

Our findings on the prevalence of microsatellite instability in colorectal NENs were compared to the published data on colorectal cancer. In a recent study of Russian researchers conducted in a Russian cohort of patients with CRC ($n = 359$), the MSI phenotype was observed in 6.4% of cases (23/359) and was correlated with younger age ($p = 0.023$), the presence

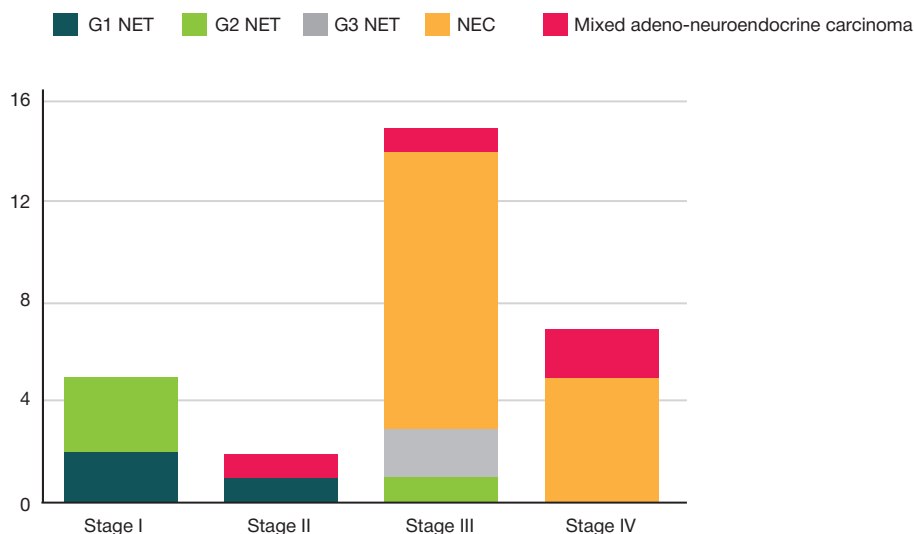


Fig. 3. Patient distribution by the histological subtype of NEN and cancer stage

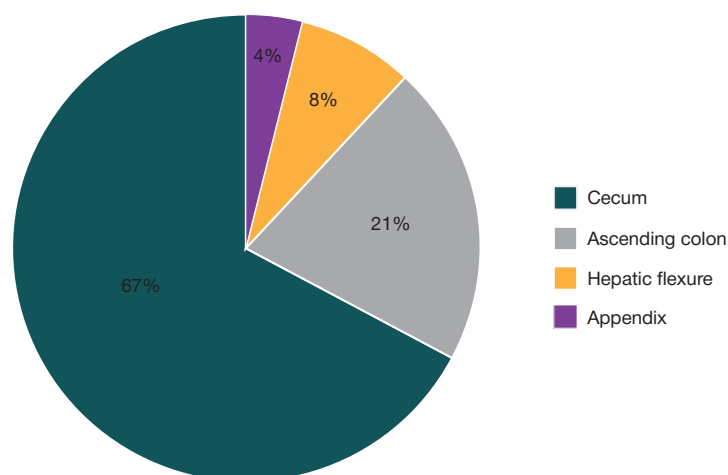


Fig. 4. Distribution of colorectal NENs with the confirmed MSS phenotype by primary location and stage

of multiple primary lesions ($p = 0.0299$), mucinous component ($p < 0.0001$), high grade ($p = 0.0025$) and right-sided location of the tumor in the colon ($p < 0.0001$) [7]. In our study, all MSI-positive NENs ($n = 5$) were low-grade and localized to the rectum.

According to the contemporary literature, there is a clear trend that the rate of MSI detection is inversely correlated with the stage of the disease [1, 3–5]. In our study, all MSI-positive NENs of the colon were stage I cancers. A larger patient sample with adequate representation of every stage of the disease is needed to check this trend for NENs of the colon.

The analysis of microsatellite instability patterns and frequency of occurrence in well-differentiated (G1/G2) neuroendocrine pancreatic tumors studied in our previous publication and NENs of the colon reveals certain differences. The MSI-positive phenotype was observed in 14% of pancreatic NENs [8] vs 17% of NENs of the colon. Besides, in pancreatic NENs, the MSI-positive phenotype was not associated with MLH1 promoter methylation. By contrast, in NENs of the colon the MSI-positive phenotype was associated only with MLH1 hypermethylation. Perhaps, this epigenetic mechanism typical for adenocarcinomas and NENs of the colon is related to their colorectal origin.

Cellular differentiation is a very important criteria in the context of gastrointestinal NENs, which is reflected in the 2019 updated WHO classification. High- and low-grade NENs are different groups of tumors completely heterogenous in terms of their genetic characteristics. Besides, NENs originating in different organs differ in their basic molecular markers. This raises the question of whether there is a link between the degree of cellular differentiation in NENs (NETs and NECs),

primary tumor location and MSI pattern distribution. The data provided in the literature is controversial. For example, of 239 studied gastrointestinal and pulmonary NENs, only 4 specimens (1 G3 NETs of the pancreas and 3 NECs of the colon) were MSI-positive [9]. In another study the prevalent primary NEC location were the stomach ($n = 21$) and the pancreas ($n = 6$), and MSI was detected in none of the total 33 lesions [10]. At the same time, according to the meta-analysis of 33 retrospective studies and 8 case reports, MSI was observed in approximately 10% of gastric and colonic NECs [11]. The MSI phenotype was not confirmed in any of 56 well-differentiated NETs of the rectum ($n = 56$), small bowel ($n = 14$), colon ($n = 38$), and pancreas ($n = 16$) [9, 12–15]. According to other reports, 10–33% of pancreatic NETs are MSI-positive [9]. In our study the majority of the specimens (55%, $n = 16$) were represented by NECs of the colon, but their MSI status was negative. However, there are reports confirming the MSI phenotype in 16%, 7%, 10%, and 14% of NECs of the colon, respectively [6, 9, 17–21]. The analysis of the relevant literature suggests that the frequency of MSI could be higher among poorly differentiated NENs. Still, our findings demonstrate the opposite: in our study, MSI was confirmed for well-differentiated grade G1 and G2 NENs of the rectum. That said, only a larger patient sample will drawing reliable conclusions about the pattern of MSI distribution in NENs of the colon.

CONCLUSIONS

The analysis of frequency of microsatellite instability in colorectal NENs depends on the tumor grade, primary location and stage

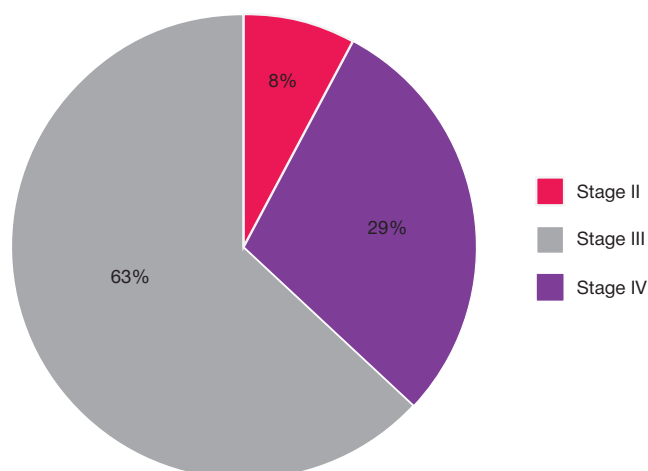


Fig. 5. Distribution of colorectal NENs with the confirmed MSS phenotype by stage

revealed that 17% the samples were MSI-positive. All of them were stage I well-differentiated G1 and G2 NENs located in the rectum. The calculated three-year survival rates demonstrate a direct correlation between the frequency of MSI occurrence in colorectal NENs and the stage of the disease. According to the currently held research, the prevalence of MSI among NENs is similar to the prevalence of MSI among adenocarcinomas of the

same organ. Comparison of our findings to the frequency of MSI in CRC reveals that well-differentiated NENs of the colon may be characterized by a higher rate of the MSI-positive phenotype (17% vs 10–15%). Notably, testing patients with NENs for MSI is not part of the standard diagnostic protocol, which we believe is wrong. We are cautiously optimistic in suggesting that novel immunotherapies may be effective against this class of tumors.

References

- Ratovomanana T, Cohen R, Svrcek M, Renaud F, Cervera P, Siret A, et al. Performance of Next-Generation Sequencing for the Detection of Microsatellite Instability in Colorectal Cancer With Deficient DNA Mismatch Repair. *Gastroenterology*. 2021; 161 (3): 814–26.
- Echle A, Grabsch HI, Quirke P, van den Brandt PA, West NP, Hutchins GGA, et al. Clinical-Grade Detection of Microsatellite Instability in Colorectal Tumors by Deep Learning. *Gastroenterology*. 2020; 159 (4): 1406–16.
- Andre T, Amonkar M, Norquist JM, Shiu KK, Kim TW, Jensen BV, et al. Health-related quality of life in patients with microsatellite instability-high or mismatch repair deficient metastatic colorectal cancer treated with first-line pembrolizumab versus chemotherapy (KEYNOTE-177): an open-label, randomised, phase 3 trial. *Lancet Oncol*. 2021; 22 (5): 665–77.
- Diao Z, Han Y, Chen Y, Zhang R, Li J. The clinical utility of microsatellite instability in colorectal cancer. *Crit Rev Oncol Hematol*. 2021; 157 (1): 103–71.
- Trjakin AA, Fedjanin MYu, Cukanov AS, Shelygin YuA, Pokataev IA, Ignatova EO, i dr. Mikrosatelitnaja nestabil'nost' kak unikal'naja harakteristika opuholej i prediktor jeffektivnosti immunoterapii. *Zlokachestvennye opuholi*. 2019; 9 (4): 59–69. Russian.
- Sahnane N, Furlan D, Monti M, Romualdi C, Vanoli A, Vicari E, et al. Microsatellite unstable gastrointestinal neuroendocrine carcinomas: a new clinicopathologic entity. *Endocr Relat Cancer*. 2015; 22 (1): 35–45.
- Musaeljan AA, Nazarov VD, Budnikova AS, Lapin SV, Vorobev SL, Jemanujel VL, i dr. Kliniko-morfologicheskij portret opuholej s mikrosatelitnoj nestabil'nost'ju. *Uspehi molekularnoj onkologii*. 2021; 8 (2): 52–59. Russian.
- Trifanov VS, Timoshkina NN, Gvaldin DYu, Mesheryakova MYu, Kolesnikov EN, Gaziev UM, et al. Study of microsatellite instability in neuroendocrine tumors of pancreas and colon. *Journal of Clinical Oncology*. 2021; 39 (15): 16196.
- Fraune C, Simon R, Hube-Magg C, Makrypidi-Fraune G, Kluth M, Büscheck F, et al. Homogeneous MMR Deficiency Throughout the Entire Tumor Mass Occurs in a Subset of Colorectal Neuroendocrine Carcinomas. *Endocr Pathol*. 2020; 31 (2): 182–9.
- Xing J, Ying H, Li J, Gao Y, Sun Z, Li J, et al. Immune Checkpoint Markers in Neuroendocrine Carcinoma of the Digestive System. *Front Oncol*. 2020; 28 (10): 132.
- Girardi DM, Silva ACB, Régo JFM, Coudry RA, Riechelmann RP. Unraveling molecular pathways of poorly differentiated neuroendocrine carcinomas of the gastroenteropancreatic system: A systematic review. *Cancer Treat Rev*. 2017; 56 (1): 28–35.
- Mitsuhashi K, Yamamoto I, Kurihara H, Kanno S, Ito M, Igarashi H, et al. Analysis of the molecular features of rectal carcinoid tumors to identify new biomarkers that predict biological malignancy. *Oncotarget*. 2015; 6 (26): 22114–25.
- Kidd M, Eick G, Shapiro MD, Camp RL, Mane SM, Modlin IM. Microsatellite instability and gene mutations in transforming growth factor-beta type II receptor are absent in small bowel carcinoid tumors. *Cancer*. 2005; 103 (2): 229–36.
- Ghimenti C, Lonobile A, Campani D, Bevilacqua G, Caligo MA. Microsatellite instability and allelic losses in neuroendocrine tumors of the gastro-entero-pancreatic system. *Int J Oncol*. 1999; 15 (2): 361–6.
- Arnold CN, Nagasaka T, Goel A, Scharf I, Grabowski P, Sosnowski A, et al. Molecular characteristics and predictors of survival in patients with malignant neuroendocrine tumors. *Int J Cancer*. 2008; 123 (7): 1556–64.
- Dudley JC, Lin MT, Le DT, Eshleman JR. Microsatellite Instability as a Biomarker for PD-1 Blockade. *Clin Cancer Res*. 2016; 22 (4): 813–20.
- Olevian DC, Nikiforova MN, Chiosea S, Sun W, Bahary N, Kuan SF, et al. Colorectal poorly differentiated neuroendocrine carcinomas frequently exhibit BRAF mutations and are associated with poor overall survival. *Hum Pathol*. 2016; 49 (1): 124–34.
- Furlan D, Sahnane N, Mazzoni M, Pastorino R, Carnevali I, Stefanoli M, et al. Diagnostic utility of MS-MLPA in DNA methylation profiling of adenocarcinomas and neuroendocrine carcinomas of the colon-rectum. *Virchows Arch*. 2013; 462 (1): 47–56.
- La Rosa S, Marando A, Furlan D, Sahnane N, Capella C. Colorectal poorly differentiated neuroendocrine carcinomas and mixed adenoneuroendocrine carcinomas: insights into the diagnostic immunophenotype, assessment of methylation profile, and search for prognostic markers. *Am J Surg Pathol*. 2012; 36 (4): 601–11.
- Kit OI, Trifanov VS, Petrusenko NA, Gvaldin DY, Kutilin DS, Timoshkina NN. Identification of new candidate genes and signalling pathways associated with the development of neuroendocrine pancreatic tumours based on next generation sequencing data. *Mol Biol Rep*. 2020; 47 (6): 4233–43.
- Kit OI, Vodolazhskij DI. Molekuljarnaja biologija kolorektal'nogo raka v klinicheskoj praktike. *Molekuljarnaja biologija*. 2015; 49 (4): 531–54. Russian.

Литература

- Ratovomanana T, Cohen R, Svrcek M, Renaud F, Cervera P, Siret A, et al. Performance of Next-Generation Sequencing for the Detection of Microsatellite Instability in Colorectal Cancer With Deficient DNA Mismatch Repair. *Gastroenterology*. 2021; 161 (3): 814–26.
- Echle A, Grabsch HI, Quirke P, van den Brandt PA, West NP, Hutchins GGA, et al. Clinical-Grade Detection of Microsatellite Instability in Colorectal Tumors by Deep Learning. *Gastroenterology*. 2020; 159 (4): 1406–16.
- Andre T, Amonkar M, Norquist JM, Shiu KK, Kim TW, Jensen BV, et al. Health-related quality of life in patients with microsatellite instability-high or mismatch repair deficient metastatic colorectal cancer treated with first-line pembrolizumab versus chemotherapy (KEYNOTE-177): an open-label, randomised, phase 3 trial. *Lancet Oncol*. 2021; 22 (5): 665–77.
- Diao Z, Han Y, Chen Y, Zhang R, Li J. The clinical utility of microsatellite instability in colorectal cancer. *Crit Rev Oncol Hematol*. 2021; 157 (1): 103–71.
- Трякин А. А., Федянин М. Ю., Цуканов А. С., Шельгин Ю. А., Покатаев И. А., Игнатова Е. О. и др. Микросателлитная нестабильность как уникальная характеристика опухолей и предиктор эффективности иммунотерапии. *Злокачественные опухоли*. 2019; 9 (4): 59–69.
- Sahnane N, Furlan D, Monti M, Romualdi C, Vanoli A, Vicari E, et al. Microsatellite unstable gastrointestinal neuroendocrine

- carcinomas: a new clinicopathologic entity. *Endocr Relat Cancer*. 2015; 22 (1): 35–45.
7. Мусаелян А. А., Назаров В. Д., Будникова А. С., Лапин С. В., Воробьев С. Л., Эмануэль В. Л. и др. Клинико-морфологический портрет опухолей с микросателлитной нестабильностью. *Успехи молекулярной онкологии*. 2021; 8 (2): 52–59.
 8. Trifanov VS, Timoshkina NN, Gvaldin DYU, Mesheryakova MYu, Kolesnikov EN, Gaziev UM, et al. Study of microsatellite instability in neuroendocrine tumors of pancreas and colon. *Journal of Clinical Oncology*. 2021; 39 (15): 16196.
 9. Fraune C, Simon R, Hube-Magg C, Makrypidi-Fraune G, Kluth M, Büscheck F, et al. Homogeneous MMR Deficiency Throughout the Entire Tumor Mass Occurs in a Subset of Colorectal Neuroendocrine Carcinomas. *Endocr Pathol*. 2020; 31 (2): 182–9.
 10. Xing J, Ying H, Li J, Gao Y, Sun Z, Li J, et al. Immune Checkpoint Markers in Neuroendocrine Carcinoma of the Digestive System. *Front Oncol*. 2020; 28 (10): 132.
 11. Girardi DM, Silva ACB, Rêgo JFM, Coudry RA, Riechelmann RP. Unraveling molecular pathways of poorly differentiated neuroendocrine carcinomas of the gastroenteropancreatic system: A systematic review. *Cancer Treat Rev*. 2017; 56 (1): 28–35.
 12. Mitsuhashi K, Yamamoto I, Kurihara H, Kanno S, Ito M, Igarashi H, et al. Analysis of the molecular features of rectal carcinoid tumors to identify new biomarkers that predict biological malignancy. *Oncotarget*. 2015; 6 (26): 22114–25.
 13. Kidd M, Eick G, Shapiro MD, Camp RL, Mane SM, Modlin IM. Microsatellite instability and gene mutations in transforming growth factor-beta type II receptor are absent in small bowel carcinoid tumors. *Cancer*. 2005; 103 (2): 229–36.
 14. Ghimenti C, Lonobile A, Campani D, Bevilacqua G, Caligo MA. Microsatellite instability and allelic losses in neuroendocrine tumors of the gastro-entero-pancreatic system. *Int J Oncol*. 1999; 15 (2): 361–6.
 15. Arnold CN, Nagasaka T, Goel A, Scharf I, Grabowski P, Sosnowski A, et al. Molecular characteristics and predictors of survival in patients with malignant neuroendocrine tumors. *Int J Cancer*. 2008; 123 (7): 1556–64.
 16. Dudley JC, Lin MT, Le DT, Eshleman JR. Microsatellite Instability as a Biomarker for PD-1 Blockade. *Clin Cancer Res*. 2016; 22 (4): 813–20.
 17. Olevian DC, Nikiforova MN, Chiosea S, Sun W, Bahary N, Kuan SF, et al. Colorectal poorly differentiated neuroendocrine carcinomas frequently exhibit BRAF mutations and are associated with poor overall survival. *Hum Pathol*. 2016; 49 (1): 124–34.
 18. Furlan D, Sahnane N, Mazzoni M, Pastorino R, Carnevali I, Stefanoli M, et al. Diagnostic utility of MS-MLPA in DNA methylation profiling of adenocarcinomas and neuroendocrine carcinomas of the colon-rectum. *Virchows Arch*. 2013; 462 (1): 47–56.
 19. La Rosa S, Marando A, Furlan D, Sahnane N, Capella C. Colorectal poorly differentiated neuroendocrine carcinomas and mixed adenoneuroendocrine carcinomas: insights into the diagnostic immunophenotype, assessment of methylation profile, and search for prognostic markers. *Am J Surg Pathol*. 2012; 36 (4): 601–11.
 20. Kit OI, Trifanov VS, Petrusenko NA, Gvaldin DY, Kutilin DS, Timoshkina NN. Identification of new candidate genes and signalling pathways associated with the development of neuroendocrine pancreatic tumours based on next generation sequencing data. *Mol Biol Rep*. 2020; 47 (6): 4233–43.
 21. Кит О. И., Водолажский Д. И. Молекулярная биология колоректального рака в клинической практике. *Молекулярная биология*. 2015; 49 (4): 531–54.

SENSORS FOR ANALYSIS OF DRUGS, DRUG-DRUG INTERACTIONS, AND CATALYTIC ACTIVITY OF ENZYMES

Agafonova LE¹✉, Bulko TV¹, Kuzikov AV^{1,2}, Masamrekh RA^{1,2}, Shumyantseva VV^{1,2}

¹ Orekhovich Research Institute of Biomedical Chemistry, Moscow, Russia

² Pirogov Russian National Research Medical University, Moscow, Russia

Development of highly sensitive methods for drug analysis is an ongoing challenge posed by modern bioanalytical and pharmaceutical chemistry. Drug analysis is essential to monitor the quality and purity of pharmaceuticals, study the delivery vehicles for therapeutic agents, to assess the effectiveness of the substance incorporation into the drug delivery system, to estimate the kinetic parameters of reactions, catalyzed by enzymes involved in xenobiotic metabolism, and to study the mechanisms of the drug-DNA interactions from the perspective of pharmacogenomics. The study was aimed to develop an electrochemical technique for detection of a number of drugs. The method is based on electrochemical oxidation of organic molecules at positive potentials between $+(0 \div 1.6)$ V. The commercially available three-contact electrodes obtained by screen printing with unmodified graphite working electrode were used for analysis. It is shown that electrochemical technique allows for simultaneous detection of several compounds at various working electrode potentials, and for detection of drugs over a wide range of the clinically meaningful drug concentrations (50 μ M – 10 mM), which could be used when working with biological fluids (blood plasma, blood serum, blood, urine), as well as when performing drug monitoring and drug-drug interaction analysis.

Keywords: electroanalysis, drugs, voltaren, nurofen, paracetamol, unmodified screen-printed graphite electrodes

Funding: the study was carried out within the framework of the Russian Federation fundamental research program for the long-term period for 2021–2030.

Author contribution: Agafonova LE — experimental procedure, data processing, manuscript writing, building graphs; Bulko TV — sample preparation, experimental procedure; Kuzikov AV — statistical data processing, manuscript writing; Masamrekh RA — sample preparation, experimental procedure; Shumyantseva VV — concept, manuscript writing, data analysis.

✉ **Correspondence should be addressed:** Lyubov E. Agafonova
Pogodinskaya, 10/8, Moscow, 119121, Russia; agafonovaluba@mail.ru

Received: 07.02.2022 **Accepted:** 21.02.2022 **Published online:** 28.02.2022

DOI: 10.24075/brsmu.2022.009

СЕНСОРЫ ДЛЯ АНАЛИЗА ЛЕКАРСТВЕННЫХ ПРЕПАРАТОВ, МЕЖЛЕКАРСТВЕННЫХ ВЗАИМОДЕЙСТВИЙ И КАТАЛИТИЧЕСКОЙ АКТИВНОСТИ ФЕРМЕНТОВ

Л. Е. Агафонова¹✉, Т. В. Булко¹, А. В. Кузиков^{1,2}, Р. А. Масамрех^{1,2}, В. В. Шумянцова^{1,2}

¹ Научно-исследовательский институт биомедицинской химии имени В. Н. Ореховича, Москва, Россия

² Российский национальный исследовательский медицинский университет имени Н. И. Пирогова, Москва

Разработка высокочувствительных методов анализа лекарственных препаратов является актуальной задачей современной биоаналитической и фармакологической химии. Анализ лекарственных препаратов необходим для мониторинга качества и чистоты, для исследования средств доставки терапевтических средств и определения эффективности включения субстанций в системы доставки, для исследования кинетических параметров реакций, катализируемых ферментами метаболизма ксенобиотиков, для исследования механизма взаимодействия лекарств с ДНК с позиций фармакогеномики. Целью работы было разработать электрохимический метод регистрации ряда лекарственных препаратов. Метод основан на реакции электроокисления органических молекул при положительных значениях потенциалов в диапазоне $+(0 \div 1,6)$ В. Для анализа использовали коммерчески доступные трехконтактные электроды, получаемые методом трафаретной печати с немодифицированным графитовым рабочим электродом. Показано, что электрохимический метод позволяет одновременно детектировать несколько соединений при разных значениях рабочих потенциалов и регистрировать препараты в широком диапазоне определяемых терапевтически значимых концентраций (50 мкМ – 10 мМ), что может быть применено при работе с биологическими жидкостями (плазмой, сывороткой, кровью, мочой), для лекарственного мониторинга и анализа межлекарственных взаимодействий.

Ключевые слова: электроанализ, лекарственные препараты, вольтарен, нурофен, парацетамол, немодифицированные печатные графитовые электроды

Финансирование: работа выполнена в рамках Программы фундаментальных научных исследований в Российской Федерации на долгосрочный период (2021–2030 гг.).

Вклад авторов: Л. Е. Агафонова — проведение экспериментов, обработка результатов, написание статьи, подготовка графиков; Т. В. Булко — подготовка образцов, проведение экспериментов; А. В. Кузиков — статистическая обработка результатов, написание статьи; Р. А. Масамрех — подготовка образцов, проведение экспериментов; В. В. Шумянцова — концепция, написание статьи, анализ результатов.

✉ **Для корреспонденции:** Любовь Евгеньевна Агафонова
Погодинская ул., д. 10, стр. 8, г. Москва, 119121, Россия; agafonovaluba@mail.ru

Статья получена: 07.02.2022 **Статья принята к печати:** 21.02.2022 **Опубликована онлайн:** 28.02.2022

DOI: 10.24075/vrgmu.2022.009

Electrochemical method of analysis is a powerful tool to estimate the drug content and purity, as well as the drug concentration both in pharmaceutical fluids and in biological fluids or tissues (urine, blood serum, blood plasma, whole blood, cell lysates). Despite the use of various drug evaluation methods (such as spectrophotometry, colorimetry, fluorescence spectroscopy, gas chromatography–mass spectrometry, high-performance liquid chromatography (HPLC), thin-layer chromatography,

titrimetry, capillary electrophoresis, high-performance liquid chromatography–tandem mass spectrometry and thermogravimetric analysis, radiometry, immunoassay) [1], electrochemical techniques are in demand as well due to high sensitivity, unique electrochemical signatures of the relevant compounds, reasonable cost, fast electrochemical analysis speed, low sample volumes (2–60 μ L), and portable equipment. Electroanalysis allows for simultaneous detection

of several pharmaceuticals and makes it possible to assess these drugs by various electrochemical methods in order to improve the test sensitivity (cyclic and stripping voltammetry, square-wave voltammetry, differential pulse voltammetry, chronoamperometry, and electrochemical impedance spectroscopy) [2–6].

Cytochrome P450 is a superfamily of heme-thiolate monoxygenases involved in metabolism of xenobiotics and endogenous compounds [7]. The method for measuring catalytic activity of this hemoprotein class by electrochemical oxidation of substrate drugs performed well in the previously published study [4], aimed at measuring the catalytic activity of cytochrome P450 3A4. Cytochrome P450 19A1 (CYP19A1, aromatase) is a key enzyme for estrogen biosynthesis [8]. Electrochemical methods for determination of estrone or β -estradiol using the electrodes, modified with various nanocomposites, had been previously developed in order to quantify the products of the CYP19A1-dependent electrocatalytic reaction [9–12]. Electrochemical oxidation of estrone or β -estradiol, being the aromatase metabolites, could be also detected on the commercially available three-prong printed graphite electrodes (PGE) [13]. Electrooxidation of (S)-7-hydroxywarfarin, being the cytochrome P450 2C9 metabolite, was used to evaluate the kinetic parameters of this hemoprotein [5].

The study was aimed to develop the reagentless electrochemical method for drug identification and quantification under physiological conditions in order to provide the possibility of assessing drugs in blood serum using the commercially available screen-printed three-prong electrodes with the graphite working electrode.

METHODS

Electrochemical measurements were performed with the PGSTAT 12 Autolab and PGSTAT 312N Autolab potentiostats (Metrohm Autolab Ins.; Netherlands) and the GPES and NOVA software, versions 4.9.7 and 2.0, respectively (Netherlands). The three-prong printed graphite electrodes (PGE, ColorElectronics; Russia) were used, together with the graphite working and auxiliary electrodes, and the silver chloride reference electrode. The diameter of working electrode was 0.2 cm (the area was 0.0314 cm²). All potentials were referred to the silver/silver chloride reference electrode (Ag/AgCl).

The following reagents were used in the study: monobasic potassium phosphate (Reachem; Russia), sodium chloride (Reachem; Russia), diclofenac sodium (substance,

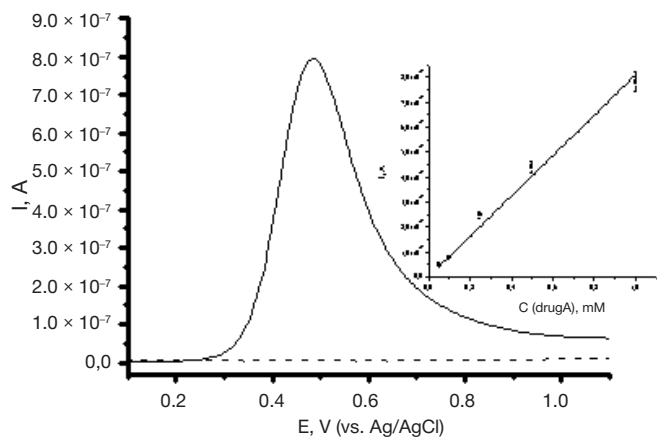


Fig. 1. Differential pulse voltammogram acquired on PGE in the 0.1 M potassium phosphate buffer containing 50 mM NaCl, pH 7.4, in the absence (---) or presence (-) of the 1 mM drug A. Insert: relationship between the oxidation peak current and the drug A concentration

Sigma-Aldrich; India), ibuprofen sodium (substance, Sigma-Aldrich; India), acetaminophen (pharmaceutical dosage form, Pharmstandard; Russia), mexidol (pharmaceutical dosage form, Pharmasoft; Russia), serum (S 1005-14, UsBiological; USA).

The 10 mM stock solutions were prepared in the 0.1 M potassium phosphate buffer (pH 7.4), containing 0.05 M NaCl, the desired concentrations were obtained by diluting with buffer and stored at +4 °C.

The real-time measurements were performed by differential pulse voltammetry (DPV) over the potential range of (0–1.6) V with the 0.01 V potential step and 25 Hz frequency, and by cyclic voltammetry (CV). Experiments were performed under aerobic conditions at room temperature. A total of 60 μ L (volume essential for uniform distribution of the drop across the electrodes) of the drug solution to be analyzed were applied to the surface of the disposable PGE, covering the working electrode, auxiliary electrode, and reference electrode [14]. At least three electrodes were used to assess the results repeatability for each concentration.

Peak current of analyte oxidation was plotted against analyte concentration in order to calculate sensitivity and the detection limit. The resulting calibration dependencies were used to calculate sensitivity (equation 1) and the detection limit (equation 2) [15]:

$$S = \Delta I / \Delta C \quad (1),$$

$$C_{lim} = 3,3\sigma / S \quad (2),$$

where S — sensitivity, I — current, C — drug concentration, C_{lim} — detection limit, σ — residual standard deviation (standard deviation of the regression coefficient b).

To remove protein components from blood serum, 2.5 mL of blood serum were collected in the 10 mL glass tube and

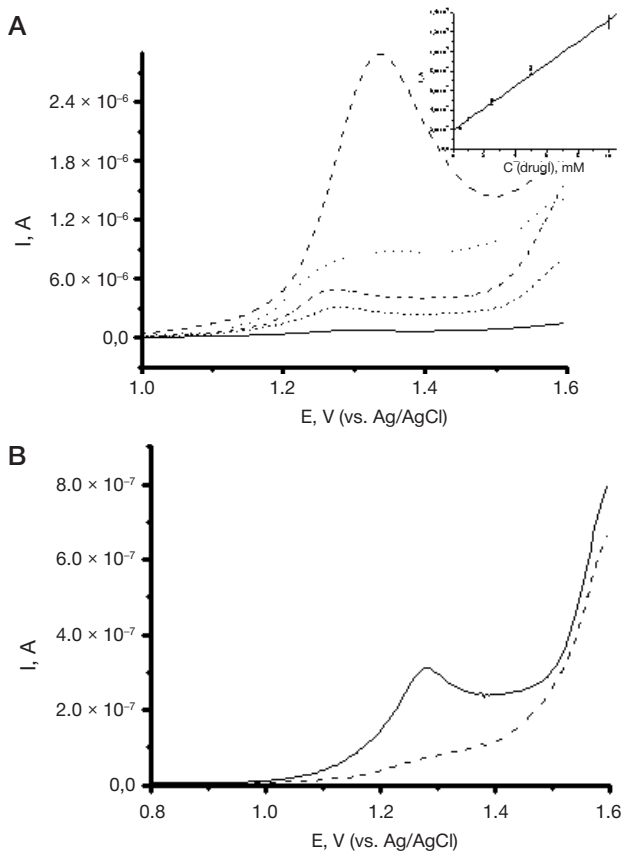


Fig. 2. A. Differential pulse voltammograms of drug I acquired on PGE in the 0.1 M potassium phosphate buffer containing 50 mM NaCl, pH 7.4, in the concentration range of 0.5 mM – 10 mM. Insert: relationship between the oxidation peak current and the drug I concentration. **B.** Differential pulse voltammograms acquired PGE in the absence (---) or presence (-) of the 1 mM drug I

Table. Electroanalytical characteristics of drugs, obtained by differential pulse voltammetry on PGE in the 0.1 M potassium phosphate buffer containing 50 mM NaCl, pH 7.4 ($n = 4-5$; $p = 0.95$)

Pharmaceutical (manufacturer)	Linear concentration range, M	E_{ox} , V	Regression equation		R^2	Sensitivity, A/M	Detection limit, M
			$I (A) = a \times C (mM) + b$				
			$a \pm \Delta a$	$b \pm \Delta b$			
Drug A (Pharmstandard)	$5 \times 10^{-5} - 1 \times 10^{-3}$	0.50 ± 0.03	$(8.6 \pm 0.5) \times 10^{-7}$	–	0.985	8.6×10^{-4}	2.9×10^{-5}
Drug I (Sigma-Aldrich)	$5 \times 10^{-4} - 1 \times 10^{-2}$	1.29 ± 0.02	$(1.2 \pm 0.1) \times 10^{-7}$	$(1.7 \pm 0.2) \times 10^{-7}$	0.983	1.2×10^{-4}	4.1×10^{-4}
Drug D (Sigma-Aldrich)	$5 \times 10^{-5} - 5 \times 10^{-4}$	0.57 ± 0.05	$(4.4 \pm 0.5) \times 10^{-7}$	$(3.3 \pm 0.6) \times 10^{-5}$	0.966	4.4×10^{-4}	4.6×10^{-5}

added 2.5 mL of the 15% (w/v) acetonitrile solution of zinc sulfate (50/40, v/v) or 10% trichloroacetic acid (1 : 10). The test tube was shaken for 20 min and equilibrated at 4 °C for 15 min, then the solution was centrifuged at 13,500 rpm for 5 min. Subsequently, supernatant was discarded, and the solution was used for further analysis [16]. After protein precipitation, blood serum was diluted 10 times with the 0.1 M potassium phosphate buffer, containing 50 mM NaCl, pH 7.4.

RESULTS

Rational selection of the electrode type is the key point of electrochemical analysis, which is essential for the most effective electron transfer and detection of molecules, biochemical events, and catalytic current, being the indicator of electrocatalysis [17]. It is shown, that modification of the electrode working surface with nanomaterials (carbon nanotubes, graphene, graphene oxide, metal nanoparticles) contributes to the increased sensor analytical sensitivity [6]. However, modified PGE may acquire background characteristics that impede direct registration of electrooxidation/electroreduction [18]. In unmodified PGE, background characteristics in the electrolyte buffer show no unintended additional signals, and the current values registered are rather low [5]. Furthermore, unmodified electrodes are commercially available, reproducibility of electrochemical analysis is high, which constitutes an essential element of the further sensors' practical utilization for drug analysis and purity evaluation, particularly in the clinical diagnostics laboratories. In this regard, we have developed methods for drug detection using precisely the unmodified graphite working electrode surfaces.

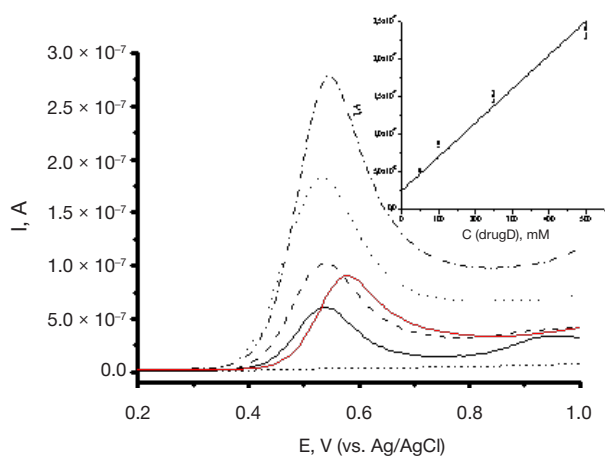


Fig. 3. Differential pulse voltammograms of drug D acquired on PGE in the 0.1 M potassium phosphate buffer containing 50 mM NaCl, pH 7.4, in the concentration range of 50 μM – 500 μM, with the drug D serum concentration of 100 μM (-) (after protein precipitation, blood serum was diluted 10 times with the 0.1 M potassium phosphate buffer, 50 mM NaCl, pH 7.4). Insert: relationship between the oxidation peak current and the drug D concentration

Electroanalytical characteristics of pharmaceuticals

N-acetyl-para-aminophenol, or drug A is an antipyretic and analgesic agent commonly used in patients with mild to moderate pain or to lower the body temperature, including in viral and bacterial infections [3]. It has been shown that *N-acetyl-p-benzoquinone imine* (NAPQI) is the main product of the drug A oxidation [3]. The mechanism, underlying the analgesic effect, is associated with prostaglandin synthesis inhibition in the central nervous system [2, 3, 19].

Fig. 1 provides the differential pulse voltammogram of the 1 mM drug A acquired on the unmodified PGE in the potential range of (0–1.2) V. Under aerobic conditions, drug A oxidation occurs at the E_{ox} potential of (0.50 ± 0.03) V (vs. Ag/AgCl). The figure insert shows the linear growth of the drug A oxidation peak current with the concentration increase from 0.05 mM to 1.00 mM. The drug A oxidation potential is stable within the margin of error.

Table provides electroanalytical characteristics (concentration range, oxidation potential), equation for the relationship between the oxidation peak current and the concentration, R^2 coefficient of determination, as well as the electrochemical system sensitivity, calculated using equation 1, and the detection limit of drug A, calculated using equation 2.

(RS)-2-(4-isobutylphenyl)-propionic acid, or drug I is a non-steroidal anti-inflammatory drug from the group of the propionic acid derivatives, which possesses analgesic and antipyretic activity [12, 13]. Fig. 2 provides the drug I differential pulse voltammograms acquired on PGE in the potential range of (0.6–1.6) V and the concentration range of (0.5–10) mM. Electrochemical oxidation of the 1 mM drug I occurs at high potential values (1.29 ± 0.02) V (see Table).

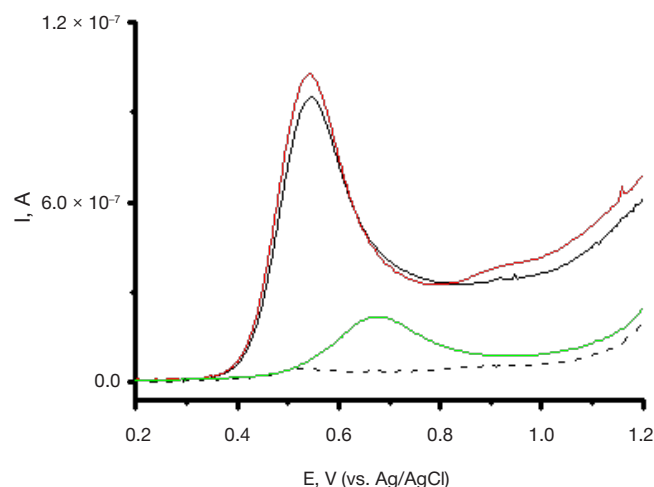


Fig. 4. Differential pulse voltammograms acquired on PGE in the 0.1 M potassium phosphate buffer containing 50 mM NaCl, pH 7.4, in the absence (---) or presence of the 98 μM drug M (-), 100 μM drug D (-), 100 μM drug D + 98 μM drug M (-)

(2-(2,6-dichloroanilino)-phenylacetic acid, or drug D is a non-steroidal anti-inflammatory drug from the group of the phenylacetic acid derivatives. The sodium salt is used in the pharmaceutical dosage forms. The drug has multiple trading names, it is prescribed to patients with many disorders, such as rheumatoid arthritis, osteoarthritis, various inflammation conditions [20, 21]. The drug has analgesic, anti-inflammatory, and anticancer effects [21]. Drug D undergoes extensive metabolism, mediated by glucosyltransferase, to form diclofenac acyl glucuronide. On exposure to cytochrome P450, drug D undergoes oxidative metabolism to form 4'-hydroxydiclofenac (catalyzed by cytochrome P450 2C9) and 5-hydroxydiclofenac (catalyzed by cytochrome P450 3A4) [22, 23].

In some cases, the drug can cause unwanted side effects: stomach hemorrhage, high blood pressure in patients with Shy-Drager syndrome and diabetes mellitus. The long-term use may result in infarction or stroke [20]. That is why the drug D analysis remains an ongoing challenge posed by bioanalytical and pharmaceutical chemistry.

Fig. 3 provides the drug D differential pulse voltammograms acquired on PGE in the potential range of (0.2 – 1.0) V and the concentration range of (50 – 500) μM . The oxidation potential of (0.57 \pm 0.05) V was stable within the margin of error in the studied concentration range. The linear relationship was found between the oxidation peak current and the drug D concentration (see Table).

DISCUSSION

CV in the scan rate range of (0.05–0.18) V/s was used to characterize the drug electrochemical oxidation processes. The CV results showed the linear relationship between the oxidation peak currents of the 1 mM drug A, 100 μM drug D and 5 mM drug I, and the scan rate square root $v^{1/2}$ (Fig. 2 (a), 4 (a), 6 (a), Appendix), reflecting the diffusion-controlled electrochemical oxidation of the drugs on the unmodified PGE in the studied range of the potential scan rates [24]. There was also a linear relationship between the oxidation peak potentials and the logarithm of scan rate, $\log v$ (Fig. 2 (b), 4(b), 6(b), Appendix), typical for irreversible electrochemical processes. This is confirmed by the CV technique: only the oxidation peaks of the 1 mM drug A, 100 μM drug D and 5 mM drug I are observed on the unmodified PGE (Fig. 1, 3 and 5, Appendix), suggesting the irreversible nature of electrochemical reactions. These results are in line with the mechanisms of the studied drugs electrochemical oxidation [2, 3, 6, 19–22, 25–30].

Polypharmacy, i.e. prescribing several medications to one patient, is widely used in clinical pharmacology and therapeutics. Pharmacokinetic and pharmacodynamic parameters should be monitored in multimorbid patients (prescribed two or more medications). Electroanalysis based on the drug electrochemical oxidation registration allows for simultaneous detection of several compounds. This approach can be used to determine the drugs' mutual influence. Thus, antioxidant metabolic drug mexidol (2-ethyl-6-methyl-3-hydroxypyridine succinate, drug M), which is prescribed to improve cerebral circulation, is commonly used in various groups of patients with comorbidities. PGE were used to analyze the drug combinations D + M (Fig. 4), D + I (Fig. 5). Electrochemical oxidation of drug M is detected at the potential of +0.67 \pm 0.06 V (Fig. 4). However, drug M (98 μM)

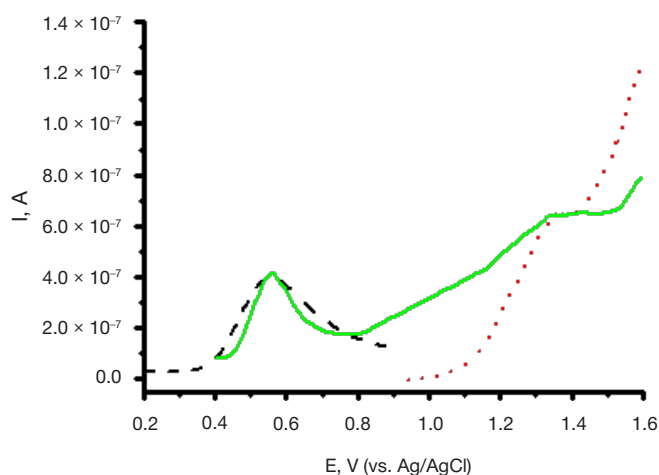


Fig. 5. Differential pulse voltammograms acquired on PGE in the 0.1 M potassium phosphate buffer containing 50 mM NaCl, pH 7.4, in the presence of 25 μM drug D (---), 200 μM drug I (...), and the combination of 25 μM drug D and 200 μM drug I (-)

has virtually no effect on the drug D (100 μM) electrochemical oxidation. There is a slight shift of the drug D oxidation potential by (5 \pm 2) mV toward the more positive (anodic) area, which is indicative of the more complicated electrochemical oxidation process. The oxidation peak current is slightly reduced (\pm 6%), which allows for the drug D quantification in the presence of drug M (Fig. 4). Fig. 5 provides DPV for the combination of the 25 μM drug D and 200 μM drug I acquired on the PGE. The measurements have been performed over the potential range of (0–1.6) V. Electrooxidation peaks of the drugs D ($E_{\text{ox}} = +0.54 \pm 0.02$ V) and I ($E_{\text{ox}} = +1.29 \pm 0.02$ V) are clearly distinguished, however, the concentration dependence remains.

Drug D was also determined by electrochemical oxidation in the blood serum samples. The concentration of drug D added to blood serum was 100 μM , and the oxidation peak current recorded was 7.5×10^{-8} A (Fig. 3). According to the insert in the Fig. 3 and the calibration dependence (see Table), the drug D concentration calculated using the regression equation was (95 \pm 5) μM .

CONCLUSIONS

The method for drug analysis using the commercially available disposable unmodified screen-printed electrodes has been developed. Sensitivity of the method corresponds to the clinically relevant concentration ranges. Electrooxidation of pharmaceuticals using electrodes as measuring tools is an effective analytical approach to the drug purity assessment and drug concentration determination, particularly in biological fluids used for therapeutic drug monitoring. The methods for drug quantification based on electrochemical oxidation may be used to assess catalytic activity of enzymes involved in the phase I metabolism, such as cytochrome P450, flavin-containing monooxygenases, aldehyde oxidase, aldehyde dehydrogenase, alcohol dehydrogenase, carboxylesterase, and to assess activity of enzymes involved in the phase II metabolism, such as UDP-glucuronosyltransferases, sulfotransferase, glutathione transferase. The method can be also used for registration of the comparative kinetics of the polymorphic variants and genetically engineered mutant enzymes in order to develop the biocatalyst isoforms important in technology.

References

- Ahuja S, Dong MW. Handbook of pharmaceutical analysis by HPLC. Elsevier, Amsterdam, 2005; 679 p.
- Akbari M, Shayani-Jam H, Yaftian MR, Parinejad M. Electrochemical oxidation of acetaminophen in the presence of diclofenac and piroxicam — Synthesis of new derivatives and kinetic investigation of toxic quinone imine/drugs interactions. *Journal of Electroanalytical Chemistry*. 2018; 827: 160–6. DOI: 10.1016/J.JELECHEM.2018.09.021.
- Cernat A, Tertis M, Sandulescu R, Bedioui F, Cristea A, Cristea C. Electrochemical sensors based on carbon nanomaterials for acetaminophen detection: A review. *Analytica Chimica Acta*. 2015; 886: 16–28. DOI: 10.1016/j.aca.2015.05.044.
- Shumyantseva VV, Bulko TV, Kuzikov AV, Masamrekh RA, Konyakhina AY, Romanenko I, et al. All-electrochemical nanocomposite two-electrode setup for quantification of drugs and study of their electrocatalytic conversion by cytochromes P450. *Electrochimica Acta*. 2020; 336: 135579. DOI: 10.1016/j.electacta.2019.135579.
- Kuzikov AV, Filippova TA, Masamrekh RA, Shumyantseva VV. Electrochemical determination of (S)-7-hydroxywarfarin for analysis of CYP2C9 catalytic activity. *Journal of Electroanalytical Chemistry*. 2022; 904: 115937. DOI: 10.1016/j.jelechem.2021.115937.
- Qian L, Durairaj S, Prins S, Chen A. Nanomaterial-based electrochemical sensors and biosensors for the detection of pharmaceutical compounds. *Biosensors and Bioelectronics*. 2021; 175: 112836. DOI: 10.1016/j.bios.2020.112836.
- Manikandan P, Nagini S. Cytochrome P450 Structure, Function and Clinical Significance: A Review. *Current Drug Targets*. 2018; 19 (1): 38–54. DOI: 10.2174/1389450118666170125144557.
- Hamadeh IS, Patel JN, Rusin S, Tan AR. Personalizing aromatase inhibitor therapy in patients with breast cancer. *Cancer Treatment Reviews*. 2018; 70: 47–55. DOI: 10.1016/j.ctrv.2018.07.014.
- Zhu Y, Liu X, Jia J. Electrochemical detection of natural estrogens using a graphene/ordered mesoporous carbon modified carbon paste electrode. *Analytical Methods*. 2015; 7: 8626–31. DOI: 10.1039/C5AY01833A.
- Moraes FC, Rossi B, Donatoni MC, de Oliveira KT, Pereira EC. Sensitive determination of 17 β -estradiol in river water using a graphene based electrochemical sensor. *Analytica Chimica Acta*. 2015; 881: 37–43. DOI: 10.1016/j.aca.2015.04.043.
- Lin X, Li Y. A sensitive determination of estrogens with a Pt nanoclusters/multi-walled carbon nanotubes modified glassy carbon electrode. *Biosensors and Bioelectronics*. 2006; 22 (2): 253–9. DOI: 10.1016/j.bios.2006.01.005.
- Hu S, Wu K, Yi H, Cui D. Voltammetric behavior and determination of estrogens at Nafion-modified glassy carbon electrode in the presence of cetyltrimethylammonium bromide. *Analytica Chimica Acta*. 2002; 464 (2): 209–16. DOI: 10.1016/S0003-2670(02)00496-8.
- Kuzikov AV, Masamrekh RA, Filippova TA, Haurychenka YI, Gilep AA, Shkel TV, et al. Electrochemical oxidation of estrogens as a method for CYP19A1 (aromatase) electrocatalytic activity determination. *Electrochimica Acta*. 2020; 333: 135539. DOI: 10.1016/j.electacta.2019.135539.
- Kulys J, D'Costa EJ. Printed amperometric sensor based on TCNQ and cholinesterase. *Biosensors and Bioelectronics*. 1991; 6 (2): 109. DOI: 10.1016/0956-5663(91)87034-9.
- Patel M, Patel DA, Gajra B. Validation of Analytical Procedures: Methodology ICH-Q2B. *International journal of review article pharmaceutical innovations*. 2011; 1 (2): 45.
- Jalalvand AR. A study originated from combination of electrochemistry and chemometrics for investigation of the inhibitory effects of ciprofloxacin as a potent inhibitor on cytochrome P450. *Microchemical Journal*. 2020; 157: 105104. DOI: 10.1016/j.microc.2020.105104.
- Shumyantseva VV, Agafonova LE, Bulko TV, Kuzikov AV, Masamrekh RA, Yuan J, et al. Electroanalysis of Biomolecules: Rational Selection of Sensor Construction. *Biochemistry (Moscow)*. 2021; 86: 140–51. DOI: 10.1134/S0006297921140108.
- Hasoň S, Fořta M, Ostatná V. Label-free electrochemical analysis of purine nucleotides and nucleobases at disposable carbon electrodes in microliter volumes. *Journal of Electroanalytical Chemistry*. 2019; 847 (15): 113252. DOI: 10.1016/J.JELECHEM.2019.113252.
- Fan Y, Liu JH, Lu HT, Zhang Q. Electrochemical behavior and voltammetric determination of paracetamol on Nafion/TiO₂-graphene modified glassy carbon electrode. *Colloids and surfaces. B: Biointerfaces*. 2011; 85 (2): 289–92. DOI: 10.1016/j.colsurfb.2011.02.041.
- Pandey SK, Yadav S, Goel Y, Temre MK, Singh VK, Singh SM. Molecular docking of anti-inflammatory drug diclofenac with metabolic targets: Potential applications in cancer therapeutics. *Journal of Theoretical Biology*. 2019; 465 (21): 117–25. DOI: 10.1016/j.jtbi.2019.01.020.
- Arisan ED, Akar RO, Rencuzogullari O, Yerlikaya OP, Gurkan AC, Akin B, et al. The molecular targets of diclofenac differs from ibuprofen to induce apoptosis and epithelial mesenchymal transition due to alternation on oxidative stress management p53 independently in PC3 prostate cancer cells. *Prostate International*. 2019; 7 (4): 156–65. DOI: 10.1016/j.prn.2019.09.003.
- Lazarska KE, Dekker SJ, Vermeulen NPE, Commandeur JNM. Effect of UGT2B7*2 and CYP2C8*4 polymorphisms on diclofenac metabolism. *Toxicology Letters*. 2018; 284: 70–8. DOI: 10.1016/j.toxlet.2017.11.038.
- Nakanishi K, Uehara S, Kusama T, Inoue T, Shimura K, Kamiya Y, et al. In vivo and in vitro diclofenac 5-hydroxylation mediated primarily by cytochrome P450 3A enzymes in common marmoset livers genotyped for P450 2C19 variants. *Biochemical Pharmacology*. 2018; 152: 272–8. DOI: 10.1016/j.bcp.2018.04.002.
- Mohammadi A, Moghaddam A, Alikhani E, Eilkhani Zadeh K, Mozaffari S. Electrochemical quantification of fluoxetine in pharmaceutical formulation using carbon nanoparticles. *Micro & Nano Letters*. 2013; 8 (12): 853–7. DOI: 10.1049/MNL.2013.0671.
- Goodarzi M, Khalilzade M, Karimi F, Gupta V, Keyvanfar M, Bagheri H, et al. Square wave voltammetric determination of diclofenac in liquid phase using a novel ionic liquid multiwall carbon nanotubes paste electrode. *Journal of Molecular Liquids*. 2014; 197: 114–9. DOI: 10.1016/J.MOLLIQ.2014.04.037.
- Sarhangzadeh K, Khatami AA, Jabbari M, Bahari S. Simultaneous determination of diclofenac and indomethacin using a sensitive electrochemical sensor based on multiwalled carbon nanotube and ionic liquid nanocomposite. *Journal of Applied Electrochemistry*. 2013; 43: 1217–24. DOI: 10.1007/s10800-013-0609-3.
- Karuppiyah C, Cheemalapati S, Chen S, Palanisamy S. Carboxyl-functionalized graphene oxide-modified electrode for the electrochemical determination of nonsteroidal anti-inflammatory drug diclofenac. *Ionics*. 2015; 21: 231–8. DOI: 10.1007/s11581-014-1161-9.
- Shalauddin M, Akhter S, Basirun WJ, Bagheri S, Anuar NS, Johan MR. Hybrid nanocellulose/f-MWCNTs nanocomposite for the electrochemical sensing of diclofenac sodium in pharmaceutical drugs and biological fluids. *Electrochimica Acta*. 2019; 304: 323–33. DOI: 10.1016/J.ELECTACTA.2019.03.003.
- Jiokeng SLZ, Tonle IK, Walcarius A. Amino-attapulgit/mesoporous silica composite films generated by electroassisted self-assembly for the voltammetric determination of diclofenac. *Sensors and Actuators B Chemical*. 2019; 287: 296–305. DOI: 10.1016/j.snb.2019.02.038.
- Karikalan N, Karthik R, Chen Sh-M, Velmurugan M, Karuppiyah Ch. Electrochemical properties of the acetaminophen on the screen printed carbon electrode towards the high performance practical sensor applications. *Journal of Colloid and Interface Science*. 2016; 483: 109–17. DOI: 10.1016/j.jcis.2016.08.028.

Литература

- Ahuja S, Dong MW. Handbook of pharmaceutical analysis by HPLC. Elsevier, Amsterdam, 2005; 679 p.
- Akbari M, Shayani-Jam H, Yaftian MR, Parinejad M. Electrochemical oxidation of acetaminophen in the presence of diclofenac and piroxicam — Synthesis of new derivatives and kinetic investigation of toxic quinone imine/drugs interactions. *Journal of Electroanalytical Chemistry*. 2018; 827: 160–6. DOI: 10.1016/J.JELECHEM.2018.09.021.
- Cernat A, Tertis M, Sandulescu R, Bedioui F, Cristea A, Cristea C. Electrochemical sensors based on carbon nanomaterials for acetaminophen detection: A review. *Analytica Chimica Acta*. 2015; 886: 16–28. DOI: 10.1016/j.aca.2015.05.044.
- Shumyantseva VV, Bulko TV, Kuzikov AV, Masamrekh RA, Konyakhina AY, Romanenko I, et al. All-electrochemical nanocomposite two-electrode setup for quantification of drugs and study of their electrocatalytic conversion by cytochromes P450. *Electrochimica Acta*. 2020; 336: 135579. DOI: 10.1016/j.electacta.2019.135579.
- Kuzikov AV, Filippova TA, Masamrekh RA, Shumyantseva VV. Electrochemical determination of (S)-7-hydroxywarfarin for analysis of CYP2C9 catalytic activity. *Journal of Electroanalytical Chemistry*. 2022; 904: 115937. DOI: 10.1016/j.jelechem.2021.115937.
- Qian L, Durairaj S, Prins S, Chen A. Nanomaterial-based electrochemical sensors and biosensors for the detection of pharmaceutical compounds. *Biosensors and Bioelectronics*. 2021; 175: 112836. DOI: 10.1016/j.bios.2020.112836.
- Manikandan P, Nagini S. Cytochrome P450 Structure, Function and Clinical Significance: A Review. *Current Drug Targets*. 2018; 19 (1): 38–54. DOI: 10.2174/1389450118666170125144557.
- Hamadeh IS, Patel JN, Rusin S, Tan AR. Personalizing aromatase inhibitor therapy in patients with breast cancer. *Cancer Treatment Reviews*. 2018; 70: 47–55. DOI: 10.1016/j.ctrv.2018.07.014.
- Zhu Y, Liu X, Jia J. Electrochemical detection of natural estrogens using a graphene/ordered mesoporous carbon modified carbon paste electrode. *Analytical Methods*. 2015; 7: 8626–31. DOI: 10.1039/C5AY01833A.
- Moraes FC, Rossi B, Donatoni MC, de Oliveira KT, Pereira EC. Sensitive determination of 17 β -estradiol in river water using a graphene based electrochemical sensor. *Analytica Chimica Acta*. 2015; 881: 37–43. DOI: 10.1016/j.aca.2015.04.043.
- Lin X, Li Y. A sensitive determination of estrogens with a Pt nanoclusters/multi-walled carbon nanotubes modified glassy carbon electrode. *Biosensors and Bioelectronics*. 2006; 22 (2): 253–9. DOI: 10.1016/j.bios.2006.01.005.
- Hu S, Wu K, Yi H, Cui D. Voltammetric behavior and determination of estrogens at Nafion-modified glassy carbon electrode in the presence of cetyltrimethylammonium bromide. *Analytica Chimica Acta*. 2002; 464 (2): 209–16. DOI: 10.1016/S0003-2670(02)00496-8.
- Kuzikov AV, Masamrekh RA, Filippova TA, Haurychenka YI, Gilep AA, Shkel TV, et al. Electrochemical oxidation of estrogens as a method for CYP19A1 (aromatase) electrocatalytic activity determination. *Electrochimica Acta*. 2020; 333: 135539. DOI: 10.1016/j.electacta.2019.135539.
- Kulys J, D'Costa EJ. Printed amperometric sensor based on TCNQ and cholinesterase. *Biosensors and Bioelectronics*. 1991; 6 (2): 109. DOI: 10.1016/0956-5663(91)87034-9.
- Patel M, Patel DA, Gajra B. Validation of Analytical Procedures: Methodology ICH-Q2B. *International journal of review article pharmaceutical innovations*. 2011; 1 (2): 45.
- Jalalvand AR. A study originated from combination of electrochemistry and chemometrics for investigation of the inhibitory effects of ciprofloxacin as a potent inhibitor on cytochrome P450. *Microchemical Journal*. 2020; 157: 105104. DOI: 10.1016/j.microc.2020.105104.
- Shumyantseva VV, Agafonova LE, Bulko TV, Kuzikov AV, Masamrekh RA, Yuan J, et al. Electroanalysis of Biomolecules: Rational Selection of Sensor Construction. *Biochemistry (Moscow)*. 2021; 86: 140–51. DOI: 10.1134/S0006297921140108.
- Hasoň S, Fojta M, Ostatná V. Label-free electrochemical analysis of purine nucleotides and nucleobases at disposable carbon electrodes in microliter volumes. *Journal of Electroanalytical Chemistry*. 2019; 847 (15): 113252. DOI: 10.1016/J.JELECHEM.2019.113252.
- Fan Y, Liu JH, Lu HT, Zhang Q. Electrochemical behavior and voltammetric determination of paracetamol on Nafion/TiO₂-graphene modified glassy carbon electrode. *Colloids and Surfaces. B: Biointerfaces*. 2011; 85 (2): 289–92. DOI: 10.1016/j.colsurfb.2011.02.041.
- Pandey SK, Yadav S, Goel Y, Temre MK, Singh VK, Singh SM. Molecular docking of anti-inflammatory drug diclofenac with metabolic targets: Potential applications in cancer therapeutics. *Journal of Theoretical Biology*. 2019; 465 (21): 117–25. DOI: 10.1016/j.jtbi.2019.01.020.
- Arisan ED, Akar RO, Rencuzogullari O, Yerlikaya OP, Gurkan AC, Akın B, et al. The molecular targets of diclofenac differs from ibuprofen to induce apoptosis and epithelial mesenchymal transition due to alternation on oxidative stress management p53 independently in PC3 prostate cancer cells. *Prostate International*. 2019; 7 (4): 156–65. DOI: 10.1016/j.prn.2019.09.003.
- Lazarska KE, Dekker SJ, Vermeulen NPE, Commandeur JNM. Effect of UGT2B7*2 and CYP2C8*4 polymorphisms on diclofenac metabolism. *Toxicology Letters*. 2018; 284: 70–8. DOI: 10.1016/j.toxlet.2017.11.038.
- Nakanishi K, Uehara S, Kusama T, Inoue T, Shimura K, Kamiya Y, et al. In vivo and in vitro diclofenac 5-hydroxylation mediated primarily by cytochrome P450 3A enzymes in common marmoset livers genotyped for P450 2C19 variants. *Biochemical Pharmacology*. 2018; 152: 272–8. DOI: 10.1016/j.bcp.2018.04.002.
- Mohammadi A, Moghaddam A, Alikhani E, Eilkanizadeh K, Mozaffari S. Electrochemical quantification of fluoxetine in pharmaceutical formulation using carbon nanoparticles. *Micro & Nano Letters*. 2013; 8 (12): 853–7. DOI: 10.1049/MNL.2013.0671.
- Goodarzi M, Khalilzade M, Karimi F, Gupta V, Keywanfar M, Bagheri H, et al. Square wave voltammetric determination of diclofenac in liquid phase using a novel ionic liquid multiwall carbon nanotubes paste electrode. *Journal of Molecular Liquids*. 2014; 197: 114–9. DOI: 10.1016/J.MOLLIQ.2014.04.037.
- Sarhangzadeh K, Khatami AA, Jabbari M, Bahari S. Simultaneous determination of diclofenac and indomethacin using a sensitive electrochemical sensor based on multiwalled carbon nanotube and ionic liquid nanocomposite. *Journal of Applied Electrochemistry*. 2013; 43: 1217–24. DOI: 10.1007/s10800-013-0609-3.
- Karuppiyah C, Cheemalapati S, Chen S, Palanisamy S. Carboxyl-functionalized graphene oxide-modified electrode for the electrochemical determination of nonsteroidal anti-inflammatory drug diclofenac. *Ionics*. 2015; 21: 231–8. DOI: 10.1007/s11581-014-1161-9.
- Shalauddin M, Akhter S, Basirun WJ, Bagheri S, Anuar NS, Johan MR. Hybrid nanocellulose/f-MWCNTs nanocomposite for the electrochemical sensing of diclofenac sodium in pharmaceutical drugs and biological fluids. *Electrochimica Acta*. 2019; 304: 323–33. DOI: 10.1016/J.ELECTACTA.2019.03.003.
- Jiokeng SLZ, Tonle IK, Walcarius A. Amino-attapulgite/mesoporous silica composite films generated by electroassisted self-assembly for the voltammetric determination of diclofenac. *Sensors and Actuators B: Chemical*. 2019; 287: 296–305. DOI: 10.1016/j.snb.2019.02.038.
- Karikalan N, Karthik R, Chen Sh-M, Velmurugan M, Karuppiyah Ch. Electrochemical properties of the acetaminophen on the screen printed carbon electrode towards the high performance practical sensor applications. *Journal of Colloid and Interface Science*. 2016; 483: 109–17. DOI: 10.1016/j.jcis.2016.08.028.

VISUAL ANALYSIS OF NIGROSOME-1 IN THE DIFFERENTIAL DIAGNOSIS OF PARKINSON'S DISEASE AND ESSENTIAL TREMOR

Moskalenko AN [✉], Filatov AS, Fedotova EYu, Kononov RN, Illarioshkin SN

Research Center of Neurology, Moscow, Russia

Differentiation between Parkinson's disease, especially in its early stages, and essential tremor, which is a phenotypically similar movement disorder, still remains an unsolved challenge for neurology. The aim of this study was to assess the diagnostic significance of nigrosome imaging (nigrosomes are dopaminergic neuron clusters in the substantia nigra of the midbrain) using 3T high-resolution SW-MRI. The study was conducted in 20 patients with Parkinson's disease and 10 patients with essential tremor. Visual analysis of the acquired nigrosome-1 images was performed using a 4-point ordinal rating scale. Differences in sex, age and duration of the disease were calculated using the Fisher exact test and the Mann-Whitney U test. The diagnostic value of the method was assessed using Pearson's chi-squared test. Nigrosome-1 was bilaterally or unilaterally absent in 70% of parkinsonian patients. Less specific changes to the substantia nigra (SN) were observed in two more parkinsonian patients (10%), whose nigrosome-1 appeared reduced in size. By contrast, nigrosome-1 was bilaterally intact in all patients (100%) with essential tremor ($p < 0.001$). Our preliminary findings demonstrate the high potential of noninvasive nigrosome-1 imaging in the differential diagnosis of Parkinson's disease and essential tremor.

Keywords: Parkinson's disease, essential tremor, nigrosome-1, magnetic resonance imaging, SWI

Author contribution: Moskalenko AN — clinical assessment, data acquisition and interpretation, literature analysis, manuscript preparation; Filatov AS — data analysis and interpretation, manuscript preparation; Kononov RN — data analysis and interpretation, study planning and supervision; Fedotova EYu, Illarioshkin SN — study planning and supervision.

Compliance with ethical standards: the study was approved by the Ethics Committee of the Research Center of Neurology (Protocol № 2–5/20 dated March 18, 2020). Informed consent was obtained from all study participants.

✉ **Correspondence should be addressed:** Anna N. Moskalenko
Volokolamskoe sh., 80, Moscow, 125367, Russia; anna_nik_kern@rambler.ru

Received: 22.12.2021 **Accepted:** 18.01.2022 **Published online:** 30.01.2022

DOI: 10.24075/brsmu.2022.002

ВИЗУАЛЬНЫЙ АНАЛИЗ НИГРОСОМЫ-1 В ДИФФЕРЕНЦИАЛЬНОЙ ДИАГНОСТИКЕ БОЛЕЗНИ ПАРКИНСОНА И ЭССЕНЦИАЛЬНОГО ТРЕМОРА

А. Н. Москаленко [✉], А. С. Филатов, Е. Ю. Федотова, Р. Н. Коновалов, С. Н. Иллариошкин

Научный центр неврологии, Москва, Россия

Дифференциальная диагностика болезни Паркинсона и фенотипически схожего двигательного расстройства — эссенциального тремора, особенно в дебюте заболевания, остается одной из нерешенных задач современной неврологии. Целью исследования было оценить диагностическую значимость визуализации нигросом — кластеров дофаминергических нейронов в черной субстанции (ЧС) среднего мозга, выявляемых при использовании SWI-режима высокоразрешающей магнитно-резонансной томографии (3 Тесла), у 20 пациентов с болезнью Паркинсона и у 10 пациентов с эссенциальным тремором. Визуальный анализ изображений нигросомы-1 проводили с использованием четырехчленной порядковой шкалы. Различия по гендерному, возрастному составу и продолжительности заболевания рассчитывали с помощью точного критерия Фишера, U-критерия Манна-Уитни. Для расчета диагностической ценности данной методики использовали критерий χ^2 Пирсона. У пациентов с болезнью Паркинсона в 70% случаев наблюдали одно- или двустороннее исчезновение нигросомы-1. Еще у двух пациентов с болезнью Паркинсона (10%) выявили менее специфичные изменения черной субстанции — уменьшение объема нигросомы-1. Напротив, у всех пациентов с эссенциальным тремором (100%) нигросома-1 оставалась сохранной с двух сторон ($p < 0,001$). Полученные предварительные результаты демонстрируют высокий потенциал методики визуального анализа нигросомы-1 в дифференциальной диагностике болезни Паркинсона и эссенциального тремора.

Ключевые слова: болезнь Паркинсона, эссенциальный тремор, нигросома-1, магнитно-резонансная томография, SWI-режим

Вклад авторов: А. Н. Москаленко — клиническая оценка, сбор, анализ и интерпретация данных, анализ литературы, подготовка рукописи; А. С. Филатов — анализ и интерпретация данных, подготовка рукописи; Р. Н. Коновалов — анализ и интерпретация данных, планирование и руководство исследованием; Е. Ю. Федотова, С. Н. Иллариошкин — планирование и руководство исследованием.

Соблюдение этических стандартов: исследование одобрено этическим комитетом Научного центра неврологии (протокол № 2–5/20 от 18 марта 2020 г.); все участники подписали добровольное согласие на участие в данном исследовании.

✉ **Для корреспонденции:** Анна Николаевна Москаленко
Волоколамское ш., д. 80, г. Москва, 125367, Россия; anna_nik_kern@rambler.ru

Статья получена: 22.12.2021 **Статья принята к печати:** 18.01.2022 **Опубликована онлайн:** 30.01.2022

DOI: 10.24075/vrgmu.2022.002

Parkinson's disease (PD) and essential tremor (ET) are common movement disorders that predominantly affect the elderly [1, 2]. Both diagnoses are clinical and rely on the sum of their typical neurological manifestations. According to the criteria for PD published by the International Parkinson and Movement Disorder Society in 2015, bradykinesia combined with resting tremor and/or rigidity in the presence of supportive criteria and the absence of absolute exclusion criteria indicates clinically definite or clinically probable PD [3]. Importantly, apart from motor manifestations, the clinical picture of PD can include non-

motor symptoms that predate motor impairment and progress gradually as the disease advances [4].

According to the updated criteria proposed by the International Parkinson and Movement Disorder Society in 2017, ET is defined as "an isolated tremor syndrome of bilateral upper limb action tremor with at least 3 years' duration, with or without tremor in other locations" [5]. In practice, patients with ET often present with additional neurological symptoms that go beyond the definition of ET, including resting tremor, impaired tandem gait, etc. Such cases are classified as ET plus. Besides motor

manifestations, many patients with ET have various non-motor symptoms [2] that usually do not have any particular clinical significance but complicate differentiation between ET and PD.

Radionuclide imaging, e.g. positron-emission tomography (PET), single photon emission computed tomography (SPECT) and transcranial sonography (TCS), can be used to differentiate between ET and PD by assessing damage to the substantia nigra (SN), the primary target of neurodegeneration in PD, which remains intact in ET [6, 7]. However, radionuclide imaging has objective limitations impeding its exploitation in clinical neurological practice.

The use of magnetic resonance imaging (MRI) for diagnosing PD and differentiating it from nondegenerative forms of parkinsonism became possible with the spread of high-field MR scanners and the introduction of additional MRI sequences into the standard MRI protocol.

Dopaminergic neurons of SN are arranged into cell clusters called nigrosomes [8]. Nigrosome-1, the largest of 5 known nigrosomes, appears on high-resolution susceptibility weighted images (SWI) as an oval slightly hyperintense region in the dorsal SN. Nigrosome-1 divides SN into 2 parts, bearing resemblance to a swallow tail, hence its name “the swallow tail sign” [9]. Recent research has shown that location of the hyperintense nigrosome-1 region in the surrounding hypointense SN structures can be quite variable and does not always fit the “swallow tail” profile [10]. Patients with PD demonstrate a loss of dorsolateral nigral hyperintensity due to the involvement of nigrosome-1 in neurodegeneration [9, 11]. In ET, structural and functional changes have been reported in the cerebellum and the brain stem (predominantly in the locus coeruleus) [12]. Despite the lack of consistency between the results of pathomorphological studies and the understudied pathogenesis of ET, so far there has been no reliable evidence about the presence of pronounced SN degeneration in patients with ET comparable to that in patients with PD. Consequently, attempts have been made to determine the diagnostic significance of visual assessment of nigrosome-1 images in discriminating between PD and ET. The method has demonstrated high sensitivity and high specificity; besides, it does not require image post-processing and therefore is effective and suitable for clinical practice [13, 14].

To our knowledge, there are no publications analyzing the described neuroimaging pattern of SN changes in the Russian cohort of patients with movement disorders. The aim of this study was to assess the biomarker role of dorsolateral nigral hyperintensity loss in differentiating between PD and ET, which is a phenotypically similar disorder.

METHODS

Participants

Participants were recruited from in- and outpatients undergoing treatment at the Research Center of Neurology from January to October 2020. The study included 20 patients with tremor-dominant/mixed types of PD (group 1) and 10 patients with ET (group 2). The diagnosis was made based on the current criteria for each of these disorders. PD staging was done using the functional Hoehn–Yahr scale: 40% of the patients had stage 1 ($n = 8$), 30% had stage 2 ($n = 6$), and 30% had stage 3 ($n = 6$). The patients gave informed consent to participate in the study and have their personal data processed.

The following exclusion criteria were applied: the past history of other neurologic/psychiatric disorders; psychoactive substance abuse; alcohol abuse; intake of tremorogenic drugs; tremor-inducing metabolic disorders; structural damage to

the brain (neoplasms, infarction, brain injury sequelae); MRI artifacts precluding the analysis of MR images; age under 18 and above 80 years.

MRI protocol and analysis of MR images

MRI protocol

All MR images were acquired using a 3T Siemens MAGNETOM Verio scanner equipped with an 8-channel head coil. SWI sequences were acquired to assess nigrosome-1 appearance (TR = 27 ms, TE = 20 ms, slice thickness = 1.5 mm, dist. factor = 20%, FoV = 172 × 230 mm², scan time = 2 min 59 s). Besides, T2, T1 MPR, T2 FLAIR and DWI images were acquired to exclude other causes of parkinsonism. The axial plane was parallel to the line connecting the anterior and posterior commissures across all brain structures.

Qualitative analysis of acquired images

On the acquired SW images, nigrosome-1 appeared as an oval slightly hyperintense region in the hypointense area of the dorsal midbrain (SN). Visual analysis of the images was performed using the following 4-point ordinal scale: 0 points — the norm (nigrosome-1 is visualized bilaterally); 1 point — the image has no diagnostic value (nigrosome-1 is poorly visualized on one or both sides or is diminished in size, i.e. partially lost); 2 points — abnormality (nigrosome-1 is absent unilaterally); 3 points — abnormality (nigrosome-1 is absent bilaterally). For illustrative purposes, MR images of 4 patients with different nigrosome-1 appearance are provided in Fig. 1. Qualitative analysis was conducted by 2 radiologists who had no access to the patients' medical records and were working independently. If their conclusions were conflicting, preference was given to the opinion of the more experienced radiologists.

Statistical analysis

The results of the study are presented below as medians and lower and upper quartiles (Med, lq, uq). Demographic characteristics of the patients (age, sex, duration of the disease) were compared using the Fisher exact test and the Mann–Whitney U-test. Nigrosome-1 scores were compared between the groups using Pearson's chi squared test. In all statistical tests, the significance threshold was assumed to be $p < 0.05$. The data were analyzed in StatTech v1.1.0, SPSS Statistics.

RESULTS

Demographic characteristics

The PD and ET groups did not differ significantly in terms of sex and age ($p = 0.246$, $p = 0.082$, respectively). The duration of the disease was significantly longer in the patients with ET than in those with PD ($p < 0.003$). The analysis of associations between the disease and sex was performed using Fisher's exact test; the associations between age and disease duration were tested using the Mann–Whitney U test. Demographic characteristics of the patients are provided in Table.

Neuroimaging data

Nigrosome-1 was clearly visible bilaterally in all patients with ET ($n = 10$), so all patients from group 2 scored 0 points on the rating scale (100%).

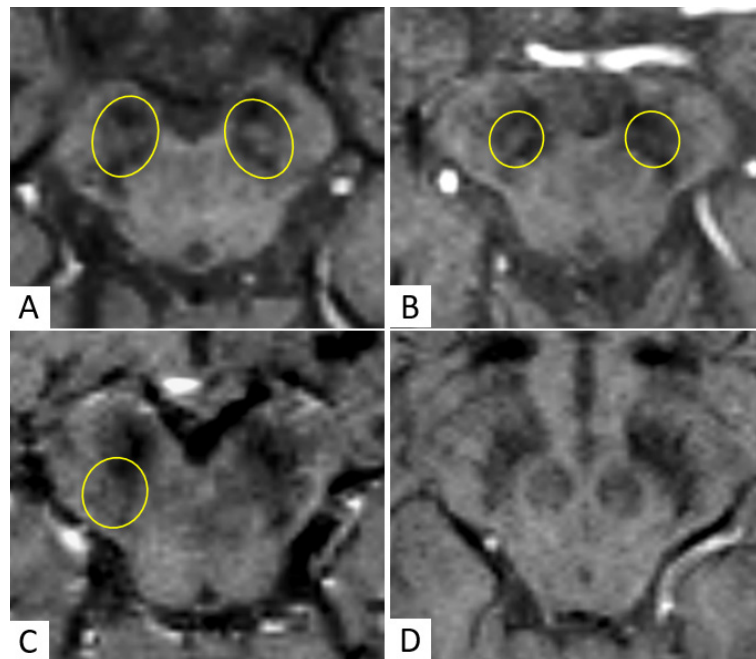


Fig. 1. Susceptibility-weighted MR images in the axial plane; slices pass through the cerebral peduncles. The substantia nigra is hypointense on SWI sequences, whereas nigrosomes-1 (yellow circles) are hyperintense. The figure shows different patterns of nigrosome-1 appearance in patients with PD (**A** — 0 points, **B** — 1 point (nigrosome-1 is reduced in volume on the left), **C** — 2 points, **D** — 3 points)

However, it was absent in 70% of patients with PD ($n = 14$); the ratio of unilateral and bilateral loss of dorsolateral nigral intensity was 1 : 1. Accordingly, 7 patients with PD scored 2 points (35%) and 7 other patients with PD scored 3 points (35%).

Nigrosome-1 was intact (0 points) in 4 patients with PD (20%); 2 more patients with PD (10%) scored 1 point: their MRI scans showed a reduction in nigrosome-1 size on one side, which was interpreted as having no diagnostic value. Comparison of the PD and ET groups demonstrated a significant difference in the results expressed as percentage ($p < 0.001$, Pearson's χ^2).

Thus, the study demonstrates a high diagnostic value of non-invasive visual nigrosome-1 assessment in differentiating between PD and ET: the sensitivity and specificity of the method were 70% and 100%, respectively. The results are provided in Fig. 2.

DISCUSSION

Oftentimes, discrimination between early-stage PD and phenotypically similar disorders poses a certain difficulty to a neurologist. The aim of this study was to assess the diagnostic significance of non-invasive nigrosome-1 assessment in differentiating PD from ET.

It has been over 20 years since heterogeneity of the SN pars compacta (i.e. identification of nigrosomes and the nigral matrix by immunohistochemical staining) was discovered

and the staging of nigrosome damage due to PD-related neurodegeneration was pathomorphologically confirmed [8, 15]. Non-invasive imaging of nigrosome-1 became possible with the spread of high-field MR scanners and the introduction of SWI sequences into the standard brain MRI protocol [9, 16]. SWI is a technique that utilizes 3D pulse MRI sequences sensitive to magnetic field inhomogeneities. It is based on the following phenomenon: iron, calcium and deoxyhemoglobin can enhance a local magnetic field and induce a positive phase shift, in comparison with the surrounding cerebral tissues. Tissues containing these paramagnetic agents appear on SW images as regions of hypointense MR signal [17, 18].

In healthy subjects, SN appears on MR images as a hypointense midbrain region dorsally divided into 2 segments by an oval hypointense area. Histopathological studies have confirmed that this dorsolateral nigral hyperintensity corresponds to nigrosome-1 and that signal enhancement may be associated with low iron content in this region in comparison with the surrounding SN [19].

Nigrosome-1 is not visualized in patients with PD. Apart from the loss of dopaminergic neurons, this may be associated with iron accumulation occurring in parallel [20, 21]. The loss of dorsolateral nigral hyperintensity is currently regarded as one of the most promising biomarkers of PD. For example, a recent meta-analysis reports that the diagnostic accuracy of nigrosome-1 imaging for the differentiation between patients with idiopathic PD and healthy individuals demonstrates high sensitivity and high specificity [22].

Table. Demographic characteristics of the patients

Characteristic	Categories / units of measurement	Disease		<i>p</i>
		PD	ET	
Sex, abs. (%)	Women	11 (55)	8 (80)	0.246
	Men	9 (45)	2 (20)	
Age, Me [Q ₁ -Q ₃]	Full years	60 [52.25-66.5]	73.5 [58.5-77.25]	0.082
Disease duration, Me [Q ₁ -Q ₃]	Full years	3 [2-6.5]	10 [8.5-15.75]	0.003

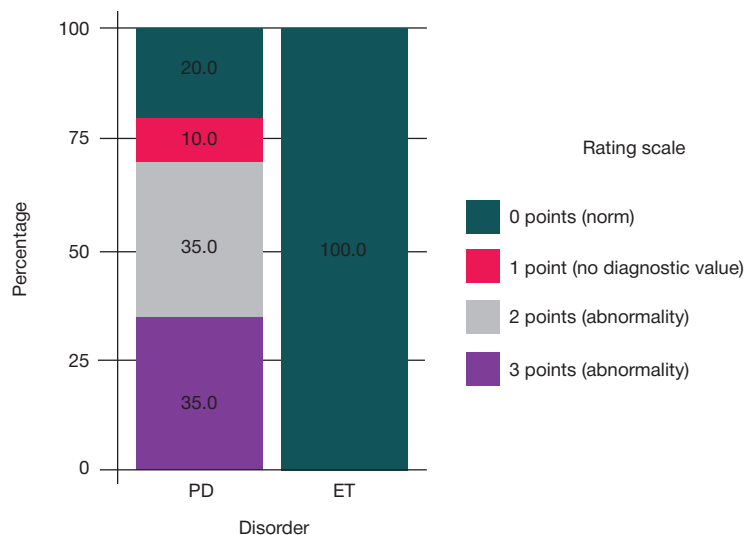


Fig. 2. Results of non-invasive nigrosome-1 assessment in patients with PD and ET

The diagnostic value of this neuroimaging marker in differentiating between PD and ET was assessed in two studies published in 2019. Jin L. et al. analyzed MR images of 68 patients with PD, 25 patients with ET and 34 control subjects. The method demonstrated high sensitivity (79.4%) and high specificity (92.0%) [13]. M. S. Perez Akly et al. studied dorsolateral nigral hyperintensity in 16 patients with PD and 16 patients with ET. The results were comparable to the results of the study by Jin L. et al. According to one of 2 involved radiologists, the sensitivity and specificity of the method were 93.75% and 87.5%, respectively. The second radiologist reported 93.75% sensitivity and 75% specificity [14]. Thus, the method was shown to be effective in differentiating between PD and ET by 2 independent research teams.

Our study also confirms the diagnostic value of noninvasive nigrosome-1 imaging. In contrast with ET patients, the absence of dorsolateral nigral hyperintensity in SN was observed in the majority of our PD patients. The sensitivity and specificity of the

method tested on the small cohort of patients were 70% and 100%, respectively.

Artifacts from motion and metal dental implants were a significant limitation of our study. From initially examined 39 patients (26 patients with PD, 13 patients with ET), only 30 whose MR images were suitable for the analysis were included in the study. To reduce the number of artifacts from motion, the patient's head can be stabilized with sand sacks or foam pillow support, and mild medical sedation can be applied [16].

CONCLUSIONS

Our findings supported by the results of foreign studies lead us to conclude that noninvasive neuroimaging has a potential to become a useful tool in the differential diagnosis of diseases accompanied by tremor and other movement disorders, including differentiation between PD and ET, especially in the early stages of the disease.

References

- Balestrino R, Schapira AHV. Parkinson disease. *Eur J Neurol*. 2020; 27 (1): 27–42. DOI: 10.1111/ene.14108. Epub 2019 Nov 27. PMID: 31631455.
- Sepúlveda Soto MC, Fasano A. Essential tremor: New advances. *Clin Park Relat Disord*. 2019; 3: 100031. DOI: 10.1016/j.prdoa.2019.100031. PMID: 34316617; PMCID: PMC8298793.
- Postuma RB, Berg D, Stern M, Poewe W, Olanow CW et al. MDS clinical diagnostic criteria for Parkinson's disease. *Mov Disord*. 2015; 30 (12): 1591–601. DOI: 10.1002/mds.26424. PMID: 26474316.
- Schapira AHV, Chaudhuri KR, Jenner P. Non-motor features of Parkinson disease. *Nat Rev Neurosci*. 2017; 18 (7): 435–50. DOI: 10.1038/nrn.2017.62. Epub 2017. Erratum in: *Nat Rev Neurosci*. 2017; 18 (8): 509. PMID: 28592904.
- Bhatia KP, Bain P, Bajaj N, Elble RJ, Hallett M, Louis ED, et al. Tremor Task Force of the International Parkinson and Movement Disorder Society. Consensus Statement on the classification of tremors. from the task force on tremor of the International Parkinson and Movement Disorder Society. *Mov Disord*. 2018; 33 (1): 75–87. DOI: 10.1002/mds.27121. Epub 2017 Nov 30. PMID: 29193359.
- Brooks DJ. Technology insight: imaging neurodegeneration in Parkinson's disease. *Nat Clin Pract Neurol*. 2008; 4 (5): 267–77. DOI: 10.1038/ncpneu0773. Epub 2008. PMID: 18382437.
- Tao A, Chen G, Mao Z, Gao H, Deng Y, Xu R. Essential tremor vs idiopathic Parkinson disease: Utility of transcranial sonography. *Medicine (Baltimore)*. 2020; 99 (20): e20028. DOI: 10.1097/MD.00000000000020028. PMID: 32443307.
- Damier P, Hirsch EC, Agid Y, Graybiel AM. The substantia nigra of the human brain. I. Nigrosomes and the nigral matrix, a compartmental organization based on calbindin D (28K) immunohistochemistry. *Brain*. 1999; 122 (Pt 8): 1421–36. DOI: 10.1093/brain/122.8.1421. PMID: 10430829.
- Blaziejewska AI, Schwarz ST, Pitiot A, Stephenson MC, Lowe J, Bajaj N, et al. Visualization of nigrosome 1 and its loss in PD: pathoanatomical correlation and in vivo 7 T MRI. *Neurology*. 2013; 81 (6): 534–40. DOI: 10.1212/WNL.0b013e31829e6fd2. Epub 2013 Jul 10. PMID: 23843466.
- Cheng Z, He N, Huang P, Li Y, Tang R, Sethi SK, et al. Imaging the Nigrosome 1 in the substantia nigra using susceptibility weighted imaging and quantitative susceptibility mapping: An application to Parkinson's disease. *Neuroimage Clin*. 2020; 25: 102103. DOI: 10.1016/j.nicl.2019.102103. Epub 2019 Nov 20. PMID: 31869769.
- Reiter E, Mueller C, Pinter B, Krismer F, Scherfler C, Esterhammer R, et al. Dorsolateral nigral hyperintensity on 3.0T susceptibility-weighted imaging in neurodegenerative Parkinsonism. *Mov Disord*. 2015; 30 (8): 1068–76. DOI: 10.1002/mds.26171. Epub 2015 Mar 15. PMID: 25773707.

12. Mavroudis I, Petridis F, Kazis D. Neuroimaging and neuropathological findings in essential tremor. *Acta Neurol Scand.* 2019; 139 (6): 491–6. DOI: 10.1111/ane.13101. Epub 2019. PMID: 30977113.
13. Jin L, Wang J, Wang C, Lian D, Zhou Y, Zhang Y, et al. Combined Visualization of Nigrosome-1 and Neuromelanin in the Substantia Nigra Using 3T MRI for the Differential Diagnosis of Essential Tremor and de novo Parkinson's Disease. *Front Neurol.* 2019 Feb 12; 10: 100. DOI: 10.3389/fneur.2019.00100. PMID: 30809189.
14. Perez Akly MS, Stefani CV, Ciancaglini L, Bestoso JS, Funes JA, Bauso DJ et al. Accuracy of nigrosome-1 detection to discriminate patients with Parkinson's disease and essential tremor. *Neuroradiol J.* 2019 Dec; 32 (6): 395–400. DOI: 10.1177/1971400919853787. Epub 2019 May 31. PMID: 31149866.
15. Damier P, Hirsch EC, Agid Y, Graybiel AM. The substantia nigra of the human brain. II. Patterns of loss of dopamine-containing neurons in Parkinson's disease. *Brain.* 1999; 122 (Pt 8): 1437–48. DOI: 10.1093/brain/122.8.1437. PMID: 10430830.
16. Schwarz ST, Afzal M, Morgan PS, Bajaj N, Gowland PA, Auer DP. The 'swallow tail' appearance of the healthy nigrosome — a new accurate test of Parkinson's disease: a case-control and retrospective cross-sectional MRI study at 3T. *PLoS One.* 2014; 9 (4): e93814. DOI: 10.1371/journal.pone.0093814. PMID: 24710392.
17. Haacke EM, Xu Y, Cheng YC, Reichenbach JR. Susceptibility weighted imaging (SWI). *Magn Reson Med.* 2004; 52 (3): 612–8. DOI: 10.1002/mrm.20198. PMID: 15334582.
18. Gao P, Zhou PY, Li G, Zhang GB, Wang PQ, Liu JZ, et al. Visualization of nigrosomes-1 in 3T MR susceptibility weighted imaging and its absence in diagnosing Parkinson's disease. *Eur Rev Med Pharmacol Sci.* 2015; 19 (23): 4603–9. PMID: 26698258.
19. Pavese N, Tai YF. Nigrosome Imaging and Neuromelanin Sensitive MRI in Diagnostic Evaluation of Parkinsonism. *Mov Disord Clin Pract.* 2018; 5 (2): 131–40. DOI: 10.1002/mdc3.12590. PMID: 30363419.
20. LeHéricy S, Bardin E, Poupon C, Vidailhet M, François C. 7 Tesla magnetic resonance imaging: a closer look at substantia nigra anatomy in Parkinson's disease. *Mov Disord.* 2014; 29 (13): 1574–81. DOI: 10.1002/mds.26043. Epub 2014. PMID: 25308960.
21. Trist BG, Hare DJ, Double KL. Oxidative stress in the aging substantia nigra and the etiology of Parkinson's disease. *Aging Cell.* 2019; 18 (6): e13031. DOI: 10.1111/accel.13031. Epub 2019 Aug 20. PMID: 31432604.
22. Chau MT, Todd G, Wilcox R, Agzarian M, Bezak E. Diagnostic accuracy of the appearance of Nigrosome-1 on magnetic resonance imaging in Parkinson's disease: A systematic review and meta-analysis. *Parkinsonism Relat Disord.* 2020; 78: 12–20. DOI: 10.1016/j.parkreldis.2020.07.002. Epub 2020 Jul 7. PMID: 32668370.

Литература

1. Balestrino R, Schapira AHV. Parkinson disease. *Eur J Neurol.* 2020; 27 (1): 27–42. DOI: 10.1111/ene.14108. Epub 2019 Nov 27. PMID: 31631455.
2. Sepúlveda Soto MC, Fasano A. Essential tremor: New advances. *Clin Park Relat Disord.* 2019; 3: 100031. DOI: 10.1016/j.prdoa.2019.100031. PMID: 34316617; PMCID: PMC8298793.
3. Postuma RB, Berg D, Stern M, Poewe W, Olanow CW et al. MDS clinical diagnostic criteria for Parkinson's disease. *Mov Disord.* 2015; 30 (12): 1591–601. DOI: 10.1002/mds.26424. PMID: 26474316.
4. Schapira AHV, Chaudhuri KR, Jenner P. Non-motor features of Parkinson disease. *Nat Rev Neurosci.* 2017; 18 (7): 435–50. DOI: 10.1038/nrn.2017.62. Epub 2017. Erratum in: *Nat Rev Neurosci.* 2017; 18 (8): 509. PMID: 28592904.
5. Bhatia KP, Bain P, Bajaj N, Elble RJ, Hallett M, Louis ED, et al. Tremor Task Force of the International Parkinson and Movement Disorder Society. Consensus Statement on the classification of tremors. from the task force on tremor of the International Parkinson and Movement Disorder Society. *Mov Disord.* 2018; 33 (1): 75–87. DOI: 10.1002/mds.27121. Epub 2017 Nov 30. PMID: 29193359.
6. Brooks DJ. Technology insight: imaging neurodegeneration in Parkinson's disease. *Nat Clin Pract Neurol.* 2008; 4 (5): 267–77. DOI: 10.1038/ncpneu0773. Epub 2008. PMID: 18382437.
7. Tao A, Chen G, Mao Z, Gao H, Deng Y, Xu R. Essential tremor vs idiopathic Parkinson disease: Utility of transcranial sonography. *Medicine (Baltimore).* 2020; 99 (20): e20028. DOI: 10.1097/MD.00000000000020028. PMID: 32443307.
8. Damier P, Hirsch EC, Agid Y, Graybiel AM. The substantia nigra of the human brain. I. Nigrosomes and the nigral matrix, a compartmental organization based on calbindin D (28K) immunohistochemistry. *Brain.* 1999; 122 (Pt 8): 1421–36. DOI: 10.1093/brain/122.8.1421. PMID: 10430829.
9. Blazejewska AI, Schwarz ST, Pitiot A, Stephenson MC, Lowe J, Bajaj N, et al. Visualization of nigrosome 1 and its loss in PD: pathoanatomical correlation and in vivo 7 T MRI. *Neurology.* 2013; 81 (6): 534–40. DOI: 10.1212/WNL.0b013e31829e6fd2. Epub 2013 Jul 10. PMID: 23843466.
10. Cheng Z, He N, Huang P, Li Y, Tang R, Sethi SK, et al. Imaging the Nigrosome 1 in the substantia nigra using susceptibility weighted imaging and quantitative susceptibility mapping: An application to Parkinson's disease. *Neuroimage Clin.* 2020; 25: 102103. DOI: 10.1016/j.nicl.2019.102103. Epub 2019 Nov 20. PMID: 31869769.
11. Reiter E, Mueller C, Pinter B, Krismer F, Scherfler C, Esterhammer R, et al. Dorsolateral nigral hyperintensity on 3.0T susceptibility-weighted imaging in neurodegenerative Parkinsonism. *Mov Disord.* 2015; 30 (8): 1068–76. DOI: 10.1002/mds.26171. Epub 2015 Mar 15. PMID: 25773707.
12. Mavroudis I, Petridis F, Kazis D. Neuroimaging and neuropathological findings in essential tremor. *Acta Neurol Scand.* 2019; 139 (6): 491–6. DOI: 10.1111/ane.13101. Epub 2019. PMID: 30977113.
13. Jin L, Wang J, Wang C, Lian D, Zhou Y, Zhang Y, et al. Combined Visualization of Nigrosome-1 and Neuromelanin in the Substantia Nigra Using 3T MRI for the Differential Diagnosis of Essential Tremor and de novo Parkinson's Disease. *Front Neurol.* 2019 Feb 12; 10: 100. DOI: 10.3389/fneur.2019.00100. PMID: 30809189.
14. Perez Akly MS, Stefani CV, Ciancaglini L, Bestoso JS, Funes JA, Bauso DJ et al. Accuracy of nigrosome-1 detection to discriminate patients with Parkinson's disease and essential tremor. *Neuroradiol J.* 2019 Dec; 32 (6): 395–400. DOI: 10.1177/1971400919853787. Epub 2019 May 31. PMID: 31149866.
15. Damier P, Hirsch EC, Agid Y, Graybiel AM. The substantia nigra of the human brain. II. Patterns of loss of dopamine-containing neurons in Parkinson's disease. *Brain.* 1999; 122 (Pt 8): 1437–48. DOI: 10.1093/brain/122.8.1437. PMID: 10430830.
16. Schwarz ST, Afzal M, Morgan PS, Bajaj N, Gowland PA, Auer DP. The 'swallow tail' appearance of the healthy nigrosome — a new accurate test of Parkinson's disease: a case-control and retrospective cross-sectional MRI study at 3T. *PLoS One.* 2014; 9 (4): e93814. DOI: 10.1371/journal.pone.0093814. PMID: 24710392.
17. Haacke EM, Xu Y, Cheng YC, Reichenbach JR. Susceptibility weighted imaging (SWI). *Magn Reson Med.* 2004; 52 (3): 612–8. DOI: 10.1002/mrm.20198. PMID: 15334582.
18. Gao P, Zhou PY, Li G, Zhang GB, Wang PQ, Liu JZ, et al. Visualization of nigrosomes-1 in 3T MR susceptibility weighted imaging and its absence in diagnosing Parkinson's disease. *Eur Rev Med Pharmacol Sci.* 2015; 19 (23): 4603–9. PMID: 26698258.
19. Pavese N, Tai YF. Nigrosome Imaging and Neuromelanin Sensitive MRI in Diagnostic Evaluation of Parkinsonism. *Mov Disord Clin Pract.* 2018; 5 (2): 131–40. DOI: 10.1002/mdc3.12590. PMID: 30363419.
20. LeHéricy S, Bardin E, Poupon C, Vidailhet M, François C. 7 Tesla magnetic resonance imaging: a closer look at substantia nigra anatomy in Parkinson's disease. *Mov Disord.* 2014; 29 (13): 1574–81. DOI: 10.1002/mds.26043. Epub 2014. PMID: 25308960.

- (13): 1574–81. DOI: 10.1002/mds.26043. Epub 2014. PMID: 25308960.
21. Trist BG, Hare DJ, Double KL. Oxidative stress in the aging substantia nigra and the etiology of Parkinson's disease. *Aging Cell*. 2019; 18 (6): e13031. DOI: 10.1111/acer.13031. Epub 2019 Aug 20. PMID: 31432604.
22. Chau MT, Todd G, Wilcox R, Agzarian M, Bezak E. Diagnostic accuracy of the appearance of Nigrosome-1 on magnetic resonance imaging in Parkinson's disease: A systematic review and meta-analysis. *Parkinsonism Relat Disord*. 2020; 78: 12–20. DOI: 10.1016/j.parkreldis.2020.07.002. Epub 2020 Jul 7. PMID: 32668370.

MEDIUM-TERM OUTCOMES OF EXTRAARTICULAR CORRECTIVE OSTEOTOMY FOR SLIPPED CAPITAL FEMORAL EPIPHYSIS

Egiazaryan KA¹, Grigoriev AV² ✉, Ratiev AP¹, But-Gusaim AB¹, Sirotin IV¹

¹ Pirogov Russian National Research Medical University, Moscow, Russia

² Moscow Regional Clinical Hospital for Trauma and Orthopedics, Moscow, Russia

Despite the diversity of surgical options for slipped capital femoral epiphysis (SCFE), there is an ongoing search for the technique that would ensure a satisfactory outcome, stable fixation of bone fragments and a low rate of complications. The aim of this study was to improve the surgical technique for SCFE in patients with moderate and severe SCFE. The study included 52 children (16 girls and 36 boys) aged 10–15 years (the mean age was 13.2 years) with chronic severe (Krethmar's stage III) stable (according to Loder's classification) SCFE. The control group ($n = 16$) underwent a classic Imhauser procedure; the main group ($n = 36$) underwent a triplane osteotomy proposed by the authors of the study. The patients were examined prior to surgery and in the late follow-up period (the mean follow-up time was 4.7 years, ranging from 1 to 10 years). The procedure included a clinical examination, history taking, radiography to measure the slip angle and the severity of the slip, and the Harris hip score to assess hip function. After 4.7 years, both groups demonstrated an increase in the range of motion, in comparison with their preoperative results ($p \leq 0.05$), good Harris hip scores (94 points in the main group and 81 points in the control group). Postoperative radiographs showed consolidation of the bone, recovery of the proximal femur anatomy. Leg length discrepancy improved significantly in both groups. The proposed technique for extraarticular osteotomy allows recovering the length of the affected leg, the anatomy and physiology of the hip joint, is simple and less traumatic.

Keywords: slipped capital femoral epiphysis, corrective extraarticular femoral osteotomy, hip joint, Imhauser procedure

Author contribution: all authors contributed equally to the study and the manuscript, all read and approved the final version of the manuscript.

Compliance with ethical standards: the study was approved by the Ethics Committee of Pirogov Russian National Research Medical University and complied with the principles of the Declaration of Helsinki. Informed consent was obtained from the patients' parents.

✉ **Correspondence should be addressed:** Alexandr V. Grigoriev
Poperechny prosek 3/5, kab. 23, Moscow, Russia; avgrigoriev@mail.ru

Received: 10.01.2022 **Accepted:** 24.01.2022 **Published online:** 31.01.2022

DOI: 10.24075/brsmu.2022.003

СРЕДНЕСРОЧНЫЕ РЕЗУЛЬТАТЫ ВНЕСУСТАВНОЙ КОРРИГИРУЮЩЕЙ ОСТЕОТОМИИ БЕДРА ПРИ ЮНОШЕСКОМ ЭПИФИЗЕОЛИЗЕ ГОЛОВКИ БЕДРЕННОЙ КОСТИ

К. А. Егизарян¹, А. В. Григорьев² ✉, А. П. Ратьев¹, А. Б. Бут-Гусаим¹, И. В. Сиротин¹

¹ Российский национальный исследовательский медицинский университет имени Н. И. Пирогова, Москва, Россия

² Московская областная клиническая травматолого-ортопедическая больница, Москва, Россия

Несмотря на множество предложенных методов хирургического лечения юношеского эпифизеолиза головки бедренной кости ЮЭГБК, продолжаются поиски варианта операции, обеспечивающей удовлетворительную коррекцию, стабильную фиксацию костных фрагментов и низкий уровень осложнений. Целью работы было усовершенствовать технику лечения пациентов с ЮЭГБК средне-тяжелой степени. В исследование вошли 52 ребенка в возрасте 10–15 лет (средний возраст 13,1), из них 16 девочек и 36 мальчиков, страдающие ЮЭГБК тяжелой степени (3-я стадия по классификации Кречмара), хронического течения, стабильного типа (классификация Loder). Пациентам контрольной группы ($n = 16$) выполнена стандартная операция по Imhauser, исследуемой ($n = 36$) — авторская трехплоскостная остеотомия. Пациентов обследовали до операции и в отдаленные сроки (средний срок наблюдения составил 4,7 года (от 1 до 10 лет) с помощью клинического метода (сбор анамнеза, объективное исследование), рентгенологического метода (определение степени соскальзывания и угла соскальзывания), а также опросника функционального состояния (Harris hip score). В среднем через 4,7 года в обеих группах отмечено увеличение объема движений в сравнении с дооперационными показателями ($p \leq 0,05$), хорошие функциональные показатели HHS (в исследуемой группе — 94 балла, в контрольной — 81 балл); на контрольных рентгенограммах отмечена консолидация костных фрагментов с сохранением коррекции проксимального отдела бедра, длина конечностей также восстановилась в обеих группах. Предложенная внесуставная остеотомия позволяет восстановить длину конечности, анатомо-физиологические взаимоотношения в тазобедренном суставе, проста в исполнении и менее травматична.

Ключевые слова: юношеский эпифизеолиз головки бедренной кости, внесуставная корригирующая остеотомия бедра, тазобедренный сустав, операция Imhauser

Вклад авторов: все авторы внесли существенный вклад в проведение исследования и подготовку статьи, прочли и одобрили финальную версию перед публикацией.

Соблюдение этических стандартов: исследование одобрено этическим комитетом РНИМУ им. Н. И. Пирогова (протокол № 213 от 13 декабря 2021 г.) выполнено в соответствии с этическими стандартами Хельсинской декларации; родители пациентов дали согласие на обработку и публикацию их персональных данных.

✉ **Для корреспонденции:** Александр Владимирович Григорьев
Поперечный просек, д. 3/5, каб. 23, г. Москва, Россия; avgrigoriev@mail.ru

Статья получена: 10.01.2022 **Статья принята к печати:** 24.01.2022 **Опубликована онлайн:** 31.01.2022

DOI: 10.24075/vrgmu.2022.003

Slipped capital femoral epiphysis (SCFE) is a relatively rare, predominantly juvenile disorder [1]. Due to a variety of causes, including endocrine, the osseous tissue of the metaphysis at the epiphyseal-metaphyseal junction undergoes structural transformation resulting in the disruption of the osteoclast/osteoblast balance and accompanied by the spatial

arrangement of the extracellular elements of connective tissue. The bone resorbs, and the epiphysis slips out of its normal position [2, 3]. The typical underlying mechanism of SCFE is associated with high axial load and is characterized by the posterior-inferior displacement of the epiphysis and its retroversion [4].

The disease occurs in 4–5 individuals per 100,000 population. It is more likely to affect pubescent boys aged 12–13 years (the male to female ratio is 3 : 2). Clinically, it presents as outer thigh pain or pain in the hip and knee joints (as a rule, pain in the knee joint is more common), which often urges the doctor to search for a possible knee joint pathology and thus misdiagnose the patient, because the true cause of pain, i.e. slipped proximal femoral epiphysis, remains overlooked.

There are a few classifications of SCFE used in clinical practice. The Southwick Slip Angle Classification is based on the epiphyseal-metaphyseal angle and categorizes the degree of epiphyseal displacement as mild (0–30°), moderate (30°–50°) and severe (> 50°). The Loder Classification evaluates epiphyseal stability and the patient's ability to bear weight. A stable slip means that the patient is able to bear weight with or without crutches; an unstable slip means that the patient is unable to bear weight even with crutches.

Another classification was proposed by Krechmar in 1982:

Stage I: pre-displacement; no signs of epiphyseal displacement, pronounced changes in the proximal physis (growth plate) and the metaphysis (femoral neck);

Stage II: the epiphysis is displaced posteriorly ($\leq 30^\circ$) and inferiorly ($\leq 15^\circ$); there are structural changes in the metaphysis; the proximal physis is open;

Stage III: the epiphysis is displaced posteriorly (> 30°) and inferiorly (> 15°); there are structural changes in the metaphysis; the physis is open;

Stage IV: acute posteroinferior displacement of the epiphysis; the physis is open;

Stage V: residual proximal femoral deformity with various degrees of epiphyseal displacement and the closed proximal physis.

This grading system integrates some of the abovementioned classifications and is, in our opinion, the most convenient.

On examination, patients with SCFE have a limp, the affected leg appears shorter, there is excessive external rotation of the hip, progressing over time; internal rotation of the hip is limited; reaching the full range of motion is painful. Krechmar's stage III is characterized by the positive Hofmeister-Drehmann's sign. The diagnosis is confirmed by anteroposterior and frog-leg lateral radiographs. In 20% of cases, SCFE is bilateral [5].

Because the condition is rare, it is often diagnosed in the advanced stage. In the majority of cases, patients with SCFE are hospitalized when the proximal femur deformity becomes very pronounced [1]. SCFE has a serious social impact, so it is important to ensure prophylaxis of early hip joint osteoarthritis, hip impingement syndrome and avascular necrosis of the epiphysis, which has been correlated with SCFE in a number of studies [6, 7].

The main goal of SCFE treatment is to prevent further femoral deformation, stabilize the proximal epiphysis and preserve blood supply to the epiphysis [8].

A diversity of surgical interventions for chronic SCFE have been proposed, including *in situ* fixation with pins, screws or plates, epiphysiodesis and various types of proximal femur osteotomy [9].

At present, the preferred treatment option for moderate and severe epiphyseal displacement (> 30°) is osteotomy [10]. Depending on its site, osteotomy can be classified into subcapital (the Dunn procedure, Fish cuneiform osteotomy), osteotomy conducted at the femoral neck base (Kramer intraarticular osteotomy Badama extraarticular osteotomy) and intertrochanteric (the Southwick and Imhauser procedures). The outcome is measured by assessing hip joint function, the presence of residual displacement, the adverse sequelae of

the surgical intervention (impaired blood supply to the femoral head), and the simplicity of the surgical technique [11].

In theory, proximal osteotomies of the femoral neck (Dunn procedures) are the ideal tool for restoring the anatomy of the proximal femur because SCFE-related deformities arise at this particular anatomical site [12]. However, there are reports that these procedures impede blood supply to the femoral head and cause avascular necrosis of the femoral head in 10–26% of patients. Due to the high risk of avascular necrosis, it was proposed to perform osteotomy in the intertrochanteric area of the femur [13].

Southwick osteotomy is a classic surgical intervention for SCFE. It corrects the metaphyseal-diaphyseal angle and eliminates excessive external rotation of the hip; however, it does not significantly affect the position of the proximal epiphysis in the acetabulum. In the past, neither surgeons, nor patients were fully satisfied with the outcome, which gave rise to multiplane osteotomies [14].

A triplane corrective osteotomy was proposed by Krasnov AI (RU 2364365, C2). It is more pathogenetically reasonable because it simultaneously corrects deformities in the frontal, horizontal and sagittal planes; fixation is performed with an angled blade plate [15].

Among the main drawbacks of the Krasnov osteotomy are its technical difficulty and the need to cut off the greater trochanter, which results in prolonged operative time. Besides, during this type of surgery, rotation is performed according to the position of the blade, i.e. around the longitudinal axis of the metaphysis. If the epiphysis is significantly displaced posteriorly (>40°) and only slightly inferiorly, which is a common occurrence, rotation of the proximal femur around the metaphyseal axis pushes the epiphysis and the metaphysis into a valgus and varus position, respectively. This results in a hip subluxation and/or the varus deformity of the metaphysis, with the high position of the greater trochanter, leading to the dysfunction of gluteal muscles and limping [16].

There is another variant of triplane corrective osteotomy with an angled blade plate (RU 2604039, C1). Advantageously, by changing the rotational axis of the proximal femur, correction can be performed in the frontal, horizontal and sagittal planes, preventing angular deformity of the femoral diaphysis, hip subluxation and varus deformity of the metaphysis [17].

In 1966, Imhauser described an intertrochanteric osteotomy that eliminated femoral varus and metaphyseal extension and rotation. The surgery is essentially a cuneiform osteotomy involving resection of the anterior or anterolateral fragment of the bone, followed by blade plate fixation [18]. There is a wealth of publications about this procedure, indicative of its popularity. It should be noted that femoral head subluxation in the setting of excessive valgization and a deformity of the proximal femur are common complications of this intervention [19–21].

Considering all currently existing surgical treatment options, their complications, stability of epiphyseal fixation, duration of postoperative immobilization and patient outcomes, we developed an original technique for SCFE correction based on the analysis of the aforementioned procedures. The aim of this study was to improve the outcomes of SCFE treatment in children and to assess the effectiveness of the proposed technique.

METHODS

Our retrospective study included 52 children with SCFE undergoing treatment at the Children's hospital of the Department of Traumatology, Orthopedics, and Disaster Surgery

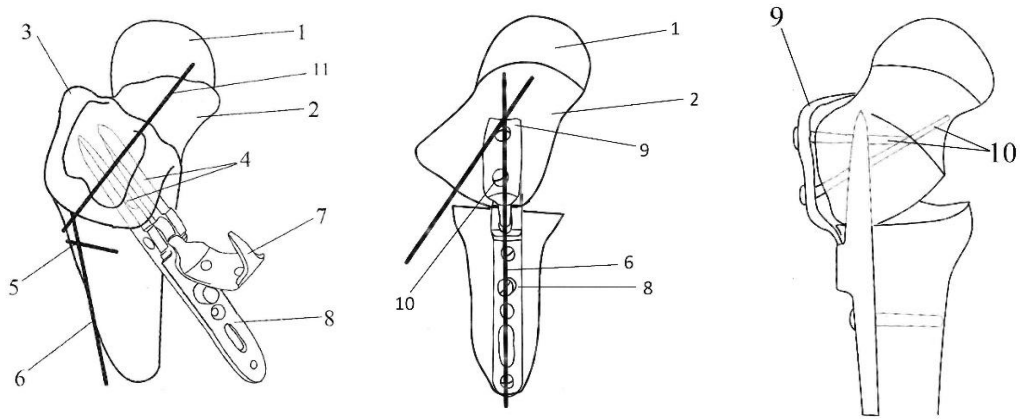


Fig. 1. The schematic representation of the proposed osteotomy technique. 1 — femoral epiphysis; 2 — femoral metaphysis; 3 — the greater trochanter; 4 — jaws of the Trotsenko–Nuzhdin plate; 5 — osteotomy site; 6 — the longitudinal axis of the femoral diaphysis; 7 — the locking part of the plate; 8 — the diaphyseal part of the plate; 9 — the part of the plate anchored to the greater trochanter; 10 — screws fixing the Trotsenko–Nuzhdin plate; 11 — the longitudinal axis of the femur

from 2010 to 2020. All patients underwent a clinical examination (medical history and complaints, demographic characteristics, symptoms, range of motion assessment) and radiography; pain and hip function were assessed using the Harris hip score [22].

The patients were divided into 2 groups. The control group included patients undergoing a classic intertrochanteric Imhauser osteotomy, the main group comprised patients undergoing the original variant of osteotomy proposed by the authors of this study [23].

The following inclusion criteria were applied: posterior (30°) and/or inferior ($>15^\circ$) displacement of the proximal femoral epiphysis, the growth plate being open; no past history of hip surgery; the absence of technical errors during surgery.

Exclusion criteria: posterior displacement of the epiphysis by $< 30^\circ$ or $> 75^\circ$; the closed growth plate; a past history of hip surgery; complete separation of the epiphysis from the metaphysis (acute slip).

The clinical examination included identification of complaints and assessment of gait, i.e. limping, the ability to ambulate, pain during ambulation, pain during movements, fixed external rotation of the affected hip; limited flexion, internal rotation and adduction of the leg.

Anteroposterior and frog-leg lateral radiographs of the hip were acquired before and after surgery and in the late follow-up period. Radiographic staging was done in accordance with Krechmar and Loder classifications [24, 25].

The main outcome measure was hip function assessment with the Harris hip score. This tool was developed to evaluate the outcomes of hip surgery. It includes 4 domains: pain, function, deformity, and range of motion. For each domain, the total score is calculated (the maximum total score is 100 points). The higher the score, the better the quality of life. The score over 90 points one year after surgery was interpreted as an excellent outcome, 80–90 points as good, 65–79 points as satisfactory, and below 65 points as unsatisfactory.

All patients were examined prior to surgery and in the late follow-up period. All patients underwent an osteotomy and were advised to unload the operated leg for 4–12 months. After 4–12 months, the plate was removed and the follow-up observation continued.

Statistical analysis was conducted in SPSS (IBM SPSS Statistics 22; USA), and Excel (Microsoft; USA). The significance of differences between the groups was assessed using the non-parametric Kruskal-Wallis test; correlations between two quantitative variables were measured using the Spearman rank correlation coefficient. Differences were considered significant at $p < 0.05$.

Surgical technique

In the proposed technique, the spatial position of the axis around which the proximal femur is rotated during femoral

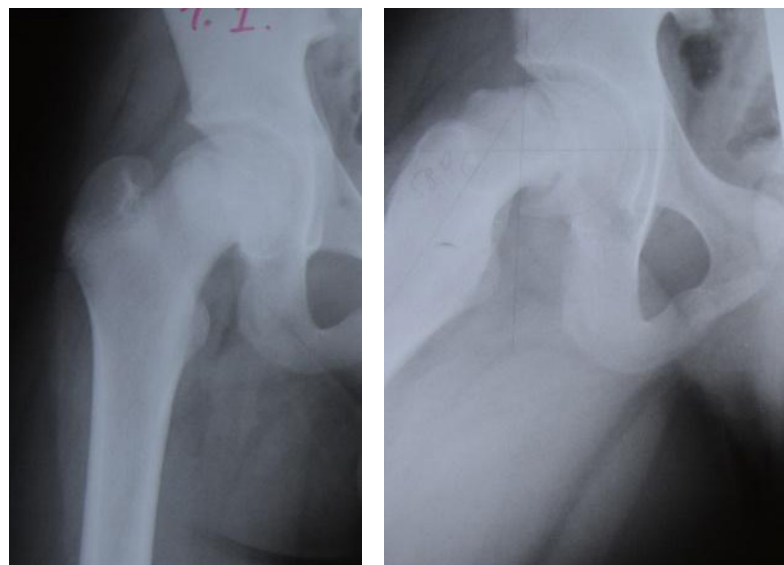


Fig. 2. The anteroposterior and frog-leg lateral radiographs of the right hip (patient M., 12 years). Stage III chronic SCFE

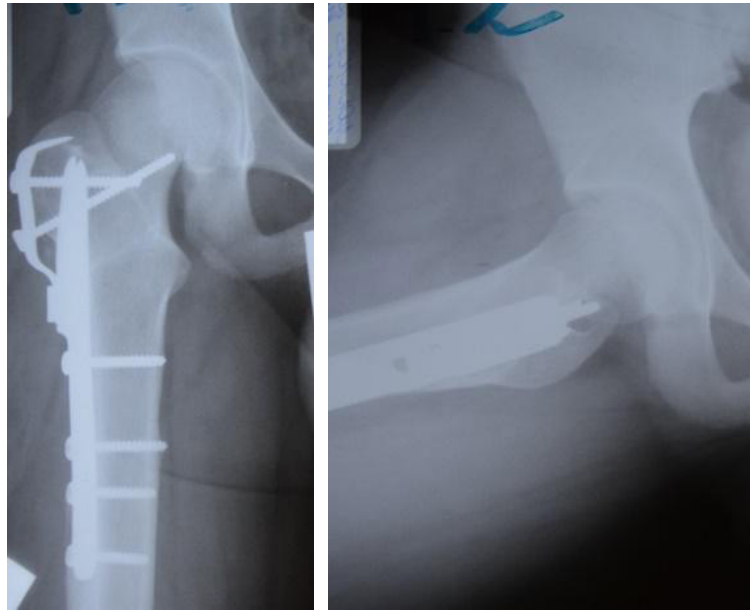


Fig. 3. The anteroposterior and frog-leg lateral radiographs of the right hip (patient M., 12 years) after an intertrochanteric osteotomy of the hip with plate fixation

osteotomy is different, as is the osteotomy type (Fig. 1). Fixation is performed with a Trotsenko–Nuzhdin plate. The points of entry for the jaws were planned 0.3–0.5 cm superior to the greater trochanter growth plate and at the posterior epiphyseal displacement distance from the midline of the lateral face of the greater trochanter. The jaws of the plate must be inserted so that the angle between the line parallel to the axis of the diaphyseal part of the plate and the line parallel to the femoral diaphysis equals the angle of epiphyseal retroversion. Blade insertion channels were formed in the proximal femur. Then, high intertrochanteric osteotomy was performed and the jaws were introduced in the prepared channels. The diaphyseal part of the plate was pulled posteriorly, keeping some space between the diaphysis and the diaphyseal part of the plate, until the midlines going through the central axis of the plate and the femoral diaphysis coincided. Thus, the femoral head was recovered from its retroverted position and derotated. Then the diaphyseal part of the plate was pressed to the femoral diaphysis and the inferior displacement of the epiphysis was eliminated. The locking part of the plate was anchored to the greater trochanter; the screws were inserted in such a way that

they passed outside the femoral neck. The diaphyseal part of the plate was anchored to the femur. Importantly, the maximum angle of forward rotation of the proximal femoral fragment should be 45°; rotation of over 45° is prohibited due to the risk of ischemic complications. If the epiphysis was displaced posteriorly by over 45°, residual displacement was corrected by derotating the proximal fragment, using the formula: $MEA - 45^\circ$ (where MEA is a metaphyseal-epiphyseal angle before surgery). If the epiphysis was displaced inferiorly, its position was corrected by valgization of the proximal fragment. To fix the Trotsenko-Nuzhdin plate, the jaws were introduced into the greater trochanter; this saves the femoral neck from injuring and helps to preserve blood supply to the proximal femur.

Postoperative rehabilitation

Postoperative rehabilitation was different in the main and control groups. In the main group, the patients remained on bed rest for 6 months and wore an antirotation foot support. The control group remained on bed rest for 3 months after surgery and wore a spica cast. Verticalization was encouraged

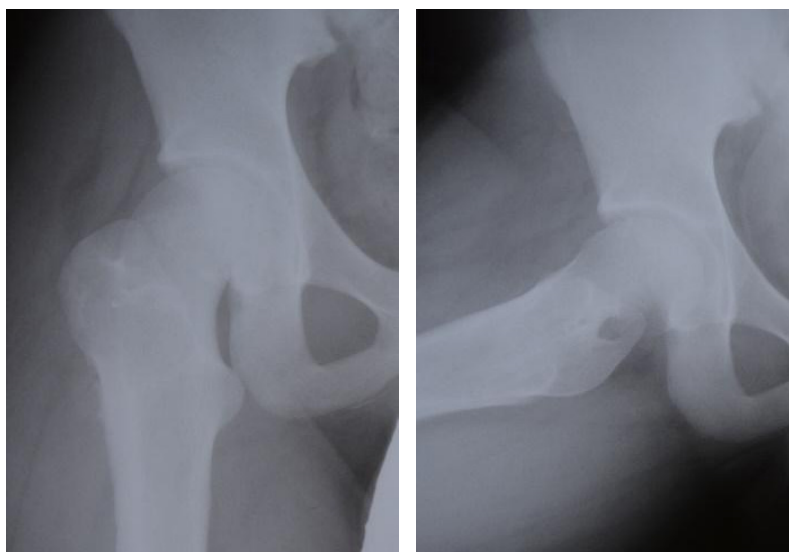


Fig. 4. The anteroposterior and frog-leg lateral radiographs of the right hip (patient M., 12 years) 12 months after the osteotomy (after bone consolidation and plate removal)

Table. Dynamics of leg length discrepancy 4.7 years after surgery

Group	Preoperative leg length discrepancy, cm		Postoperative leg length discrepancy, cm	
	Me	Q ₁ -Q ₃	Me	Q ₁ -Q ₃
Main	1.25	0.63-2	0	0-0.5
Control	1	0.5-1.38	1	0.5-1

at week 6 in the main group and at week 3 in the control group. Early rehabilitation was carried out only in the control group and included passive and, later, active physical exercise.

The plate was removed 10–12 months after the intervention.

RESULTS

A total of 52 patients were included in the study. Of them, 16 (30.8%) were girls and 36 (69.2%) were boys. The main group comprised 36 patients and the control group consisted of 16 patients. All patients were 10–15 years old; the mean age was 13 ± 1.1 years.

In the main group, there were 12 girls (33.4%) and 24 boys (66.6%); the control group included 4 girls (25%) and 12 boys (75%). The mean age in the main group was 13 ± 1.1 years ($p = 0.1$).

In both groups, all patients (100%) presented with pain and gait disturbance. All of them had a positive Hofmeister-Drehmann sign on examination.

In all patients, a positional deformity was observed in one of the legs due to excessive external rotation. For external rotation, the postoperative range of motion was 41.2° on average (40.8° in the main and 42.2° in the control groups, respectively; $p = 0.3$). Preoperatively, it was 69.0° (68.4° and 69.9° in the main and control groups, respectively; $p = 0.2$).

Internal rotation of the hip was limited in all patients; the average range of motion was 5.2° (4.8° and 6.9° in the main and control groups, respectively; $p = 0.006$). The leg length discrepancy was comparable between the groups, equaling 1.25 cm on average (1.20 cm in the main vs 1 cm in the control group; $p = 0.02$).

The metaphyseal-epiphyseal and the epiphyseal-diaphyseal angles were measured in the frog-leg lateral and the anteroposterior radiography views, respectively (Fig. 2–4). The average angle of posterior epiphyseal displacement was 46.8° (47.7° and 45.8° in the main and control groups, respectively; $p = 0.002$).

Due to the risk of acute epiphyseal slippage, the Harris hip score for hip function assessment was not used during the preoperative examination.

The average length of hospital stay was 14.4 in the main group vs 15.7 days in the control group ($p = 0.0075$). Average operative times were 71 min in the main group vs 137 min in the control group ($p = 0.0011$).

The follow-up examination performed 4.7 years (on average) after the surgical procedure revealed an improvement in internal hip rotation by an average of 16.7° (20.1° in the main group vs 9.1° in the control group; $p = 0.0024$). The leg length discrepancy was compensated and was now 0.5 cm on average (0 cm in the main group vs 1 cm in the control group; $p = 0.5$) (see Table).

Hip function assessment was performed only in the late follow-up period (4.7 years after the osteotomy), so it is impossible to track how hip function had been changing over that period, but the end result can be measured in both groups. The average Harris score in the late follow-up period was 89 points (94 points in the main group vs 81 points in the control group; $p = 0.001$) (Fig. 5).

Chondrolysis is a serious complication of surgery for SCFE and the disorder itself. Chondrolysis was observed in one patient in the main group (2.8%) and two patients in the control group (5.6%; $p = 0.0013$).

DISCUSSION

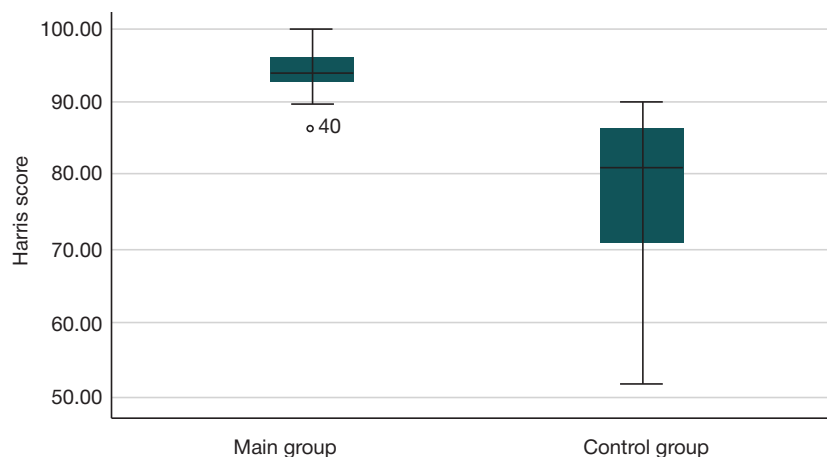
The literature offers a diversity of surgical techniques for treating chronic SCFE. The choice of the technique depends on the stage of the disorder and the experience and skills of the operating surgeon.

Today, SCFE is usually managed with intertrochanteric and subtrochanteric osteotomies of the femur involving fixation with an angled blade plate and screws or by an osteotomy of the femoral neck with screw fixation.

The original technique for metaphyseal osteotomy proposed by the authors of this study has demonstrated good outcomes and a low rate of complications.

Demographic parameters (age and sex), the average range of motion for external rotation of the hip and leg length discrepancy were comparable between the groups ($p \geq 0.05$). There was a significant difference in the range of motion for internal rotation: 4.8° in the main vs 6.9° in the control group ($p = 0.006$). The length of hospital stay was comparable, but the average operative times differed significantly, being shorter in the main group.

The follow-up examination conducted 4.7 years after the osteotomy revealed an increase in internal rotation, which was

**Fig. 5.** Harris scores 4.7 years after surgery in the main and control groups

significant in the main group (20.1°), compared to the control group (9.1°; $p = 0.0024$).

Hip function was assessed 4.7 after the osteotomy using the Harris hip score; the average score was 94 points for the main group and 81 points for the control group ($p = 0.001$).

The analysis of the obtained data showed that the main group subjected to a triplane osteotomy and fixation with the Trotsenko-Nuzhdin blade plate tolerated the procedure better (the intervention was shorter due to its technical simplicity). The duration of postoperative immobilization with antirotation foot support was minimal in the main group, which facilitated the early commencement of rehabilitation. Consequently, most patients in the main group were able to improve internal hip rotation and restore the length of the affected leg to the maximum possible extent. Owing to the design of the Trotsenko–Nuzhdin plate (the bifurcated blade is introduced into the greater trochanter), the femoral neck was not traumatized intraoperatively, which had a positive effect on blood supply to the epiphysis.

Corrective femoral osteotomy involving correction of the proximal femur rotation axis allows recovering the proper centration of the femoral epiphysis, prevents angular deformation of the femoral diaphysis, hip subluxation and varus deformity of the metaphysis, reduces the risk of avascular necrosis of the epiphysis and articular cartilage chondrolysis, delays progression of hip arthrosis, and puts off the need for hip replacement until much later.

CONCLUSIONS

The proposed technique for corrective osteotomy of the femur in patients with stage 3 chronic SCFE prevents subluxation of the affected hip, deformity of the proximal femur and shortens rehabilitation time. The simplicity of the technique and stability of fixation result in shorter operative time, less intraoperative blood loss and make postoperative patient management less complicated.

References

- Sokolovskij AM, Sokolovskij OA, Goldman RK, Junosheskij jepifizeoliz golovki bedrennoj kosti. Medicinskie novosti. 2006; 2. Russian.
- Witbreuk M, van Kemenade FJ, van der Sluijs JA, Jansma EP, Rotteveel J, van Royen BJ. Slipped capital femoral epiphysis and its association with endocrine, metabolic and chronic diseases: a systematic review of the literature. *J Child Orthop*. 2013; 7 (3): 213–23.
- Tayton K. The epiphyseal tubercle in adolescent hips. *Acta Orthop*. 2009; 80: 416–9.
- Gholve PA, Cameron DB, Millis MB. Slipped capital femoral epiphysis update. *Curr Opin Pediatr*. 2009; 21 (1): 39–45.
- Carney BT, Weinstein SL. Natural history of untreated chronic slipped capital femoral epiphysis. *Clin Orthop Relat Res*. 1996; (322): 43–7.
- Abu Amara S, Cunin V, Ilharrebordé B; French Society of Pediatric Orthopaedics (SOFOP). Severe slipped capital femoral epiphysis: a French multicenter study of 186 cases performed by the SoFOP. *Orthop Traumatol Surg Res*. 2015; 101 (6 Suppl): S275–9.
- Bittersohl B, Hosalkar HS, Zilkens C, Krauspe R. Current concepts in management of slipped capital femoral epiphysis. *Hip Int*. 2015; 25 (2): 104–14.
- Mahran MA, Baraka MM, Hefny HM. Slipped capital femoral epiphysis: a review of management in the hip impingement era. *SICOT J*. 2017; 3: 35.
- Meier MC, Meyer LC, Ferguson RL. Treatment of slipped capital femoral epiphysis with a spica cast. *J Bone Joint Surg Am*. 1992; 74: 1522–9.
- Bellemore JM, Carpenter EC, Yu NY, Birke ODG. Little Biomechanics of Slipped Capital Femoral Epiphysis: Evaluation of the Posterior Sloping Angle. *J Pediatr Orthop*. 2016; 36 (6): 651–5.
- Thawrani DP, Feldman DS, Sala DA. Current practice in the management of slipped capital femoral epiphysis. *J Pediatr Orthop*. 2016; 36 (3): e27–e37.
- Slongo T, Kakaty D, Krause F, Ziebarth K. Treatment of slipped capital femoral epiphysis with a modified Dunn procedure. *J Bone Joint Surg Am*. 2010; 92 (18): 2898–908.
- Rathey T, Piehl F, Wright JG. Acute slipped capital femoral epiphysis. Review of outcomes and rates of avascular necrosis. *J Bone Joint Surg Am*. 1996; 78: 398–402.
- Salvati EA, Robinson JH Jr, O'Down TJ. Southwick osteotomy for severe chronic slipped capital femoral epiphysis: results and complications. *J Bone Joint Surg Am*. 1980; 62 (4): 561–70.
- Barsukov DB, Baidurashvili AG, Pozdnikin IYu, Baskov VE, Krasnov AI, Bortulov PI. Novyj metod korririrujushhej osteotomii bedra u detej s junosheskim jepifizeolizom golovki bedrennoj kosti. *Genij ortopedii*. 2018; 24 (4): 450–9. Russian.
- Tihonenkov ES, Krasnov AI, redaktory. Diagnostika, hirurgicheskoe i vosstanovitel'noe lechenie junosheskogo jepifizeoliza golovki bedrennoj kosti u podrostkov: metod. rekomendacii. SPb., 1994; 39 s. Russian.
- Pozdnikin IYu, Barsukov DB, avtory. Sposob korririrujushhej osteotomii bedra pri junosheskom jepifizeolize golovki bedrennoj kosti. Patent RF # 2604039. 18.05.2015. Russian.
- Imhäuser GZ. Imhäuser's osteotomy in the flirid gliding process. Observations on the corresponding work of B.G. Weber. *Orthop Ihre Grenzgeb*. 1966; 102 (2): 327–9.
- Kartenbender K, Cordier W, Katthagen BD. Long-term follow-up study after corrective Imhäuser osteotomy for severe slipped capital femoral epiphysis. *J Pediatr Orthop*. 2000; 20 (6): 749–56.
- Trisolino G, Pagliazzi G, Di Gennaro GL, Stilli S. Long-term Results of Combined Epiphysiodesis and Imhäuser Intertrochanteric Osteotomy in SCFE: A Retrospective Study on 53 Hips. *J Pediatr Orthop*. 2017; 37 (6): 409–15.
- Erickson JB, Samora WP, Klingele KE. Treatment of chronic, stable slipped capital femoral epiphysis via surgical hip dislocation with combined osteochondroplasty and Imhäuser osteotomy. *J Child Orthop*. 2017; 11 (4): 284–8.
- Aguilar CM, et al. Clinical evaluation of avascular necrosis in patients with sickle cell disease: Children's Hospital Oakland Hip Evaluation Scale--a modification of the Harris Hip Score. *Arch Phys Med Rehabil*. 2005.
- Egiazarjan KA, Gordienko DI, Grigorev Aleksandr V, Grigorev Aleksej V, Chebotarev VV, avtory. Sposob hirurgicheskogo lechenija junosheskogo jepifizeoliza golovki bedrennoj kosti. Patent RF # 2692325. 24.06.2019. Russian.
- Krechmar AN. Junosheskij jepifizeoliz golovki bedra (kliniko-jeksperimental'noe issledovanie) [dissertacija]. L., 1982; 34 s. Russian.
- Loder RT, Skopelja EN. The epidemiology and demographics of slipped capital femoral epiphysis. *ISRN Orthop*. 2011; 2011: 486512.

Литература

- Соколовский А. М., Соколовский О. А., Гольдман Р. К., Юношеский эпифизеолиз головки бедренной кости. Медицинские новости. 2006; 2.
- Witbreuk M, van Kemenade FJ, van der Sluijs JA, Jansma EP, Rotteveel J, van Royen BJ. Slipped capital femoral epiphysis and its association with endocrine, metabolic and chronic diseases: a systematic review of the literature. *J Child Orthop*. 2013; 7 (3): 213–23.
- Tayton K. The epiphyseal tubercle in adolescent hips. *Acta Orthop*. 2009; 80: 416–9.
- Gholve PA, Cameron DB, Millis MB. Slipped capital femoral epiphysis update. *Curr Opin Pediatr*. 2009; 21 (1): 39–45.
- Carney BT, Weinstein SL. Natural history of untreated chronic slipped capital femoral epiphysis. *Clin Orthop Relat Res*. 1996; (322): 43–7.
- Abu Amara S, Cunin V, Ilharreborde B; French Society of Pediatric Orthopaedics (SOPOP). Severe slipped capital femoral epiphysis: a French multicenter study of 186 cases performed by the SoPOP. *Orthop Traumatol Surg Res*. 2015; 101 (6 Suppl): S275–9.
- Bittersohl B, Hosalkar HS, Zilkens C, Krauspe R. Current concepts in management of slipped capital femoral epiphysis. *Hip Int*. 2015; 25 (2): 104–14.
- Mahrn MA, Baraka MM, Hefny HM. Slipped capital femoral epiphysis: a review of management in the hip impingement era. *SICOT J*. 2017; 3: 35.
- Meier MC, Meyer LC, Ferguson RL. Treatment of slipped capital femoral epiphysis with a spica cast. *J Bone Joint Surg Am*. 1992; 74: 1522–9.
- Bellemore JM, Carpenter EC, Yu NY, Birke ODG. Little Biomechanics of Slipped Capital Femoral Epiphysis: Evaluation of the Posterior Sloping Angle. *J Pediatr Orthop*. 2016; 36 (6): 651–5.
- Thawrani DP, Feldman DS, Sala DA. Current practice in the management of slipped capital femoral epiphysis. *J Pediatr Orthop*. 2016; 36 (3): e27–e37.
- Slongo T, Kakaty D, Krause F, Ziebarth K. Treatment of slipped capital femoral epiphysis with a modified Dunn procedure. *J Bone Joint Surg Am*. 2010; 92 (18): 2898–908.
- Rathey T, Piehl F, Wright JG. Acute slipped capital femoral epiphysis. Review of outcomes and rates of avascular necrosis. *J Bone Joint Surg Am*. 1996; 78: 398–402
- Salvati EA, Robinson JH Jr, O'Down TJ. Southwick osteotomy for severe chronic slipped capital femoral epiphysis: results and complications. *J Bone Joint Surg Am*. 1980; 62 (4): 561–70.
- Барсуков Д. Б., Баиндурашвили А. Г., Поздникин И. Ю., Басков В. Е., Краснов А. И., Бортулёв П. И. Новый метод корригирующей остеотомии бедра у детей с юношеским эпифизеолизом головки бедренной кости. *Гений ортопедии*. 2018; 24 (4): 450–9.
- Тихоненков Е. С., Краснов А. И., редакторы. Диагностика, хирургическое и восстановительное лечение юношеского эпифизеолиза головки бедренной кости у подростков: метод. рекомендации. СПб., 1994; 39 с.
- Поздникин И. Ю., Барсуков Д. Б., авторы. Способ корригирующей остеотомии бедра при юношеском эпифизеолизе головки бедренной кости. Патент РФ № 2604039. 18.05.2015.
- Imhäuser GZ. Imhäuser's osteotomy in the florid gliding process. Observations on the corresponding work of B.G. Weber. *Orthop Ihre Grenzgeb*. 1966; 102 (2): 327–9.
- Kartenbender K, Cordier W, Katthagen BD. Long-term follow-up study after corrective Imhäuser osteotomy for severe slipped capital femoral epiphysis. *J Pediatr Orthop*. 2000; 20 (6): 749–56.
- Trisolino G, Pagliazzi G, Di Gennaro GL, Stilli S. Long-term Results of Combined Epiphysodesis and Imhäuser Intertrochanteric Osteotomy in SCFE: A Retrospective Study on 53 Hips. *J Pediatr Orthop*. 2017; 37 (6): 409–15.
- Erickson JB, Samora WP, Klinge KE. Treatment of chronic, stable slipped capital femoral epiphysis via surgical hip dislocation with combined osteochondroplasty and Imhäuser osteotomy. *J Child Orthop*. 2017; 11 (4): 284–8.
- Aguilar CM, et al. Clinical evaluation of avascular necrosis in patients with sickle cell disease: Children's Hospital Oakland Hip Evaluation Scale--a modification of the Harris Hip Score. *Arch Phys Med Rehabil*. 2005.
- Егизарян К. А., Гордиенко Д. И., Григорьев Александр В., Григорьев Алексей В., Чеботарев В. В., авторы. Способ хирургического лечения юношеского эпифизеолиза головки бедренной кости. Патент РФ № 2692325. 24.06.2019.
- Кречмар А. Н. Юношеский эпифизеолиз головки бедра (клинико-экспериментальное исследование) [диссертация]. Л., 1982; 34 с.
- Loder RT, Skopelja EN. The epidemiology and demographics of slipped capital femoral epiphysis. *ISRN Orthop*. 2011; 2011: 486512.

ADHERENCE TO TREATMENT IN VISUALLY IMPAIRED INDIVIDUALS

Bikbov MM, Israfilova GZ [✉], Gilmanshin TR, Zainullin RM, Yakupova EM

Ufa Eye Research Institute, Ufa, Russia

Adherence to treatment is one of the major challenges posed by modern medicine. Today, cataract is the leading cause of reversible blindness and visual disability. The study was aimed to assess adherence to timely surgical treatment in individuals with cataract. The data of the cross-sectional, population-based Ural Eye and Medical Study were assessed. Among 546 participants, there were 46.3% men and 53.7% women, 59.6% urban residents, 40.4% rural residents. Their average age was 66.36 ± 9.47 years (40–88 years). Statistical data analysis was performed using the IBM SPSS Statistic software package. The findings showed that the lack of awareness of the disorder and low interest in surgery were the main factors, affecting the patients' motivation for cataract treatment. At the same time, the frequency of ophthalmology visits was inversely related to the patients' age (OR 1.24; 95% CI 1.04–1.49) and the duration of vision loss (OR 1.08; 95% CI 0.81–1.43), and directly related to the cataract diagnosis age (OR 1.20; 95% CI 1.04–1.38), the presence of ophthalmologist in the community clinic (OR 1.71; 95% CI 1.29–2.26), trust in the doctor (OR 3.62; 95% CI 3.02–4.35), ophthalmologist's explanation of the cataract complications and advanced treatment methods (OR 1.62; 95% CI 1.34–1.97). Understanding the main factors, contributing to low treatment adherence in patients with cataracts, would make it possible to optimize the measures to improve healthcare delivery to such patients, associated with the increased coverage of surgical treatment.

Keywords: adherence to surgical treatment, cataract, awareness, quality of life

Author contribution: Bikbov MM — study concept and design, advising, editing; Israfilova GZ, Gilmanshin TR — data acquisition and processing, manuscript writing and editing.

Compliance with ethical standards: the study was approved by the Ethics Committee of the Ufa Eye Research Institute and conducted in accordance with the fundamental ethical principles of the Declaration of Helsinki, GCP (Good Clinical Practice) principles, and current regulatory requirements; the informed consent was submitted by all study participants.

✉ **Correspondence should be addressed:** Gulnara Z. Israfilova
Pushkina, 90, 450008, Ufa, Russia; israfilova_gulnara@mail.ru

Received: 01.02.2022 **Accepted:** 15.02.2022 **Published online:** 22.02.2022

DOI: 10.24075/brsmu.2022.008

ПРИВЕРЖЕННОСТЬ К ЛЕЧЕНИЮ ЛИЦ С НАРУШЕНИЕМ ЗРЕНИЯ

М. М. Бикбов, Г. З. Исрафилова [✉], Т. Р. Гильманшин, Р. М. Зайнуллин, Э. М. Якупова

Уфимский научно-исследовательский институт глазных болезней, Уфа, Россия

Проблема приверженности к лечению — одна из наиболее значимых для современной медицины. На сегодняшний день основной причиной обратимой слепоты и инвалидности по зрению является катаракта. Целью исследования было оценить приверженность к своевременному хирургическому лечению у лиц с катарактой. В работе использованы данные поперечного популяционного исследования «Ural Eye and Medical Study». Из 546 участников 46,3% мужчин и 53,7% женщин, жителей города — 59,6%, жителей села — 40,4%, средний возраст которых составил 66,36 ± 9,47 года (диапазон 40–88 лет). Статистический анализ данных проводили с использованием пакета прикладных программ IBM SPSS Statistic. Результаты исследования показали, что основной фактор, влияющий на мотивацию пациента к лечению катаракты, — недостаточная информированность о заболевании и заинтересованность в хирургическом лечении. При этом частота посещений офтальмолога находится в обратной зависимости от возраста пациентов (ОШ 1,24; 95% ДИ 1,04–1,49), длительности снижения зрения (ОШ 1,08; 95% ДИ 0,81–1,43) и в прямой зависимости от длительности времени с момента установления диагноза катаракты (ОШ 1,20; 95% ДИ 1,04–1,38), наличия офтальмолога в поликлинике по месту жительства (ОШ 1,71; 95% ДИ 1,29–2,26), доверия врачу (ОШ 3,62; 95% ДИ 3,02–4,35), разъяснения офтальмологом осложнений и современных методов лечения катаракты (ОШ 1,62; 95% ДИ 1,34–1,97). Понимание основных причин, снижающих приверженность пациентов с катарактой к лечению, позволит разработать наиболее эффективные мероприятия по совершенствованию медицинской помощи, связанной с увеличением охвата хирургическим лечением пациентов с данной патологией.

Ключевые слова: приверженность к хирургическому лечению, катаракта, информированность, качество жизни

Вклад авторов: М. М. Бикбов — концепция и дизайн исследования, консультирование, редактирование; Г. З. Исрафилова, Т. Р. Гильманшин — сбор и обработка материала, написание текста; Г. З. Исрафилова, Т. Р. Гильманшин, Р. М. Зайнуллин, Э. М. Якупова — написание текста, редактирование.

Соблюдение этических стандартов: исследование одобрено этическим комитетом Уфимского НИИ глазных болезней; выполнено в соответствии с основополагающими этическими принципами Хельсинкской декларации, правилами GCP и действующими нормативными требованиями; все участники подписали добровольное информированное согласие на участие в исследовании.

✉ **Для корреспонденции:** Гульнара Зуфаровна Исрафилова
ул. Пушкина, д. 90, 450008, г. Уфа, Россия; israfilova_gulnara@mail.ru

Статья получена: 01.02.2022 **Статья принята к печати:** 15.02.2022 **Опубликована онлайн:** 22.02.2022

DOI: 10.24075/vrgmu.2022.008

The term "adherence to treatment" emerged in the domestic scientific literature about 20 years ago, but it has become widely used recently, in the last 5–6 years. According to the World Health Organization (WHO), adherence to treatment is the degree to which a patient's behavior matches the doctor's prescriptions for taking medications, following dietary recommendations and/or lifestyle changes. It is believed that the patients' non-compliance with medical recommendations results from the lack of effective doctor–patient communication. The patients' personal and psychological characteristics, clinical features

of the disease, treatment type, socio-economic factors, and the features of healthcare delivery in different countries are the other reasons for low treatment adherence [1]. This issue is particularly relevant for eye diseases, since eye lesions are not potentially fatal, especially when the lesions could be removed. Many patients pay little attention to cataracts, since they usually have no prominent subjective symptoms for a long time. However, even the treatable eye lesions constitute a major medical and social challenge. The patient's psychology in terms of the cataract treatment and prevention is one of the

leading causes of blindness and low vision in the world [2]. High medical and social significance of cataracts is determined by a number of factors: high levels of blindness (reversible) and vision disability, significant direct (expenses for surgery, conservative treatment, and management of postoperative complications) and consequential (loss of labor potential of the society, traffic accidents, injuries, and falls due to visual impairment) economic losses, high prevalence of the disorder, clear upward trend in the number of individuals with reduced lens transparency of both retirement and working age [3–7].

It should be noted that the treatment success depends not only on the properly constructed healthcare system, but also on the patient's compliance with the recommendations on the prevention and treatment of the disease, given by healthcare professionals [8, 9]. Poor adherence is a proven risk factor of any disorder, which reduces the effectiveness and increases the cost of treatment, increases the risk of various complications, worsens the outcome, and reduces the patients' quality of life [10, 11]. Experts from the WHO have identified a large number of factors that affect the patient's adherence to treatment. According to the WHO classification (2003), the factors are divided into five interconnected groups: 1) patient-related factors; 2) factors related to medical personnel and healthcare system organization; 3) factors associated with ongoing therapy; 4) factors associated with the patient's condition (disease); 5) socio-economic factors [12]. In this regard, the papers, which propose structured approach to describing the causes of low treatment adherence, are of great interest. The causes are divided into five major categories: socio-demographic; psychological; resulting from the disorder or the disease treatment; economic; related to the healthcare system [1].

Filling the gap in studying various factors, negatively affecting the capability of overcoming the treatment adherence-related barriers in patients with cataracts, would result in the significantly decreased incidence of this socially significant disorder. This is especially important in terms of improving the cooperation between the doctor and the patient, which contributes to faster recovery, improved quality of life and healthy lifestyle creation, and makes it possible to develop the measures to improve the quality of care provided to patients with cataracts.

For that reason, identification and analysis of the existing factors, including the psychological factors, which affect treatment adherence in patients with cataract, seem to be relevant.

The study was aimed to assess the attitude towards factors, affecting adherence to timely surgical treatment, in individuals with cataracts.

METHODS

Data of the cross-sectional, population-based Ural Eye and Medical Study (UEMS), conducted in 2015–2017 in the Ufa Eye Research Institute, were assessed. Currently, UEMS is the largest ophthalmological population-based study in the Russian Federation, which is aimed at studying the prevalence of socially significant eye diseases and associated risk factors.

The stages of the study were in line with the generally accepted standards. The study included the following: protocol development and the research instrument selection, data acquisition, scaling and database creation, statistical processing, analysis, and interpretation of the results [13, 14]. Inclusion criteria: voluntary consent to participate in the project; age over 40; permanent residence in the studied urban and rural areas.

To assess alterations in lens transparency, we used the LOCS III grading scale (Lens Opacities Classification System, 1993), according to which three types of lens opacification were distinguished: nuclear, cortical, and subcapsular [15]. According to this classification, nuclear lens opacities were divided into six grades. It should be noted that the most important are the changes in the lens nucleus, corresponding to grade 3 and above. For that reason, in the paper we link the nuclear cataract to these changes.

To study the respondents' awareness of the lens disorder and their adherence to timely treatment, we conducted a questionnaire survey among people diagnosed with cataracts. The study was carried out by the written survey using the specially compiled questionnaire, which contained 25 questions concerning demographic information (gender, age), socio-economic data (level of education), the frequency and the possibility of ophthalmology visits, individual's awareness of the disease, risk factors, and treatment methods, as well as the questions to assess the reasons, preventing the timely cataract surgery.

The study involved 546 individuals: 253 men (46.3%) and 293 women (53.7%), 325 urban residents (59.6%), 221 rural residents (40.4%). The average age was 66.36 ± 9.47 years (40–88 years). The number of observations required was justified using the method, developed by Otdelnova KA [16].

Statistical analysis was carried out using the IBM SPSS Statistic software package, version 23.0 (SPSS: An IBM Company; USA). The methods of descriptive and comparative statistics for quantitative characteristics were selected based on the distribution type assessment using the Shapiro–Wilk test. The groups were compared based on the qualitative characteristics using the Pearson's chi-squared (χ^2) test or Fisher's exact test (in case there were less than five observations in at least one cell of the contingency table). To characterize the univariate regression models and assess the degree of influence of each predictor on the disease development (outcome), the following parameters were calculated: regression coefficient (β), standard error of the coefficient (SE), Wald chi-square statistics (W), Odds ratios (OR), 95% confidence intervals (CI) for OR, and predictor significance were calculated based on these data. When performing statistical analysis, the achieved significance level (p) was calculated; the differences were considered significant at $p < 0.05$.

RESULTS

The analysis revealed that the majority of the respondents (60.85%) noted they had a secondary specialized education. A total of 21.70% respondents had higher education, 13.62% had secondary general education, and only 3.83% had incomplete school education. A survey of people over 40 years of age on their health-related behaviour showed that 39.2% of respondents got their ophthalmic checkups annually, 33.7% visited a doctor twice a year or more frequently, and 27.1% visited a specialist less than once a year. It should be noted that women were much more likely to seek ophthalmological care within a year (78.9 vs. 66.4%, $\chi^2 = 8.34$; $p = 0.01$). Furthermore, almost all patients (68.9% of men and 71.9% of women, $\chi^2 = 6.51$; $p = 0.04$) noted that they needed constant medical supervision. Among rural residents, characterized by the lack of healthcare access, the proportion of those who contacted a healthcare institution throughout the year was slightly less than among urban residents (71.6 and 73.6%, respectively, $\chi^2 = 1.13$; $p = 0.2$). Thus, rural residents remain active in applying to healthcare institutions.

Table 1. Reasons preventing the cataract patients from ophthalmology visits

Reasons of non-attendance for ophthalmologic examination	Answers, <i>n</i> (%)
Was unaware of the need to see a doctor	29 (19.6)
Being busy (due to employment, household activities, agricultural activities, etc.)	27 (18.2)
No visual impairment	22 (15.2)
No ophthalmologist in the community clinic	20 (13.4)
Long queue to ophthalmologist	12 (8.2)
No accompanying person	9 (6.3)
Transport problems	8 (5.8)
Other	21 (14.1)
Total responses	148

It was found that the lack of knowledge about the need to see a doctor (19.6%) because of reduced vision was the main reason, preventing the respondents with cataracts from visiting an ophthalmologist on the annual basis. According to the respondents, the equally important reasons were as follows: being busy (18.2%), and no specialist physician in the community clinic (13.4%) (Table 1).

Patients with cataracts are characterized by low anxiety, and often by the condition severity underestimation. They do not consider their disorder to be the condition, significantly limiting their daily living activities, and assume that surgical treatment is fully capable to restore visual functions.

To investigate the respondents' knowledge about cataract, the questions were included in the questionnaire, allowing us to assess the respondent's awareness of the features of his/her eye disorder. The survey revealed a good knowledge on the disorder in the majority of respondents (60.2%); 17.8% of individuals had some ideas about the cataract, 5.9% were completely unaware, and 16.1% found it difficult to answer the question.

At the same time it should be noted that a large proportion of patients took an active stand on the matter. Thus, 60.4% of patients would like to know as much as possible about their disorder; 25.1% of individuals thought it was enough that the doctor was aware of the disease. The majority of patients (65.6%) would like to receive additional information about the disease from an ophthalmologist, as from a competent specialist. Furthermore, 19.3% of respondents would obtain

such information from the online resources, 11.1% would get information in healthcare institutions (stands, brochures), 2.6% would read popular science magazines, and 1.4% would discuss the matter with their friends.

The doctor's high professional level and positive personal qualities are essential for the patients' compliance with recommendations, and the lack of this component increases the likelihood of self-treatment [10, 20]. The survey showed that the majority of the respondents (63.6 %) fully trusted their attending physicians and highly appreciated the physicians' professional level. One third of the respondents (27.9%) noted the doctor's high professional qualification and good personal qualities. The minority of respondents (1.4%) seemed not to fully trust their doctors and did not consider them to be the highly qualified professionals. Only 7.1% of respondents found it difficult to express their attitude. The following factors were among the reasons for "dissatisfaction" with the doctor: insufficient attention paid by the doctor (52.7%), the doctor's inability to win over the patient (14.9%), and the doctor's low level of competence (12.4%). However, the findings might indicate the high level of confidence in the doctors' professional qualification and personality.

When a patient comes to see an ophthalmologist, it is extremely important for a doctor to explain the clinical features of cataract, such as functional vision impairment, which reduces the quality of life, and to provide information about the modern personalized treatment methods in case of reversible vision loss. Thus, 70.3% of individuals in the studied group indicated

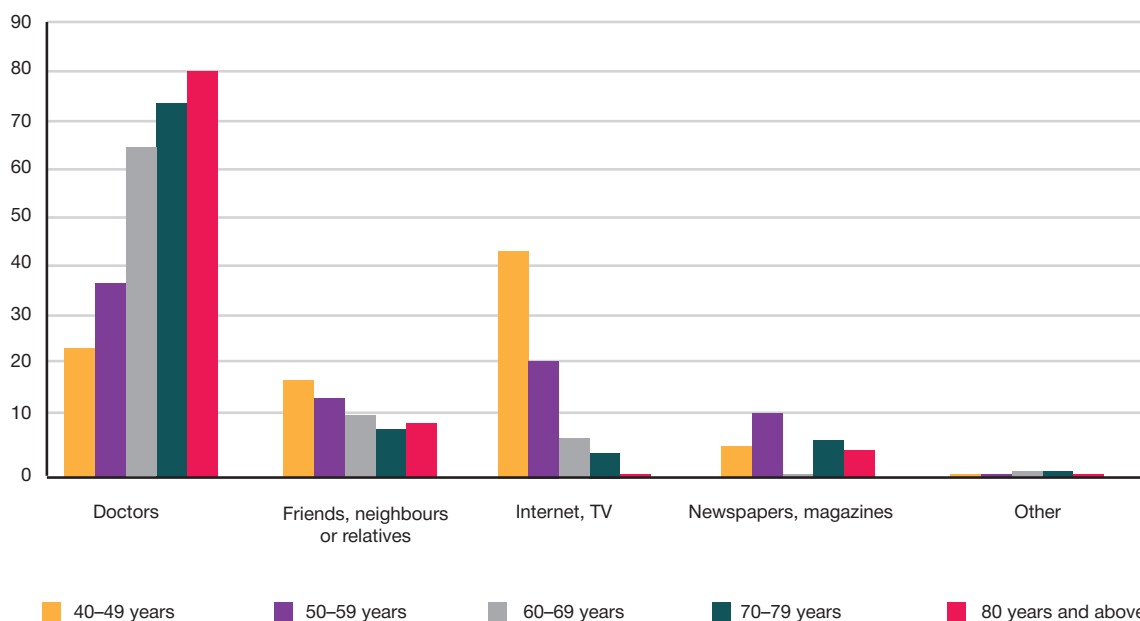
**Fig. 1.** Age distribution of respondents taking into account the source of information about cataracts

Table 2. Factors associated with the frequency of ophthalmology visits in patients with cataracts

Indicator (factor)	β	W	p	OR	95% CI
Age (years)	-1.54	22.54	< 0.001	1.24	1.04–1.49
Duration of vision loss (years)	-0.39	8.26	0.004	1.08	0.81–1.43
Time since the diagnosis of cataract (years)	0.59	6.39	0.01	1.2	1.04–1.38
Presence of ophthalmologist in the community clinic (1 — present, 2 — absent)	0.55	13.54	< 0.001	1.71	1.29–2.26
Confidence in the doctor (1 — yes, 2 — no)	0.33	19.248	< 0.001	3.62	3.02–4.35
Have the ophthalmologist explained about cataracts and treatment methods (1 — yes, 2 — no)	0.48	23.63	< 0.001	1.62	1.34–1.97

Note: β — regression coefficient; SE — standard error of the coefficient, W — Wald chi-square statistics, OR — odds ratio, 95% CI — two-sided 95% CI for OR.

that they learned about their eye disease when talking with the doctor; 15.2% of individuals got information from their friends and relatives, and 14.5% of respondents obtained information from mass media, such as TV, Internet, and press. Younger patients more often received information from the online resources, friends or relatives, while the respondents of the older age groups received information from ophthalmologists (Fig. 1).

We have defined the frequency of ophthalmology visits depending on the duration of visual impairment, the patients' age, and the presence of ophthalmologist in the community clinic (Table 2).

The analysis revealed the impact of the patients' age on the frequency of ophthalmology visits. Thus, every one-year increase in age reduces the probability of visiting a specialist physician by 1.24 times. Longer time since the diagnosis of cataract in the surveyed patients results in the 1.2 higher frequency of visits to ophthalmologists. Among individuals, who have ophthalmologists in their community clinics, the probability of annual ophthalmology visits is 1.71 times higher compared to individuals, having no ophthalmologists in their community clinics.

Studying the trust towards doctors as a factor affecting the patients' adherence to regular medical visits, and their willingness to comply with the specialists' recommendations, revealed the direct relationship. The calculated odds ratio (OR — 3.6) indicates that the chances to undergo ophthalmic examination are higher in individuals, who trust their doctors. A significant relationship has been also found between the frequency of ophthalmology visits and explaining the existing

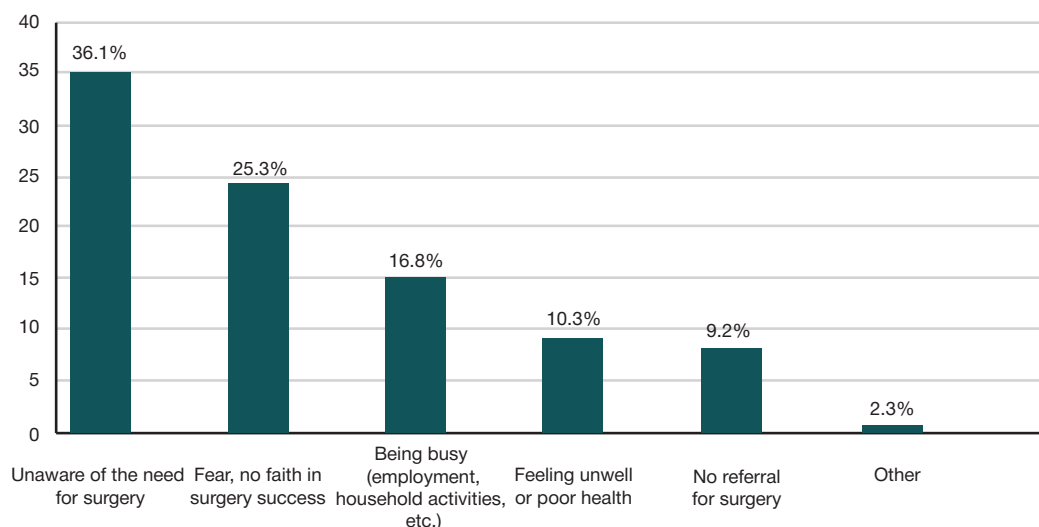
eye disorder. Thus, individuals, to whom the the specialists explain the course and complications of cataract, as well as the advanced treatment methods, have a 1.6 times higher probability of the ophthalmology visits.

We have ranked the factors that, according to the respondents, prevent the timely cataract surgery (Fig. 2). It was found that 36.1% of respondents were unaware of the need for cataract surgery. In every fourth respondent, his/her professional or household activity was one of the key factors, constraining the decision on the timely cataract surgery. A total of 16.8% individuals reported they were afraid of the forthcoming treatment; 10.3% of individuals postponed surgical treatment due to the concomitant somatic disease.

These findings indicate the lack of the patients' awareness of the disease and modern treatment methods. In this regard, informing the population, especially people over the age of 40, about cataract as a serious disease, which contributes to reversible blindness, is an urgent task.

DISCUSSION

The study has shown that insufficient awareness of the disease and the lack of interest in surgical treatment are the major factors, which reduce the patient's motivation for cataract treatment. At the same time, ophthalmology visit frequency is inversely related to the patients' age and the duration of vision loss, and is directly related to the presence of ophthalmologist in the community clinic, trust in the doctor, and ophthalmologist's explanation of the cataract complications and advanced treatment methods. It should be noted that the lack of knowledge about the need

**Fig. 2.** Distribution of reasons for refusal of the cataract surgery

for cataract surgery has been the main obstacle to timely cataract surgery according to 36.1% of respondents, being busy due to employment or household activities was identified by 25.3%, being afraid of the forthcoming treatment was reported by 16.8%, and concomitant somatic disorders were mentioned by 10.3%. These findings are in line with the results of studying the patients' treatment adherence in certain areas of medicine. Thus, a survey of patients with cardiovascular diseases revealed that the key factors contributing to low treatment motivation were as follows: misunderstanding of the doctor's instructions (33.7%), fear of side effects or building up a tolerance (40.2%), comorbidity (35.9%) [17], no symptoms of the disease [18], patient's refusal to depend on drugs or medical personnel, denial of the disease [19].

When studying dental patients, the key factors, negatively affecting the treatment motivation, were as follows: patients' age (the vast majority of individuals were 35–49 years old); gender (women sought medical attention more often than men) [20]; quality of dental care [21]; underestimation of the condition severity by the patient; treatment costs [22]; painful procedure-related fear. In most cases the need for visiting a dentist is associated with acute pain (58.9%), 31.1% of patients schedule their dental visits, and only 22.8% of respondents would have routine check ups [23].

Thus, the study has shown that the factors associated with the patient's personality (lack of awareness, being busy,

fear, etc.), including psychosocial factors (beliefs, perceptions, lack of motivation), as well as the lack of trust in the doctor-patient communication, are the most significant barriers for the cataract treatment adherence. The patient's limited knowledge about cataract and its sequelae together with the lack of motivation and positive preoperative expectations, as well as limited awareness of the advanced treatment methods, result in the delayed application for effective surgical intervention, and reduced quality of life.

CONCLUSIONS

To date, strengthening the prevention and treatment of sociomedical conditions, being the main cause of blindness and low vision, is a major challenge posed by the healthcare system. At the current stage, increasing the patients' adherence to treatment is one of the main factors of improving the health status and the quality of life of the population. When analyzing attitudes towards factors that affected adherence to timely treatment in individuals with cataracts, it was found that the patient-related factors were the most significant (lack of awareness of the disorder, low patient's interest). The findings make it possible to optimize the measures to improve healthcare delivery to patients with cataracts in order to increase the coverage of surgical treatment in such patients.

References

- Likhodey NV, Kalashnikova MF, Likhodey EM, Fadeev VV. Analiz faktorov, prepjatstvujushih formirovaniju priverzhennosti lecheniju sredi bol'nyh saharnym diabetom, i strategij, sposbstvujushih ee povysheniju. *Saharnyj diabet*. 2018; 21 (1):5–14. Russia.
- Brian G, Taylor H. Cataract blindness – challenges for the 21st century. *Bull World Health Organ*. 2001;79 (3): 249–56.
- Branchevsky SL, Malyugin BE. Rasprostranennost' narushenija zrenija vsledstvie katarakty po dannym issledovanija RAAB v Samare. *Oftal'mohirurgija*. 2013; 3: 82–85. Russia.
- Libman E. S., Shahova E. V. Slepota i invalidnost' vsledstvie patologii organa zrenija v Rossii. *Vestnik oftal'mologii*. 2006; 1: 35–37. Russia.
- Sinjapko SF. Sostojanie normal'noj ostroty zrenija, slabovidenija, slepoty, vidov refrakcii, vospalitel'nyh i nevospalitel'nyh zabolevanij glaz u naselenija Krasnojarskogo kraja. *Voprosy oftal'mologii*. Abakan. 2004: 4–13. Russia.
- Juzhakov AM. Osnovnye napravlenija v likvidacii ustranimoj slepoty v Rossijskoj Federacii. *Likvidacija ustranimoj slepoty: Vsemirnaja iniciativa VOZ. Materialy Rossijskogo mezhrregional'nogo simpoziuma*. Moskva, 2003; s. 27–31. Russia.
- World Health Organization Press Office Control of major blinding diseases and disorders: Vision 2020: the Right to Sight, WHO Fact Sheet. Geneva. 2010. № 214. Available from: <http://www.who.int/inf-fs/en/fact214.html/>.
- Chowdhury R, Khan H, Heydon E, Shroufi A, Fahimi S, Moore C, et al. Adherence to cardiovascular therapy: a meta-analysis of prevalence and clinical consequences. *Eur Heart J*. 2013; 34 (38): 2940–8. DOI: 10.1093/eurheartj/ehd295.
- Shvarc YuG, Naumova EA. Priverzhennost' pacientov k lecheniju s pozicij dokazatel'noj mediciny. *Mezhdunarodnyj medicinskij zhurnal*. 2005; 3: 120–125.
- Koichuev AA. Priverzhennost' v lechenii: metodiki ocenki, tehnologii korekcii nedostatochnoj priverzhennosti terapii. *Medicinski vestnik Severnogo Kavkaza*. 2013; 8 (3): 65–69.
- Lukina YuV, Kutishenko NP, Marcevic SYu. Priverzhennost' lecheniju: sovremennij vzgljad na znakomuju problemu. *Kardiovaskuljarnaja terapija i profilaktika*. 2017; 16 (1): 91–95. DOI: 10.15829/1728-8800-2017-1-91-95. Russia.
- World Health Organization. Adherence to long-term therapies: evidence for action. WHO Library Cataloguing-in-Publication Data, Geneva, WHO 2003; 230 pp. Available from: http://www.who.int/chp/knowledge/publications/adherence_report/en.
- Bikbov MM, Kazakbaeva GM, Gilmanshin TR, Zainullin RM, Arslangareeva II, Salavatova VF, et al. Axial length and its associations in a Russian population: The Ural Eye and Medical Study. *PLoS One*. 2019; 14 (2): e0211186. DOI: 10.1371/journal.pone.0211186.
- Bikbov M, Fayzrakhmanov RR, Kazakbaeva G, Jonas JB. Ural Eye and Medical Study: description of study design and methodology. *Ophthalmic Epidemiol*. 2018; 25 (3): 187–98. DOI: 10.1080/09286586.2017.1384504.
- Chylack LT Jr, Wolfe JK, Singer DM, Leske MC, Bullimore MA, Bailey IL, et al. The Lens Opacities Classification System III. The Longitudinal Study of Cataract Study Group. *Arch Ophthalmol*. 1993; 111 (6): 831–6. DOI: 10.1001/archophth.1993.01090060119035.
- Otdelnova KA. Opređenje neobhodimogo chisla nabljudenij v social'no-gigienicheskikh issledovanijah. *Sbornik trudov 2-go MMI*. 1980; 150 (6): 18–22. Russia.
- Semenova ON, Naumova EA. Faktory, vlijajushhie na priverzhennost' k terapii: parametry VOZ i mnenie pacientov kardiologicheskogo otdelenija. *Bjul med Internet-konferencij*. 2013; 3 (3): 507–11. Russia.
- Kachkovskij MA, Simerzin VV, Krasnoslobodskaya OV. Priverzhennost' lecheniju bol'nyh s fibriljaciej predserdij v uslovijah ambulatorno-poliklinicheskoj praktiki. *Izvestija Samarskogo nauch. centra Ros. akad. nauk*. 2010; 12; 1 (6): 1606–9. Russia.
- Konobeeva EV, Shvarc YuG, Korsunova EN, Gafanovich EYa. Vozmozhnosti povyshenija osoznannoj motivacii pacientov kardiologicheskogo profilja. *Ispol'zovanie standartizirovannyh nagladnyh rekomendacij. Fundamental'nye issledovanija*. 2013; 9 (1): 58–61. Russia.
- Ivanova EI. Motivacija obrashhenija pacientov za parodontologicheskoi pomoshh'ju. *Molodij uchenyj*. 2014; 6: 298–301. Russia.
- Avanesyan RA, Sirak SV, Hodzhayan AB, Gevandova MG. Social'nyj sostav i motivacija pacientov pri obrashhenii za implantologicheskoi stomatologicheskoi pomoshh'ju. *Sovrem.*

- probl. nauki i obrazov. 2013; 4. Russia.
22. Firsova IV, Mihalchenko VF, Popova AN, Chaplieva EM. K voprosu izucheniya komplaentnosti stomatologicheskogo pacienta. Volgostom. Volgogradskii stomatologicheskii portal. Dostupno po ssylke: <http://www.volgostom.ru/k-voprosu-izucheniya-komplaentnosti-stomato-logicheskogo-patsienta>. Russia.
23. Firsova IV. Konceptija komplaentnosti v stomatologicheskoi praktike [dissertacija]. Volgograd, 2009; 52 s. Russia.

Литература

1. Лиходей Н. В., Калашникова М. Ф., Лиходей Е. М., Фадеев В. В. Анализ факторов, препятствующих формированию приверженности лечению среди больных сахарным диабетом, и стратегий, способствующих ее повышению. Сахарный диабет. 2018; 21 (1): 5–14.
2. Brian G, Taylor H. Cataract blindness – challenges for the 21st century. Bull World Health Organ. 2001;79 (3): 249–56.
3. Бранчевский С. Л., Малюгин Б. Э. Распространенность нарушения зрения вследствие катаракты по данным исследования РААВ в Самаре. Офтальмохирургия. 2013; 3: 82–85.
4. Либман Е. С., Шахова Е. В. Слепота и инвалидность вследствие патологии органа зрения в России. Вестник офтальмологии. 2006; 1: 35–37.
5. Синяко С. Ф. Состояние нормальной остроты зрения, слабовидения, слепоты, видов рефракции, воспалительных и невоспалительных заболеваний глаз у населения Красноярского края. Вопросы офтальмологии. Абакан. 2004: 4–13.
6. Южачов А. М. Основные направления в ликвидации устранимой слепоты в Российской Федерации. Ликвидация устранимой слепоты: Всемирная инициатива ВОЗ. Материалы Российского межрегионального симпозиума. Москва, 2003; с. 27–31.
7. World Health Organization Press Office Control of major blinding diseases and disorders: Vision 2020: the Right to Sight, WHO Fact Sheet. Geneva. 2010. № 214. Available from: <http://www.who.int/inf-fs/en/fact214.html/>.
8. Chowdhury R, Khan H, Heydon E, Shroufi A, Fahimi S, Moore C, et al. Adherence to cardiovascular therapy: a meta-analysis of prevalence and clinical consequences. Eur Heart J. 2013; 34 (38): 2940–8. DOI: 10.1093/eurheartj/ehd295.
9. Шварц Ю. Г., Наумова Е. А. Приверженность пациентов к лечению с позиций доказательной медицины. Международный медицинский журнал. 2005; 3: 120–125.
10. Койчув А. А. Приверженность в лечении: методики оценки, технологии коррекции недостаточной приверженности терапии. Медицинский вестник Северного Кавказа. 2013; 8 (3): 65–69.
11. Лукина Ю. В., Кутишенко Н. П., Марцевич С. Ю. Приверженность лечению: современный взгляд на знакомую проблему. Кардиоваскулярная терапия и профилактика. 2017; 16 (1): 91–95. DOI: 10.15829/1728-8800-2017-1-91-95.
12. World Health Organization. Adherence to long-term therapies: evidence for action. WHO Library Cataloguing-in-Publication Data, Geneva, WHO 2003; 230 pp. Available from: http://www.who.int/chp/knowledge/publications/adherence_report/en.
13. Bikbov MM, Kazakbaeva GM, Gilmanshin TR, Zainullin RM, Arslangareeva II, Salavatova VF, et al. Axial length and its associations in a Russian population: The Ural Eye and Medical Study. PLoS One. 2019; 14 (2): e0211186. DOI: 10.1371/journal.pone.0211186.
14. Ural Eye and Medical Study: description of study design and methodology. Ophthalmic Epidemiol. 2018; 25 (3): 187–98. DOI: 10.1080/09286586.2017.1384504.
15. Chylack LT Jr, Wolfe JK, Singer DM, Leske MC, Bullimore MA, Bailey IL, et al. The Lens Opacities Classification System III. The Longitudinal Study of Cataract Study Group. Arch Ophthalmol. 1993; 111 (6): 831–6. DOI: 10.1001/archoph.1993.01090060119035.
16. Отдельнова К. А. Определение необходимого числа наблюдений в социально-гигиенических исследованиях. Сборник трудов 2-го ММИ. 1980; 150 (6): 18–22.
17. Семенова О. Н., Наумова Е. А. Факторы, влияющие на приверженность к терапии: параметры ВОЗ и мнение пациентов кардиологического отделения. Бюл. мед. Интернет-конференций. 2013;3 (3): 507–11.
18. Качковский М. А., Симерзин В. В., Краснослободская О. В. Приверженность лечению больных с фибрилляцией предсердий в условиях амбулаторно-поликлинической практики. Известия Самарского науч. центра Рос. акад. наук. 2010; 12; 1 (6):1606–9.
19. Конобеева Е. В., Шварц Ю. Г., Корсунова Е. Н., Гафанович Е. Я. Возможности повышения осознанной мотивации пациентов кардиологического профиля. Использование стандартизированных наглядных рекомендаций. Фундаментальные исследования. 2013; 9 (1): 58–61.
20. Иванова Е. И. Мотивация обращения пациентов за пародонтологической помощью. Молодой ученый. 2014; 6: 298–301.
21. Аванесян Р. А., Сирак С. В., Ходжкян А. Б., Гевандова М. Г. Социальный состав и мотивация пациентов при обращении за имплантологической стоматологической помощью. Соврем. пробл. науки и образов. 2013; 4.
22. Фирсова И. В., Михальченко В. Ф., Попова А. Н., Чаплиева Е. М. К вопросу изучения комплаентности стоматологического пациента. Volgostom. Волгоградский стоматологический портал. Доступно по ссылке: <http://www.volgostom.ru/k-voprosu-izucheniya-komplaentnosti-stomato-logicheskogo-patsienta>.
23. Фирсова И. В. Концепция комплаентности в стоматологической практике [диссертация]. Волгоград, 2009; 52 с.